Characterizing and controlling structural and mechanical properties of type I collagen self-assembly

Jieling Zhu

Submitted in partial fulfillment of the
requirements for the degree of
Doctor of Philosophy
in the Graduate School of Arts and Sciences

COLUMBIA UNIVERSITY

2015

Abstract

Characterizing and controlling structural and mechanical properties of type I collagen self-assembly

Jieling Zhu

Type I collagen matrices are used across a variety of applications in bioengineering and biophysical studies; however, a fuller understanding of the collagen self-assembly process is required to optimize control of the matrix structural and mechanical properties in these applications. The work in this thesis sought to 1) characterize collagen self-assembly using simultaneous imaging, spectroscopy, and rheological methods, 2) use collagen gels as three-dimensional microenvironments to study glioma invasion, and 3) develop a model using experimental research data to teach data analysis tools to undergraduate students.

Chapter 1 provides a brief overview of collagen in the body, its applications, structural details about the collagen monomer, and descriptions of *in vivo* and *in vitro* fibrillogenesis. Advantages and disadvantages of methodologies used to study collagen self-assembly are discussed for *in vitro* fibrillogenesis. The materials and methods used in this thesis are described in Chapter 2.

Chapters 3 and 4 describe insights into collagen self-assembly using multiple modalities. In Chapter 3, turbidity and confocal reflectance microscopy were simultaneously employed to

track collagen fibrillogenesis and reconcile the information reported by the two techniques, with confocal fluorescence microscopy used to supplement information about early events in fibrillogenesis. Chapter 4 describes the novel use of simultaneous rheology and confocal microscopy to study the development of mechanical and structural properties of collagen gels.

In Chapter 5, glioma migratory and invasive behaviors are observed and perturbed in the context of well-controlled *in vitro* two- and three-dimensional environments, including implanting multicellular tumor spheroids in collagen gels across several concentrations to test the effects of pore size on glioma invasion. This chapter serves as a preliminary investigation into how glioma behavior changes depending on environment dimensionality and lays out further studies to fully investigate the mechanisms underlying glioma invasion.

Finally, Chapter 6 describes the development, evaluation, and redesign of a Microsoft Excel-based activity where data analysis from contemporary research (published in Chapter 3) was adapted into a training exercise for students taking an introductory General Chemistry Laboratory course. This activity humanized the research enterprise for the undergraduate students and can serve as a model for future collaborations between research and instructional laboratories.

Table of Contents

List of Figures

List of Tables

List of Acronyms

AFM	Atomic force microscopy
AS	Acid-solubilized (collagen)
CRM	Confocal reflectance microscopy
CFM	Confocal fluorescence microscopy
CRS	Collagen recognition sequence
DLS	Dynamic light scattering
DMEM	Dulbecco's Modified Eagle Medium
DMSO	Dimethyl sulfoxide
ECM	Extracellular matrix
ER	Endoplasmic reticulum
FBS	Fetal bovine serum
GBM	Glioblastoma multiforme
IST	*In situ* turbidity
MMP	Matrix metalloproteinase
MTS	Multicellular tumor spheroid
OI	Osteogenesis imperfecta
PBS	Phosphate buffer saline

PMT	Photomultiplier tube
PT	Pepsin-treated (collagen)
SEM	Scanning electron microscope
SLRP	Small leucine-rich repeat proteoglycan
TAs	Teaching assistants
TEM	Transmission electron microscope

Acknowledgements

Many people have provided guidance and support to me throughout my graduate career, so it is my greatest pleasure to express my gratitude to everyone who contributed to my personal and professional development.

I would like to thank my thesis advisor, Professor Laura Kaufman, for her continued mentorship and friendship these past five years. I chose to attend Columbia after speaking with her about potential research projects, and I was very happy that she accepted me into her research group right away. As a graduate student, I have pursued several exciting projects, guided by her research interests and experimental expertise. I am grateful for all the scientific advice and encouragement that she has provided me, as well as for her support with activities outside of lab, including teaching activities, outreach events, and running. I thank her for her edits on all of my scientific writing, including fellowship applications, paper drafts, and this thesis. As a scientist, teacher, mother, wife, runner, avid reader, and pet-lover (not exhaustive, and in no particular order), Laura is my role model and has shown me the importance of being adaptable, persistent, and resourceful.

Laura's personality and management style has created a collaborative and supportive lab environment full of smart, creative, and passionate scientists that I have had the pleasure of working with during my time in graduate school. I watched our lab grow in size and research breadth as people arrived and departed, learning new things with every individual. I would like to thank all of the people that have contributed to my research and helped me in some way in the lab: Dr. Keewook Paeng, for being the go-to person for any malfunctioning instruments, providing

helpful discussions and ingenious problem-solving ideas, and for conceptualizing, building, and machining our rheomicroscopy set-up; Dr. Yali Yang, for working on biopolymers in the lab before me, and Dr. Khanh-Hoa Tran-Ba, for taking over the biopolymer projects now that I am leaving; Matt Wilhelm and Chai Medicherla, for initial training with cells and collagen gels; Dr. Asja Guzman and Michelle Ziperstein, as resources for cell work and for their valuable feedback during bio sub-group meetings; Dat Hoang, for helping me with programming, math, and error analysis; Yen Nguyen and Michelle Ziperstein, for preliminary studies in fibrin; Dr. Abdel-Mohsan Abdel-Lattif, for collagen-hyaluronic acid studies; all the undergraduates that I have worked with: Chai Medicherla, Benjamin Kwok, Sriram Garikapati, Hector Acaron, Matt Levine, Esha Maharishi, Alana Warhit, John Raffles Durbin, and Akul Akora; Dr. Heungman Park, for always being in lab late in the evenings to check on why my computer is malfunctioning or why my files at not syncing properly; Dr. Zhihua An, for providing distractions from work with talk of kittens; and all the other people in lab that have helped me, offering encouragement or listening to me complain: Dr. Stephan Mackowiak, Dr. Lindsay Leone, Dr. Kevin Stokely, Dr. Jaesung Yang, Alyssa Manz, Karen Kwon, James Kweon, Daniel Lee, Catherine Zhang, and Holly Hajare. I especially want to thank Dr. Lindsay Leone, Dat Hoang, and Michelle Ziperstein for being some of my closest friends in and out of the lab.

The Chemistry department has been my home outside of home for the last five years and I would like to thank the faculty and staff here that have helped me. First, I am grateful to the professors who were part of my committee, for providing great feedback and ideas: Ann McDermott, Ruben Gonzalez, and Wei Min (and Helen Lu, from the Department of Bionegineering). Second, I would like to thank the faculty that I have had the pleasure of TAing for: Joseph Ulichny and Sarah Hansen for Fall 2010 General Chemistry Lab, Laura and Ruben for

Spring 2011 General Chemistry II, and Ruben and visiting Professor Bruce Bursten for Spring 2012 General Chemistry II. I would especially like to thank Bruce for encouraging me to pursue teaching opportunities and being accepting of a potentially non-traditional career path. Third, I am grateful to Dr. Sarah Hansen for working closely with me on the chemical education project, being a great resource for chemical education questions, and providing me a unique opportunity to work on curriculum development with her, Joseph Ulichny, Jessica Karch, and Cristina Sorrento. Fourth, I would like to thank Dr. Luis Avila for his help with instrumentation, and for always being the friendliest professor to ride an elevator with; I am also very grateful to the administrative staff for helping me with issues tangentially related to research, such as problems with teaching, lab conditions, and ordering supplies from foreign companies: Jay Kirschenbaum, Dani Farrell, Carlos Garcia, Alix Lamia, Socky Lugo, Maureen Carothers, and Emilia Warlinski-Tokiwa. Last but not least, I would like to thank all of my graduate student colleagues, especially those that have provided me instrumentation assistance and for helpful scientific discussions.

These acknowledgements would be incomplete without thanking my previous research mentors from my late high school and undergraduate years. I am very grateful to Kirk Brown, my high school IB Biology I/II and Biotechnology I/II teacher, who instilled in me a love for the natural sciences. Kirk trained me in molecular biology techniques and gave me access to scientific resources beyond that of a typical high school biology course. He encouraged me to do research for the first time, helping me get into the Young Scholars Program at UC Davis where I studied plant defense mechanisms with Dr. Andy McCall, then-graduate student who is now a professor at Denison University. This field-based research experiment led me to pursue several projects with fieldwork components, including the summer that I spent in the South Dakota Badlands chasing prairie dogs on a project led by Dr. Dean Biggins for the U.S. Geological Survey. Despite having

little experience working with small animals outdoors, Dean took a chance on me—I still remember how hard those first few days were, waking up at 4 am every morning to set out hundreds of prairie dog traps (manual labor?!). I also remember how astoundingly beautiful the Badlands are, camping for the first time (and many times thereafter), hiking 15 miles a day in completely inappropriate shoes, and watching Fourth of July fireworks at Mount Rushmore (only to realize that the fireworks were actually better in our small town of Interior). I am so grateful to my amazing team (Amanda, Mario, Casey, Pam, Lauren, Samantha, David, Erica, Sara) for taking pity on my non-existent animal handling and general outdoor survival skills. I especially thank Amanda and Casey for helping me discover the great outdoors and introducing me to camping and hiking as lifelong hobbies. Leaving NYC for the weekend to spend time outdoors is the best thing that I can do for myself in times of stress, and I am so thankful to be able to share this activity with loved ones.

Additionally, in college I expanded my research exposure to include areas such as viral bioinformatics and epidemiology, natural resource conservation, craniofacial diseases, industrial analytical processes, and the molecular biology of acute lung injury and sepsis. I learned so many new things from each experience and from all of my mentors, and would like to thank Dr. Frederick Leung from the University of Hong Kong, Drs. George Su and Dean Sheppard from UC San Francisco, Ed Hoff from Genentech, and Dr. Maria Tolarova from the University of Pacific School of Dentistry. I am especially grateful to George for his constant encouragement and for his personal and professional guidance then, which continues even now as I make decisions about my career and future life. I would also like to thank Ed for all the times we played hooky to go sailing.

Finally, and most importantly, I would like to thank my family and friends for all their love and support. My parents have sacrificed so much so that my sisters and I could have a better life,

and there are no words that fully capture my gratitude to them. That being said, thank you especially, Mom and Dad, for giving me sisters and for accepting that I will never go to medical school. Thank you, Jessie and Joanna, for being the best younger sisters that I could boss around growing up. I am so proud of the young women that you have both grown up to be. Graduate school and thesis writing could not have happened without my wonderful fiancé Steven. I am so lucky that you fell in love with me and I look forward to spending the rest of our lives together with Martin by our side.

One more thing: research cannot exist without funding. The research discussed in this thesis is supported by grants from the National Science Foundation and the National Institutes of Health. Stipend support comes from the Chemistry department, the NSF Graduate Research Fellowship Program, and the GSAS Lead Teaching Fellows Program. I have had the privilege of being part of the LTF inaugural class, and the program has been a great resource for me to see different approaches to teaching across departments.

Jieling Zhu

Columbia University

September 2015

1 Introduction

Extracellular matrix (ECM) plays an important role in regulating many cellular processes by maintaining the proper biochemical and biophysical conditions for cells to develop and function. Research in the past several decades has found that cellular microenvironments provide many of the biochemical, biophysical, and mechanical cues underlying both desired and undesired biological functions, and the need to better understand the interplay between ECM components has driven much of the research on collagen. As a prevalent component in ECM, collagen provides structural support and has domains that bind other ECM molecules and macromolecules.

1.1 Collagen

Collagen is the most abundant protein in the human body, comprising one-third of total protein content, and is produced by many different types of cells to maintain local and overall structural integrity of the body. Collagen molecules are composed of three polypeptide α chains, characterized by their repetitive X-Y-Gly sequence. More than 28 distinct types of collagen have been discovered to participate in a broad variety of functions, including tissue scaffolding, cell adhesion and migration, angiogenesis, and wound healing (1, 2). Approximately 80-90% of collagen in the body consist of types I, II, and III, which form long thin fibers that are arranged differently in different tissues (3). Other types of collagens, like type IV, form two-dimensional sheets or, like type VI, are associated with fibrillar collagens to link them to other extracellular matrix components (1, 2). While fibroblasts are responsible for the majority of collagen in the body, epithelial cells also produce a significant amount of collagen in basement membranes (4-8).

1.1.1 Type I collagen

Collagen I is the most prevalent form of collagen and is fibrillar, providing connective structure and support for tendons, skin, ligaments, cornea, dentin, blood vessels, and other non-cartilaginous tissues. Collagen I can be associated with several other collagens in the body, most commonly type III and type V (9-11). It is a versatile material, organizing itself differently in tissues with different mechanical requirements. Much of what is known about collagen is from studies of type I collagen because it is easily isolated from animals in large quantities.

An example of type I collagen's unique function is in tendons and ligaments, which have unique structural and mechanical properties that arise from their high collagen I content (65-80% of its dry mass) (12-14). Tendons are organized in bundles of parallel fibers that facilitate the effective transmission and absorption of tensile forces and also provide the structural and biochemical support for tendon fibroblasts to thrive (15). The tensile strength of collagen in tendons is 100-140 MPa and its stiffness is 1.0-1.5 GPa (9), which makes tendons very strong and stiff for transmission of muscle forces. Tendons and ligaments exhibit non-linear elastic properties, like greater compliance at low stresses than at high stress, which reduces the chances of injury (9, 16).

1.1.1.1 Collagen I-related diseases

There are many pathologies associated with mutations in collagen genes that code for the α polypeptide chains that make up collagen molecules. About 85% of the more than 1000 known mutations occur in only 5 genes: *COL1A1*, *COL1A2*, *COL3A1*, *COL4A5* and *COL7A1* (17). Gene names are designated by collagen type and alpha chain; for example, *COL1A1* is the gene that codes for the α1 chain of type I collagen. Patients with collagen diseases usually display

heterogeneous symptoms due to the variety of mutations. The majority of these mutations are single base substitutions that lead to the wrong amino acid being incorporated in place of glycine (1, 17).

Osteogenesis imperfecta (OI) is a disease characterized by brittle bones. Almost all patients with OI have mutations in *COL1A1* and *COL1A2* that cause early termination of the polypeptide chain, although patients typically have mutations in other collagens as well (17, 18). Patients who have OI vary in their symptoms and severity, but have in common bones with structural defects and compromised mechanics. The disease occurs every 1 in 20,000 live births, and there is no cure. Treatments are aimed at increasing bone strength, including the intake of bisphosphonates (to increase bone mass, reduce bone pain and fracture), surgery, physiotherapy, and the use of physical aids (19).

Ehlers-Danlos syndrome is a group of heterogeneous disorders characterized by joint hypermobility, skin hyperextensibility, thinness and fragility, skeletal deformities, and complications with cardiovascular and other bodily systems due to likelihood of artery and organ rupture. Patients have mutations in several genes causing defects in type I, III, and V collagen; additionally, some variants of the disease are caused by mutations that inactivate important enzymes that cleave or crosslink collagens (17). The disease is relatively common, seen in 1 in 10,000 to 1 in 20,000 births worldwide. Palliative treatment includes medications for pain or to control blood pressure (blood vessels are more fragile), physical therapy, and surgery to repair joints damaged by repeated dislocations (20, 21).

1.1.2 Other collagens

Collagens are typically classified based on their structural homology and suprastructural assembly. In addition to classical fibrillar collagens, there are also network-forming collagens (including long chain, short chain, and basement membrane types), filamentous collagens, fibril-associated collagens with interrupted triple helices (FACITs), membrane-associated collagens with interrupted triple helices (MACITs), multiple triple-helix domains and interruptions (multiplexins). FACITs are usually bound to type I (XII, XVI, XIX, XXI) and type II (IX, XVI, XIX) collagen fibrils. Type IV is typically found in basement membranes and is a network structure comprised of collagen, laminins, and other proteins. MACITs have transmembrane domains that are recognized by signaling molecules. Multiplexins are domains with interruptions containing chondroitin sulfate and heparin sulfate glycosaminoglycans.

Table 1.1 summarizes the different types of collagen seen in vertebrates. There is a large body of research focused on all the different types of collagens. The following work focuses on type I collagen specifically as it is the most prevalent type of collagen in the body and can be purchased commercially from several sources.

Table 1.1: Vertebrate collagens

Table adapted from References (1) and (15)

Class	Type	Genes	Distribution	Pathology
Fibrillar	I	*COL1A1* and *COL1A2*	Widespread: dermis, bone, tendon, ligament	Osteogenesis imperfecta, Ehlers-Danlos, osteoporosis
	II	*COL2A1*	Cartilage, vitreous	Osteoarthrosis, chondrodysplasias
	III	*COL3A1*	Skin, blood vessels, intestine	Ehlers-Danlos, arterial aneurysms
	V	*COL5A1*, *COL5A2*, and *COL5A3*	Widespread: bone, dermis, cornea, placenta	Ehlers-Danlos
	XI	*COL11A1*, *COL11A2*, and *COL11A3*	Cartilage, intervertebral disc	Chondrodysplasia, osteoarthrosis
	XXIV	*COL24A1*	Bone, cornea	
	XXVII	*COL27A1*	Cartilage	
Network	IV	*COL4A1*, *COL4A2*, *COL4A3*, *COL4A4*, *COL4A5*, and *COL4A6*	Basement membranes	Alport syndrome
Long chain	VII	*COL7A13*	Dermis, bladder	Epidermolysis bullosa acquisita
Short chain	VIII	*COL8A1*	Widespread: dermis, brain, heart, kidney	Fuchs endothelia corneal dystrophy
	X	*COL10A1*	Cartilage	Chondrodysplasia
Filamentous	VI	*COL6A1*, *COL6A2*, *COL6A3*, *COL6A5*, and *COL6A6*	Widespread: bone, cartilage, cornea, dermis	Bethlem myopathy
FACIT	IX	*COL9A1*, *COL9A2*, and *COL9A3*	Cartilage, cornea, vitreous	Osteoarthrosis, multiple epiphyseal dysplasia
	XII	*COL12A1*	Dermis, tendon	
	XIV	*COL14A1*	Widespread: bone, dermis, cartilage	
	XVI	*COL16A1*	Dermis, kidney	
	XIX	*COL19A1*	Basement membrane	
	XX	*COL20A1*	Cornea (chick)	
	XXI	*COL21A1*	Stomach, kidney	
	XXII	*COL22A1*	Tissue junctions	
	XXVI	??	Testis, ovary	
Multiplexins	XV	*COL15A1*	Capillaries, testis, kidney, heart	
	XVIII	*COL18A1*	Basement membrane, liver	Knobloch syndrome
MACIT	XIII	*COL13A1*	Endothelial cells, dermis, eye, heart	
	XVII	*COL17A1*	Hemidesmosomes in epithelia	Generalized atrophic epidermolysis bullosa
	XXIII	*COL23A1*	Heart, retina	
	XXV	??	Brain, heart, testis	Amyloid formation?
Unknown	XXVIII	??	Dermis, sciatic nerve	Neurodegenerative disease?

1.2 Applications

Collagen is biocompatible, biodegradable, and exhibits weak antigenicity, making it ideal for biomedical applications (22). Collagen gels, having tunable structural and mechanical properties, are used widely to approximate extracellular environments for studying cellular behavior in normal and disease systems.

1.2.1 Wound healing and tissue repair

Collagen has been used widely in wound healing and exhibits several functions at the wound site, including attracting and guiding cell aggregation and proliferation, serving as a nucleation agent and attachment site for the formation of fibrillar structures and capillary growth, and promoting blood coagulation (23-26). As a scaffold, collagen provides a permeable, hydrophilic, and stable structure for all wound healing processes to take place and has also been found to be resistant to bacteria and help keep wounds clean (24, 27). Collagen is used frequently in reconstructive surgery, for example, on burn victims as artificial skin and burn dressing that increases healing. Tissues grafts made of collagen have been used for surgical repair, and collagen has been used as a surgical adhesive (22).

1.2.2 Dental composites

Dentistry has long used polymeric materials that confer desired properties similar to what is already present in teeth, with the right amount of resilience, abrasion resistance, low toxicity, and stability (28). The bulk of teeth under the enamel is made of dentin, a biomaterial that is primarily hydroxyapatite, water, and collagen (mostly type I). It is a softer material than enamel and more prone to decay once exposed but supports the enamel and transmission of forces within

teeth (29, 30). Collagen is an important component in manmade dental composites used for fillings—a typical dental root canal filling contains ~10-30% collagen, along with additives that strengthen and stabilize the composite (28).

1.2.3 Drug delivery

Collagen fibers have desirable properties as a drug delivery system since they can be cross-linked with various agents to control *in vivo* absorption. Some applications of collagen in drug delivery include collagen eye bandages, sponges for wounds, tablets for protein delivery, sustained drug delivery gels, and nanoparticles for gene delivery (22). The drugs can be loaded into collagen membranes by hydrogen bonding, covalent bonding, or physical entrapment, and given to patients by injection or ingestion.

1.2.4 Cell studies

Type I collagen, present abundantly in extracellular matrix, is useful for studying cell-matrix interactions in two- and three-dimensional *in vitro* environments. Cells interact with collagen in multiple ways: through integrins, cell-surface receptors that cluster and pull strongly on fibrils to gain traction and migrate, producing matrix metalloproteinases that can digest collagen, and producing their own collagen. The combination of these actions results in heavy matrix reorganization to facilitate cellular functions in normal and disease states. Our lab has produced several papers that discuss the various ways in which cancer cells interact in collagen environments that can be tuned for specific structural and mechanical properties (31-34).

An interesting occurrence of upregulation of collagen is in the extracellular matrix of patients with malignant gliomas, a type of aggressive tumor that is characterized by diffuse

infiltration into brain parenchyma and an especially poor prognosis in patients (35). The extracellular environment of a normal brain is generally very rich in proteoglycans, hyaluronic acid, and glycoaminoglycans, and also contains some collagen that surrounds vascular endothelial cells. Glioma cells tend to preferentially invade along blood vessels and white matter tracts (36, 37), which point to interesting interactions with components in the extracellular environment. Glioma cells can also synthesize types I and IV collagen (38, 39). Chapter 5 provides an example of one application of collagen I gels in the understanding of glioma invasive behavior.

Recently, there has been intense interest in the use of collagen for microfabrication and patterning cells. Because cellular functions and morphology are strongly affected by extracellular topography and composition, a developing area of research has been to deposit collagen in specific patterns and see how cells respond to localized changes in the collagen scaffold (40-45).

1.2.5 Mimetic peptides

Although collagen is readily isolated from various animal sources, its heterogeneity, potential immunogenicity, and loss of structural integrity from the isolation process can make it animal collagen difficult to work with, depending on the application (28). Synthetic collagen or collagen-like peptide chains have been successfully produced, with properties that promote self-assembly into fibrils (1, 46). Some of this work has confirmed hypotheses about requirements for triple helix formation and the importance of single amino acid substitutions in supramolecular assembly (47). The consensus seems to be that synthetic methodologies have not quite reached the level of control to create peptides with desired morphological, biochemical, or mechanical traits for many of the applications previously mentioned, but is well on its way.

1.2.6 Other applications

The same properties that make collagen an ideal material for bioengineering applications (biocompatibility, degradability, and weak antigenicity) also allow it to be used widely in the food, cosmetic, and pharmaceutical industries. Traditionally, collagen for these products was isolated from land-based animals (cows and pigs), but there have been several outbreaks of diseases like bovine spongiform encephalopathy that have made consumers and manufacturers more cautious about their collagen sources (48). Collagen is now commonly obtained from many types of fish, as it can be isolated from their scales, skin, bones, and swim bladders (49).

1.2.6.1 Food industry

Gelatin, the denatured form of collagen, is used heavily in processed foods as a gelling agent and/or emulsifier (giving the desired consistency and texture) and in the formulation of packaging films and coatings to preserve foods and extend shelf life (49). Other uses for gelatin in food include as a cryoprotective additive, which reduces ice crystal growth, useful for example in an ice cream mixture, (50), and as a carrier for aroma compounds, like essential oils, that can affect flavor release and increase antimicrobial properties (51).

1.2.6.2 Cosmetics industry

Because collagen makes up such a large percentage of the human body protein content, it has been widely exploited in the cosmetic industry. Within this realm, collagen has been used in many different ways, including taken as a supplement, injected into the skin for the treatment of wrinkles, or applied topically to give skin a more youthful appearance. Scientific validation of the health claims of ingesting or topical application of collagen is limited and controversial, but some

studies have shown beneficial results in terms of better hydrated skin and a reduction in wrinkles (52-54). Gelatin has also been studied for its potential biological benefits, such as antioxidant, antihypertensive, anticancer, and cholesterol-lowering effects (49).

1.3 Structure of collagen monomer

Members of the collagen protein superfamily have in common a right-handed triple helix formed by three left-handed coiled polypeptide α chains, which may be homo- or heterotrimeric. More than forty distinct α chains have been identified in humans, and each chain has a chain recognition sequence (CRS) that is recognized by neighboring chains during trimerization (55, 56). Collagen chains are characterized by their repetitive X-Y-Gly sequence, where X and Y are commonly proline or hydroxyproline residues. Glycine, as every third residue and having the smallest side chain, ends up in the interior axis of the helix, and creates tightly packed helices (1, 2, 9). Hydroxyproline is an unusual amino acid derivative that is the result of post-translational modifications. The polypeptide chains in a collagen monomer are stabilized mainly by hydrogen bonds (1, 57, 58). The unique properties of different collagens result from polypeptide segments that interrupt the X-Y-Gly repeats.

This triple helix structure was first correctly identified in 1951 by Pauling and Corey (58) from x-ray diffraction patterns and further refined by several groups throughout the decade. In the 1990s and 2000s, high-resolution crystal structures made from collagen-related peptides were studied to understand the structural impact of a single amino acid substitution, confirm the existence of hydrogen bonds that stabilize the triple helix, and observe the interaction of collagen with integrin α2β1 (59-61). The helical pitch from crystal structures varied according to proline

content, from 20.0 Å per axial repeat for proline-rich structures to 28.6 Å predicted for natural collagen by fiber diffraction (1).

In human collagen, 22% of all residues are either proline or hydroxyproline, which organizes the polypeptide chains in a way that decreases the entropic cost for collagen folding (62). However, proline residues can form tertiary amides within the chain so all peptide bonds must isomerize from *cis* to *trans* configuration (1). Proline is often modified by an enzyme to form hydroxyproline, where the γ-carbon is hydroxylated. Hydroxyproline increases the thermal stability of triple helices and decreases the entropic cost for folding when it is in the Y position via a stereoelectronic effect, where the electronegative substituents on the pyrrolidine ring forces a twisted pucker that preorganizes the main chain torsion angles to those of the triple helix (1). It has been proposed that the high percentage of proline and glycine residues in collagen prevent aggregation by avoiding the formation of β-sheets, which are found in amyloid fibrils and associated pathologies (1, 63-66).

Studies estimate the fracture strength of a collagen monomer to be 11 GPa, which is at least ten times that of a collagen fibril, because breaking the monomer would involve unraveling the triple helical structure (67). Measurements of the Young's modulus of the monomer range from 5-11 GPa (68), and the shear modulus was found to be G ~ 33 MPa (69). All of these values varied somewhat depending on the isolation source, hydration state, extent of crosslinking, and measurement technique. Some ideal amount of crosslinking is favorable for mechanical properties of collagen; excessive crosslinking results in extremely brittle collagen fibrils which is a symptom of aging (70).

Simulations indicate that the length of a collagen monomer is ideal for assembly into fibrils with desired mechanical properties and efficient energy dissipation, and any other length would

not produce fibrils with the right mechanical properties (71). In particular, the type I collagen monomer consists of two α1(I) and one α2(I) chains, each 1050 amino acids long, and monomers are 300 nm long and 1.5 nm in diameter, flanked by short segments called telopeptides that are non-helical and do not have the X-Y-Gly repeat.

1.4 *In vivo* synthesis

Collagen triple helices assemble hierarchically into many different secondary and tertiary structures, forming fibrils, basement membranes, and even complex network structures in skin, bone, and other tissues. In the body, the process of collagen synthesis is as follows:

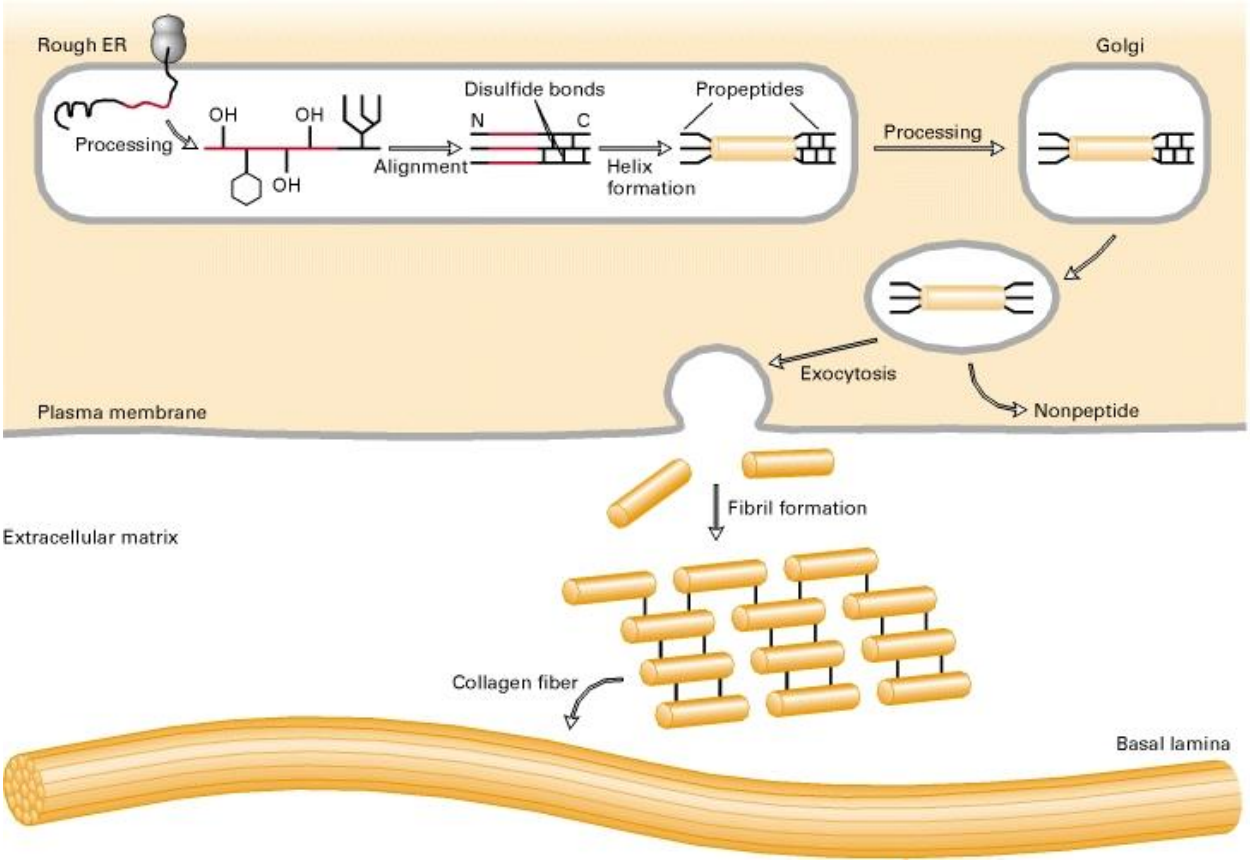

Figure 1.1: In vivo *collagen assembly*

Reprinted from (3)

Collagen mRNA transcripts are translated into polypeptide chains at ribosomes attached to the rough endoplasmic reticulum (ER). The N-terminal of the peptide is recognized and directed through the rough ER for post-translational modifications, producing procollagen. Procollagen is generally unstable in the cell and would be rapidly degraded if not for the presence of vitamin C, which is also required for hydroxylating certain amino acids (72). In addition to hydroxylation, procollagen undergoes glycosylation, and disulfide-bond formation within the rough ER. The disulfide bonds between three chains of procollagen align themselves to initiate the formation of the triple helix, with loose ends called telopeptides. Assembly into the triple helix is also aided by C-propeptide domains of procollagen that have short chain recognition sequences (CRS) that recognize the correct α chains to trimerize, mainly through favorable electrostatic interactions between side chains (55, 56). Mutations in the CRS region can cause severe disease phenotypes (56).

Once assembled, the triple helix is transported to the Golgi apparatus, where it undergoes further modification and is packaged for exocytosis and secreted out of the cell. Although it was initially thought that fibril assembly only occurred in the extracellular space once N- and C-terminal proteinases cleave off part of the non-helical region, there has been evidence showing that assembly is initiated in Golgi to plasma membrane carrier vesicles (73).

Once cleaved of propeptide domains and outside the cell, mature collagen fibrils containing helices assembled in a staggered manner are produced. Each molecule in a fibril is staggered by 67 nm, creating the striated banding pattern that is seen in electron micrographs. This staggered length is known as ‘D’, with each D-period repeat contains two parts, one with five molecules in the cross-section, called the “overlap”, and another part containing four molecules, called the “gap”. AFM has shown that a single collagen fibril has different mechanical properties in the

overlap and gap regions (74). Collagen monomers are packed in a quasi-hexagonal manner that results in a twisted right-handed coil seen in mature collagen fibrils. The presence of collagen V is proposed to be a strong regulator fibrillogenesis *in vivo* through interactions with adjacent collagen I molecules (11, 75).

Mature collagen fibrils are crosslinked by lysyl oxidase, an enzyme that acts on the lysine and hydroxylysine residues to induce covalent bonding and give strength and stability to the fibrils. Crosslinks also hold several fibrils together to form the thick fibers seen in some tissues. This process is regulated by ECM molecules including small leucine-rich repeat proteoglycans (SLRPs) like decorin and FACIT collagens that can affect fibril and fiber properties (76, 77). In the body, fibrils and fibers interact with various ECM components to carry out proper cell, tissue, and organ functions, and individual cells can interact with different types of collagen fibers via cell-surface receptors called integrins.

1.5 *In vitro* fibrillogenesis

Collagen self-assembly is an entropy-driven process, similar to that of microtubules and actin filaments—as collagen monomers aggregate to form fibrils, solvent molecules are freed from the surface of protein molecules creating an entropic gain (78). While the previous section described the biological synthesis of fibrillar collagen *in vivo*, the majority of studies attempting to better understand the fibrillogenesis process have occurred with *in vitro* collagen purified from animal tissues, which allows for control over specific factors and measurements of fibril properties and assembly kinetics. Generally, fibrils are 50 – 200 nm in diameter, and *in vitro* fibrillogenesis does not lead to thicker fibers without the use of additional crosslinking agents. Fibrillogenesis is affected by many factors such as concentration, temperature, pH, ionic strength, and the

introduction of cross-linkers and secondary gel components, which result in collagen gels with tunable structural and mechanical properties. The specific effect of each factor will not be discussed in detail in this thesis, other than what is relevant to the studies in Chapters 3 and 4.

Collagen monomers can be purchased with or without its telopeptides, depending on the isolation procedure. Acid-solubilization maintains the telopeptides while treating the collagen with pepsin removes them; the experiments in this thesis use collagen from rat tail tendon and bovine hides, which are, respectively, acid-solubilized (AS) and pepsin-treated (PT) from the specific manufacturers chosen. The N- and C- terminal telopeptides appear to have different functions; loss of either N- or C-telopeptides are linked to loss of diameter uniformity, loss of unidirectional packing, and formation of non-banded fibrous aggregates to various degrees (79-81). However, triple helices lacking telopeptides can still undergo fibrillogenesis and produce fibrils (15). The PT collagen purchased from Nutragen for studies in Chapter 5 forms fibrils that are much thicker than that of AS collagen and no bundling is seen, even at lower gelation temperatures. Broadly, PT collagen from this source is much less susceptible to changes in fibril structure and gel properties.

Initial studies from more than half a century ago used turbidity to monitor the type I collagen self-assembly process and showed that fibrillogenesis follows a nucleation-and-growth pattern, where monomers assemble with little change in turbidity in the lag phase followed by a period of exponential growth and eventual plateau as the gel reaches an equilibrium state (82). Turbidity is an observable that depends on the fibrils' ability to scatter light, so classic light scattering theory has been used to derive important gel properties such as equilibrium diameter and mass to length ratio (83-85). According to this theory, and also supported by more recent literature (86), events during the initial lag phase are critical to how the structural and mechanical properties develop and how the gel behaves at equilibrium (31). In both *in vivo* and *in vitro* studies,

models suggest that the fibrillogenesis process is nucleated and modulated by collagen V, usually present as less than 5% of collagen content in tissues, which interacts with adjacent collagen molecules and limits lateral growth (11, 87). While turbidity continues to be a popular method by which to monitor gelation, its main disadvantage is that there is no direct corresponding image of gel network structure, especially at non-equilibrium times where assumptions in applying light scattering theory are no longer valid (86, 88).

Another technique that has been used to study collagen structure and gelation kinetics is dynamic (quasi-elastic) light scattering (DLS). DLS is a sensitive technique typically used for measuring the size of particles dispersed in liquid, which scatters light that fluctuates in intensity as particles diffuse due to Brownian motion. The correlation and autocorrelation in intensity fluctuation can give many characteristics of the particles in solutions, such as its size, translation and rotational diffusion coefficients, and degree of dispersity. Historically, most of these measurements have been done on different types of collagen freshly isolated from animal parts, so these numbers vary tremendously across the literature (89). Although using DLS to monitor the motion of non-spherical particles is complex, the technique has been successfully used on collagen monomers or small aggregates kept in acidic solution to prevent full gelation as well as collagen molecules during fibrillogenesis (90, 91). More specialized types of light scattering techniques, like small-angle light scattering, have also been used to provide quantitative information about enzymatic degradation and its effects on fibril mechanical properties (92).

Light scattering studies are usually coupled with some microscopy (most often SEM or TEM) to observe what fibrils look like at certain time points. Bard and Chapman (1973) took electron micrographs of fibrils at various points along their turbidimetric gelation curve, made measurements of fibril diameters, and found that the number of fibrils holds constant when about

20% of collagen molecules had assembled into fibrils (93). This result showed that the gel network structure is set relatively early during gelation, and suggests that the remainder of gelation consists of remaining monomers contributing to the thickness of fibrils rather than the creation of new fibrils. Although a few groups have shown the presence of fibril intermediates and evidence for a multi-step fibrillogenesis mechanism (94), most publications support the nucleation-and-growth process for collagen fibrillogenesis.

In more recent literature, the collagen I self-assembly process continues to be monitored with turbidity or DLS but also has been studied using imaging techniques and rheology. Non-invasive imaging methods such as confocal reflectance or fluorescence microscopy provide a direct image narrative for how gel structure develops. Fluorescence microscopy seems to provide better imaging of early aggregates, but has been limited by the fast bleaching of the fluorophores and the potential for the disruption of normal collagen fibrillogenesis. On the other hand, confocal reflectance microscopy is simple to perform on unlabeled collagen and does not require the use of high power lasers like with two-photon fluorescence or second harmonic generation microscopy, but is limited by poor resolution of early aggregates immediately after gelation has been initiated (86). Atomic force microscopy has also been used to determine the elastic properties of collagen I fibrils, but AFM scans are time consuming and are not capable of producing an accurate depiction of quick gelation processes (74).

Additionally, rheology has been used in collagen literature primarily to assess the mechanical properties of equilibrium gels, with few studies focused on the properties of the gel during the self-assembly process (95-97). In oscillatory rheology, a (usually small, non-perturbative) deformation is created in the material to form a measurable time-dependent viscoelastic response reported frequently as storage (G') and loss (G'') moduli. Typical rheological

tests include frequency and strain sweeps of equilibrium gels, with a particular focus on the underlying mechanisms involved in the complex biological phenomenon of strain stiffening (98-101). Microrheology, an emergent method for measuring local heterogeneity tracking the thermal fluctuations of fluorescent molecules, has been employed but only provides indirect clues about the assembly process (102-105). These tests have not been fully explored for a gel as it is undergoing the self-assembly process. Previous research has also attempted to characterize collagen gelation with traditional sol-gel transition theories with varying degrees of success (106, 107). This approach is difficult because biopolymer gelation is much more complicated than simple polymer chains engaging in chemical or physical gelation. Furthermore, only a few studies have ever characterized collagen gelation with both imaging and rheological studies (95, 104, 106-108). The ability to perform simultaneous measurements would enhance fundamental biopolymer studies by allowing for the visualization of a developing network while also monitoring the gel mechanical development; a direct correlation of the observables from these two methodologies would avoid encountering issues like non-uniform sample size and gelation conditions that may be present these methodologies are employed alone.

1.6 Motivation

The Kaufman lab studies the structural and mechanical properties of biopolymer gels towards designing gels with particular properties for studying the invasive behavior of cancer cells. This thesis is motivated by the goal of enhancing our fundamental understanding of mechanisms driving gelation and to develop methodologies for better design and characterization of collagen gels. Multiple modalities, including turbidity, confocal reflectance, confocal fluorescence, and rheology, are employed to understand the coupling of such gel properties.

2 Materials and methods

2.1 Preparation of collagen gels used in self-assembly studies

High concentration acid-solubilized rat tail collagen I (8–10 mg/ml) was obtained from BD Biosciences (later acquired by Corning). Collagen gels of various concentrations were prepared by diluting the stock collagen solution with 10% Dulbecco's modified Eagle's medium (DMEM, Sigma) 10X, 2.5% HEPES, and distilled H_2O. For fixed wavelength studies, DMEM 10X contained phenol red, and for wavelength-dependent studies (see Chapter 3), phenol red free DMEM (Life Technologies, Carlsbad, CA) 10X was employed. For gels that contain acid-solubilized fluorescein isothiocyanate (FITC)-labeled collagen I (bovine skin, Sigma, ≈ 1 mg/ml, see Chapter 3.2.2), a 10:1 by weight mixture of unlabeled to labeled collagen was employed. In all cases, 1N NaOH was added to each solution to achieve a pH of 7.4. Final ionic strength of all gel solutions was $I \approx 0.15$. All solutions were prepared on ice or in a cold room at 4°C and neutralized immediately before measurements.

2.2 Standard turbidity assay

Turbidity of 1.0 mg/ml collagen gels forming at 27°C and 37°C was monitored at 400, 458, 488, 515, 543, and 633 nm using a dual-beam Cary 5000 spectrophotometer. In this measurement, absorbance (A) was reported, where $A = -\log(I/I_0) = \alpha l$ with I the intensity of transmitted light, I_0 the intensity of transmitted light in the reference solution (the solution without collagen), α the absorption coefficient (cm^{-1}), and l the pathlength in cm. Changes to A over time during gel formation represent an increase in scattering. Turbidity was then calculated via $\tau = A/l$ ln

10 (88, 109). Temperature control was maintained with a water circulator and heated sample holder. Both the sample and reference were held in 1 cm quartz cuvettes. Measurements were taken every 10 s for up to 30 min and averaged across two to three samples per wavelength.

2.3 Microscopy

Different microscopy set-ups were utilized for the different chapters discussed in the text.

2.3.1 Simultaneous IST, CRM, and CFM (Chapter 3)

A schematic diagram of the multimodal microscope set-up employed for imaging collagen gelation in Chapter 3 is shown in Figure 2.1. Samples were illuminated on an inverted confocal laser scanning microscope (Olympus Fluoview 300) with an NA = 1.42 oil objective. Except where specified, a 488 nm Argon ion laser was used to illuminate samples on a microscope stage equipped with an incubator system (Neue Biosciences). The objective was modified with a heating ring and both the incubator and objective heater were pre-warmed and maintained at 27°C, 32°C, or 37°C during collagen gelation. The same excitation power was used for all measurements and the same detector settings were employed. In tri-modal videos, fluorescence and reflected light were collected through a confocal pinhole on two photomultiplier tube (PMT) detectors while light that passed through the sample was collected through a condenser in the forward direction on a third PMT detector. For bi-modal videos where only reflectance and transmittance images were collected, the set-up was identical but PMT 1 in Figure 2.1 was not employed. These transmittance images were collapsed to provide turbidity curves as described below.

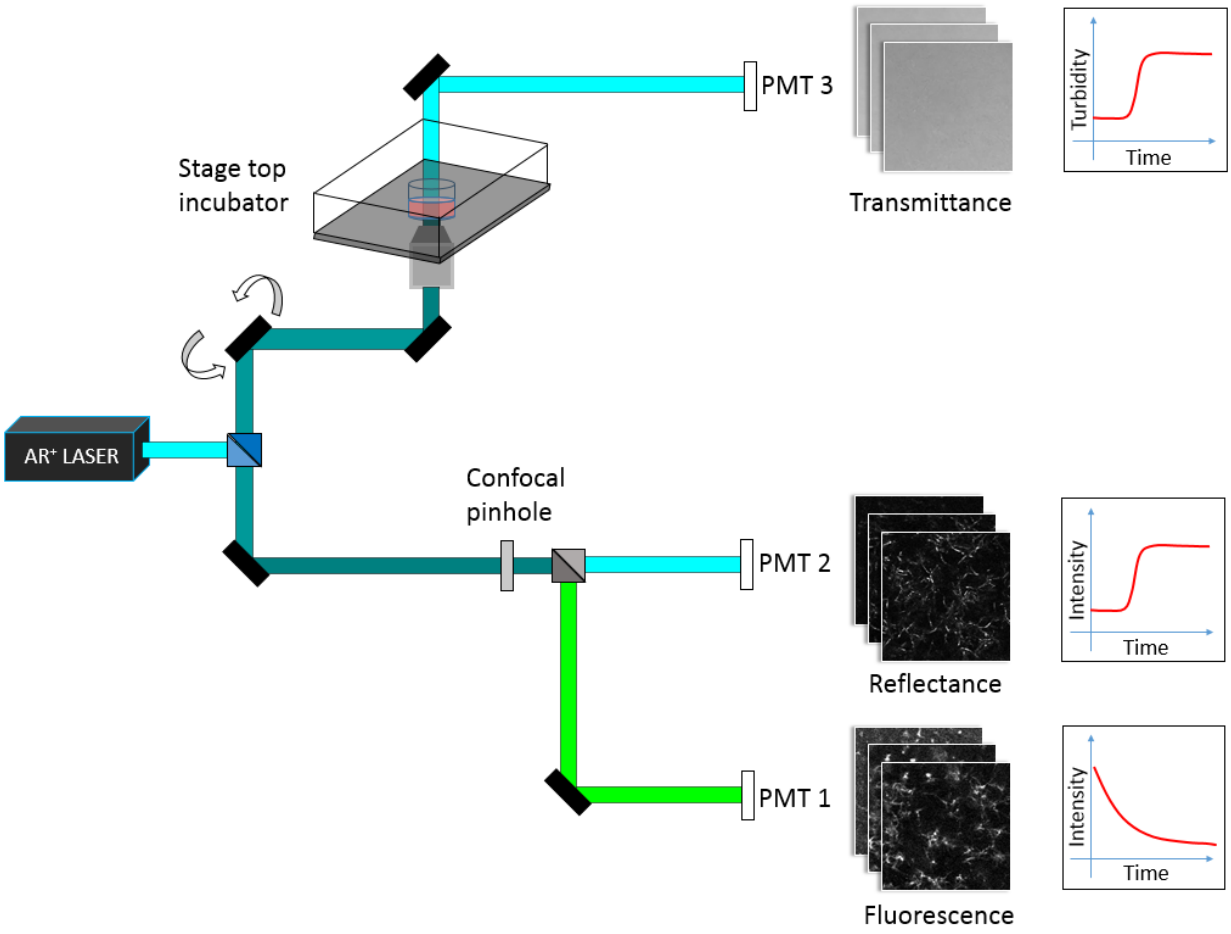

Figure 2.1: Multi-modal microscopy set-up for simultaneous IST, CRM, and CFM

For wavelength-dependent scans, measurements were performed on additional samples of 1.0 mg/ml collagen formed at 37°C using the 488 nm line of the Argon ion laser as well as two HeNe lasers at 543 nm and 633 nm. In these measurements, laser power at the sample was kept constant. Detector settings were optimized for visualization of confocal reflectance in the lowest intensity scans and were kept constant across all wavelength-dependent measurements. CRM images were corrected for the wavelength-dependent transmission of the optics in the detection path.

Collagen samples were prepared as described and upon neutralization were placed in the microscope incubator preset to and equilibrated at 27°C, 32°C, or 37°C. Imaging began as soon as neutralization of the gel was complete, the sample was placed on the stage, and the desired imaging plane—≈ 50 μm into the sample—was found. The time between neutralization and the beginning of imaging varied between samples, from 1 to 2 min. Time zero was considered the time at which neutralization of the gel was performed. Scans were collected at 3.26 s per scan, and the time interval between imaged scans was 10 s. In all cases, scans were 1024 × 1024 pixels (235 × 235 μm), and 12 bit images were collected. Two to four samples of unlabeled 0.5 mg/ml, 1.0 mg/ml, and 2.0 mg/ml collagen gelling at 27°C, 32°C, and 37°C were imaged and analyzed for combined IST/CRM studies illuminated with the Argon ion 488 nm laser. Additional samples were prepared for both wavelength-dependent scans described previously and for tri-modal imaging in which CFM was also performed. A representative movie showing tri-modal time-lapse images of a 1.0 mg/ml FITC-labeled collagen gel forming at 32°C is presented in Video S1 (110).

2.3.2 Simultaneous rheology and CRM (Chapter 4)

A schematic diagram of the rheomicroscope is shown in Figure 2.2. Experiments were conducted on a modified modular Anton Paar MCR 302 instrument outfitted with an open bottom configuration that allowed for the placement of a 60X water immersion objective. The rheometer is outfitted with a solvent trap system to minimize sample evaporation as well as double-sided Peltier temperature control (heating from both the bottom of the rheometer stage and inner hood of solvent trap) to ensure a gradient-free sample temperature. A 1º polycarbonate cone geometry (diameter 25 mm, 100 μm truncation) was used to conduct experiments in shear oscillatory mode. Glass cover slips were custom made (UQG Optics) to fit the round bottom of the rheometer stage.

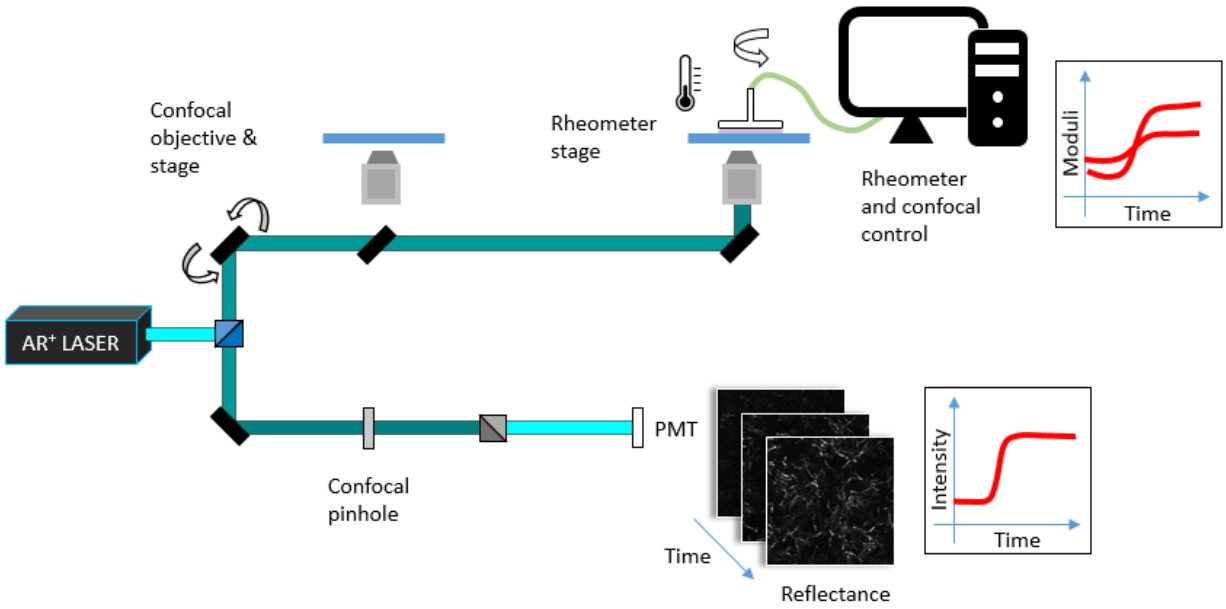

Figure 2.2: Rheomicroscope set-up

Samples were illuminated using an Argon ion 488 nm laser redirected out the back of an inverted confocal laser scanning microscope (Olympus Fluoview 300) through a custom multiple lens/mirror system to ensure the same magnification as if imaging on the confocal stage. The objective, modified with a homebuilt heater, was placed slightly off-center (gap size of field of view is ~ 140 μm) to avoid imaging directly at the truncation point of the cone. Light reflected from sample components was collected through a confocal pinhole on a PMT detector. The same laser excitation power was used for all measurements, but detector settings were changed to optimize the dynamic range and signal-to-noise ratio depending on manually-controlled z-position depth of objective.

Gel were prepared as described earlier and placed on the rheometer stage with settings as described in the Rheology methods section. Scans were collected at 3.26 s per scan, and the time interval between imaged scans was 5 s. In all cases, scans were 1024 x 1024 pixels (235 x 235

μm), and 12 bit images were collected. Collection of CRM images proceeded for different times depending on the gelation temperature and concentration.

2.3.3 Cell studies (Chapter 5)

All imaging for cell studies was performed on the Olympus Fluoview 300 laser scanning confocal microscope. The transmittance mode was utilized most frequently to image cells using a 10X air objective, and cells in collagen gels were imaged using the 60X water objective. The stage incubation chamber and objective heater were also used during imaging to keep cells at 37°C with 5% carbon dioxide. Further detail for imaging in cell experiments is described within the procedures for each assay.

2.4 Image analysis

2.4.1 Confocal reflectance images

Because CRM images had an artifact due to reflection from optical elements in the microscope, the central portion of each image was replaced by a copy of the upper left corner of the image before further analysis. From these center-replaced CRM images, total intensity and mesh size were obtained. Total intensity was obtained by summing all individual pixel values. Total intensity of the first image collected (when no features can be imaged and very little scattering is expected) was subtracted from all subsequent images to account for background. In Chapter 3, CRM total intensity was reported as the sum value, while in Chapter 4, it was normalized for each sample to account for different detector settings. All graphs showing CRM total intensity evolution over time were linearly scaled in both x and y-axes.

2.4.2 Confocal fluorescence images

Although CFM images are discussed qualitatively in Chapter 3, further analyses with total intensity curves of these images were discarded because they were dominated by photobleaching. Although attempts were made to distinguish between intensity loss due to photobleaching and intensity loss due to aggregation as collagen molecules assembled into fibrils, this proved to be a difficult task but may be addressed in future studies.

2.4.3 Scanning transmittance images

From scanning transmittance images, total intensity was calculated by summing the intensity at every pixel of unprocessed images. That total intensity, I, was then transformed for comparison with traditional turbidity measurements via $A = -\log(I/I_0)$, with I_0 the intensity of the first image collected. As in the standard turbidity measurement, turbidity was then calculated via $\tau = A/l \ln 10$. We refer to turbidity obtained in this manner as IST.

2.4.4 Mesh size determination

Determination of mesh size required thresholding. Several ways of thresholding were tested for optimal removal of extraneous pixels. Iterative thresholds were set using CRM images from gels that had developed much of their ultimate structure, at a time denoted the plateau time, t_{PL} (Chapter 3) or $t_{Pl,CRM}$ (Chapter 4), described below. The threshold determined from a gel image at this image was then applied to all images in that time series to distinguish between fibers and background pixels. Following threshold determination, mesh size was determined as described previously (34). Briefly, mesh size was calculated by fitting a distribution of the distance between

fibers across each row and down each column per image to the equation $y = Ae^{-\beta x}$, and 1/β was extracted as the characteristic mesh size, ξ_{char}.

2.4.5 Identification of key time points from CRM and IST

IST and the CRM variables of total intensity and mesh size were plotted against time. Key time points in the gelation process were identified from both IST and CRM intensity curves. In Chapter 3, these time points of interest were lag time (t_{LAG}), inflection point (t_{INF}), and plateau time (t_{PL}), while in Chapter 4, these were lag time ($t_{LAG,CRM}$), inflection point ($t_{INF,CRM}$), and plateau time ($t_{PL,CRM}$), identified in the same way but has an additional subscript to differentiate these values from those identified in rheological curves. Two additional time points, arrest time (t_{ARR}) and the time at which the mesh size is no longer evolving (t_{MS}), were identified from CRM images. In Chapter 3, the rates of increase of IST and CRM intensity during the growth phase (k_G) were also obtained. The manner in which these values were determined is described below and depicted in Figure 2.3 for a representative 2.0 mg/ml sample gelled at 37°C.

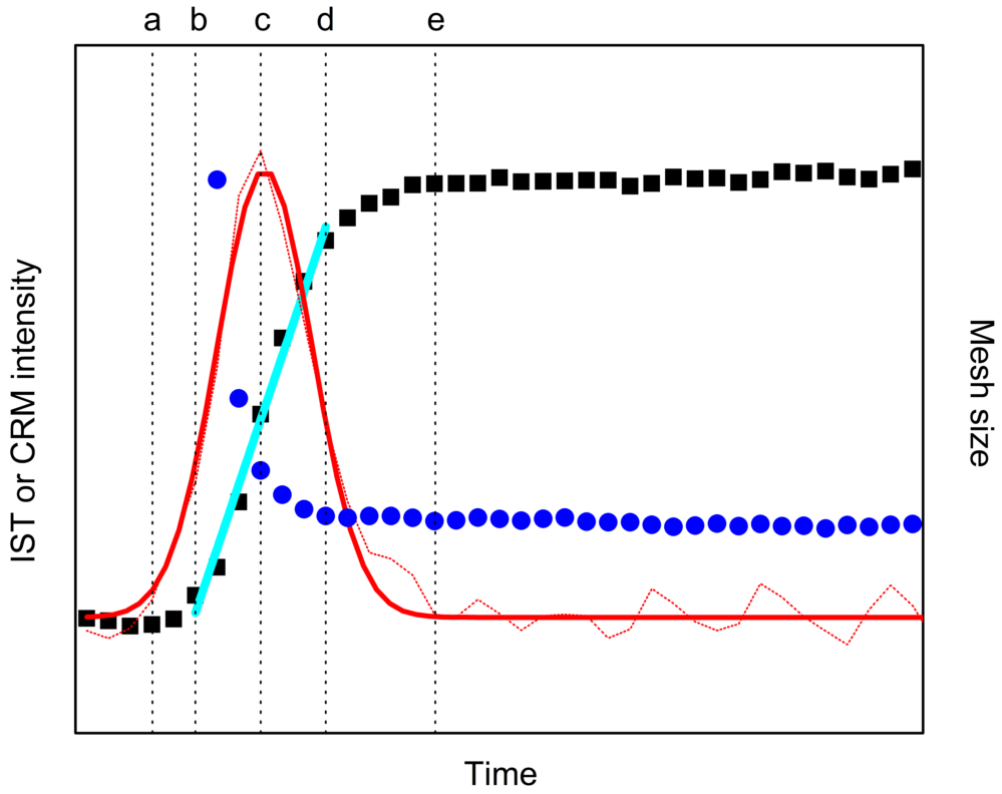

Figure 2.3: Determination of time points of interest

Representative IST curve obtained from a 2.0 mg/ml sample gelled at 37ºC (black squares). The first derivative (red dashed line) and Gaussian fit to the first derivative (red solid line) are shown. Mesh size (blue circles) evolution is also shown. Relevant variables discussed in the text are **A** t_{LAG}, **B** t_{ARR}, **C** t_{INF}, **D** t_{MS}, and **E** t_{PL} (indicated by dotted lines from left to right) and slope of growth curve, k_G (cyan line).

The inflection time, t_{INF}, was defined as the time at which half the CRM intensity or IST had developed. Due to noise in the data at the end of the measurement, particularly in IST curves, this point was chosen as the maximum of the fit of the first derivative curve. t_{LAG} was chosen as the point at which the fit to the first derivative curve had increased 5–10% over its initial value: this point also corresponded to the time at which the CRM intensity or IST curve started increasing abruptly from a near zero value. The plateau time, t_{PL}, was determined as the time at which the fit

to the first derivative curve had attained 95% of its value at the conclusion of the measurement. To identify the rate of increase of the CRM intensity or IST, k_G, a linear portion of the data between t_{LAG} and t_{PL} was fit to a line using least squares fitting.

Arrest time, t_{ARR}, and the time at which the mesh size was set, t_{MS}, could only be identified from CRM images rather than from both CRM and IST. t_{ARR} was defined as the time at which visualized fibrils were fixed relative to each other. In Chapter 3, for time-lapse images taken at the lower temperatures, some fibrils became fixed relative to each other before the gel structure was fixed in the field of view. In these cases, t_{ARR} was set as the time at which not only structures were set relative to others in the frame but also those same structures were seen through the remainder of the movie, as this approximated the time at which a network spanning structure was in place. In Chapter 4, t_{ARR} occurred as soon as any fibrils were seen. Although t_{ARR} was identified through visualization of the time-lapse images, it was validated through cross-correlation analysis. Correlation coefficients between subsequent images were computed via $r = \sum_m \sum_n (A_{mn} - \overline{A})\ (B_{mn} - \overline{B}) / ((\sum_m \sum_n (A_{mn} - \overline{A})^2)(\sum_m \sum_n (B_{mn} - \overline{B})^2))^{0.5}$ with $A(B)_{mn}$ the pixel intensity value of the first (second) image in the mth row and nth column and $\overline{A}(\overline{B})$ the mean pixel value of the images. The correlation coefficient was near zero and increased steeply over several frames to a plateau. The arrest time determined visually was in close accord (within 10%) with the time at which the cross-correlation coefficient began increasing. Mesh size set time, t_{MS}, was chosen as the point at which mesh size was 110% of its value at the conclusion of the experiment.

2.5 Rheology

Preliminary strain sweep tests at a fixed frequency were performed to determine the strain amplitude range of the linear viscoelastic regime. For all remaining measurements, the controlled variable was set to be strain, with stress varying to achieve a strain amplitude of 1% for all experiments. Then, keeping strain constant, frequency sweeps (not shown) were used to determine frequencies of equilibrium gels that minimized moduli differences. Angular frequencies 5, 10, and 15 rad/s were chosen for rheological time sweeps because these resulted in same moduli of equilibrium gels but subtly different moduli during gel formation. Rheological time sweeps were purposely performed at 24ºC and 32ºC to investigate the effects of collagen bundling at lower temperatures and non-bundling at higher temperatures while ensuring that gelation at high temperatures would be slow enough to capture early time points. In order to ensure minimum temperature variation, the Peltier temperature system and objective heater were equilibrated for an hour before start of measurements.

2.0 and 3.0 mg/ml gels of AS collagen were prepared as described earlier, and 600 µl samples were added to the rheometer stage as quickly as possible after neutralization to monitor in situ gelation dynamics with storage and loss moduli measurements taken every 15-30 s (actual timing of measurement did not affect reported moduli values). While lowering the tool, confocal reflectance microscopy was initiated manually; rheology runs were then initiated after tool was completely lowered onto the sample (sample did not require trimming), and solvent trap hood was lowered. Exact timing of all steps during the set-up process was accounted for in data analyses; approximately 1.5 min lapsed between neutralization of the collagen solution and starting rheological runs. Time 0 describes the start of rheological measurements. Collection of rheology data lasted for different times depending on the gelation temperature and concentration.

2.5.1 Identification of key time points from rheology

Plateau time for rheological curve, $t_{PL,R}$, was determined in the same way as $t_{PL,CRM}$. All graphs showing storage and loss moduli evolution over time were logarithmically scaled in the y axis and linearly scaled in the x axis, in keeping with traditional rheology measurements that obey power-law scaling behavior and span several orders of magnitude (111).

Multiple ways of determining the gel point were utilized: a) obtaining the crossover time between G' and G'', t_C, calculated using Anton Paar proprietary software RheoPlus interpolation methodology (using x = time and y = moduli, both on log scale, as inputs, it approximates where the exact time and modulus at crossover despite only obtaining moduli measurements every 15 – 30 s), and b) calculating the frequency-independent crossover time often used in describing critical gels, t_G, defined by eye as the time at which the tan δ curves across different frequencies merged (106, 112, 113). The latter method predicts that storage and loss moduli at a specific frequency will scale as follows:

$$G'(\omega) \alpha G''(\omega) \alpha \omega^{\Delta} \qquad \textit{(Equation 1)}$$

The loss tangent at gel point, which is independent of the frequency of the dynamic experiment, is defined as:

$$\text{Tan } \delta = G'' / G' \qquad \textit{(Equation 2)}$$

At gel point, the critical loss angle δ_c is related to the exponent Δ by

$$\delta_c = (\pi / 2)\,\Delta \qquad \textit{(Equation 3)}$$

An analytical method was developed to verify t_G identified above. The curves for tan δ for each gelation condition were averaged using spline interpolation. The frequency-independent gelation time was set equal to the time at which the ratio of the standard deviation of the averaged curve to the average value was equal to 0.20.

2.6 Calculating fibril diameter

2.6.1 Standard turbidity or IST

Quantitative information on fiber dimensions may be accessed through wavelength dependent turbidity measurements (83, 109), using the following relationship:

$$\tau\lambda^5 = A\mu(\lambda^2 - Br^2) \qquad \textit{(Equation 4)}$$

where A and B are defined as follows:

$$A = \frac{88}{15}\frac{\pi^3 cn(\frac{dn}{dc})^2}{N_A}$$

$$B = \frac{92}{77}\pi^2 n^2$$

In the above, τ is turbidity, λ wavelength of light, μ mass per unit length, c mass concentration of collagen, n the refractive index of the solvent, dn/dc the refractive index increment, N_A Avogadro's number, and r the fibril radius (114). For collagen in water, n = 1.33 and dn/dc = 0.186 g/cm^3 (115). From Equation 4, plotting $\tau\lambda^5$ vs. λ^2 yields a slope of $A\mu$ and a y-intercept of $-A\mu Br^2$.

2.6.2 Moduli and mesh size

Simultaneous rheology and microscopy provides the unique opportunity to apply semiflexible polymer theories to calculate fibril diameter from two parameters G' and ξ, using the established relationship from the MacKintosh model (116)

$$G' \sim \xi^{-22/5} d^{28/5} \qquad \textit{(Equation 5)}$$

In a previous publication where gelation was examined separately with microscopy and rheology, graphing $\log(G')$ against $\log(\xi^{-22/5} d^{28/5})$ across several temperatures provided proportionality constants that were utilized here to calculate fibril diameter.

2.7 Cell culture

Immortalized C6 glioma cells were purchased from ATCC. Cells were cultured at 37°C with 5% carbon dioxide in high glucose DMEM (Life Biotechnologies) supplemented with 10% (v/v) HyClone FBS (GE Healthcare) and 1% (v/v) 100X antibiotic solution (MP Biomedicals). Cells were subcultured every other day upon 70-80% confluence in 100 mm tissue culture plates (Corning), using trypsin 0.05% with EDTA (Life Technologies) to detach cells.

2.8 Gap closure assay

Cells in culture dish were serum-starved for 24 hrs before the experiment. 2D gap closure assays were set up using cell culture inserts (Ibidi), which have a defined 500 µm gap with cells on both sides. 70 µl of cells at a concentration of 7 x 10^5 cells/ml were plated into the appropriate wells on the insert and spread evenly with a pipette tip. PBS was added to the well to surround the insert and the dish was placed in an incubator for 24 hrs to allow cells to spread and grow to confluence. After incubation, cell culture inserts were removed to expose the gap, and cells were washed with PBS several times to remove any loose cells. Media was layered over cells and incubated for 8 hrs. For drug studies, blebbistatin (Sigma) dissolved in DMSO (Sigma) was added to the regular culture media at 10 µM and 20 µM concentrations; control culture dishes with regular culture media only and with DMSO added were also maintained. Culture dishes were imaged using transmittance microscopy after 8 hrs with a 10X objective. Gap distances were measured seven times per image and averaged.

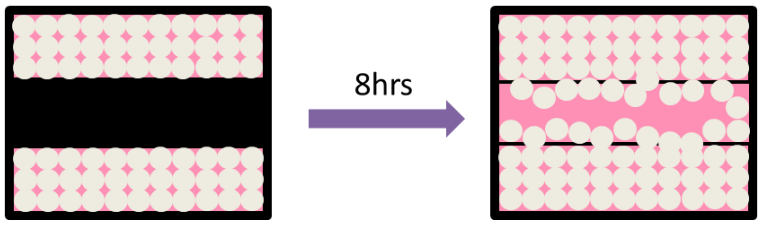

Figure 2.4: Schematic of gap closure assay

2.9 Transwell migration assay

C6 cells were detached using trypsin-EDTA solution and resuspended in DMEM containing 2% (v/v) FBS and 1% (v/v) antibiotic solution to a concentration of 1 x 10^6 cells/ml. 300 µl of cell suspension was plated into 8 µm and 3 µm FluoroBlok Transwell inserts (BD Biosciences) placed in a 24-well cell culture plate with 500 µl DMEM containing 10% (v/v) FBS and 1% (v/v) antibiotic solution at the bottom of each well to create a FBS gradient for cells to migrate downward through Transwell. For drug studies, all culture media was supplemented with desired concentration of blebbistatin, with DMSO as a control. Cells were allowed to invade for 6 hrs under normal incubation conditions. After invasion, cotton swabs were used to remove excess liquid or cells from above the filter, and filters were fixed in -20°C acetone, stained with 0.01% (v/v) propidium iodide for 1 hour at 37°C and washed with PBS. Membranes were excised from Transwell inserts, mounted on microscope slides, and imaged with a fluorescence microscope. Cells were counted from ten images per sample of different fields of view and normalized to that counted in the DMSO control.

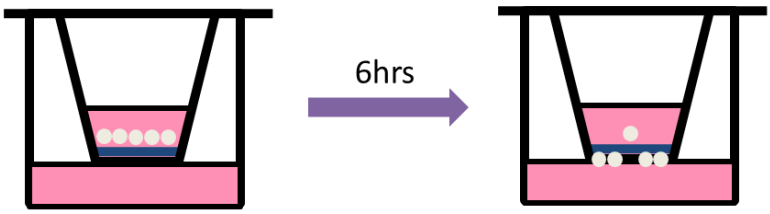

Figure 2.5: Schematic of Transwell migration assay

2.10 3D collagen gel invasion assays

Multicellular tumor spheroids (MTS) were formed using the hanging drop procedure (117). 25 µl drops containing 1000 cells were placed on the inside of a tissue culture plate lid, and the lid was inverted over 10 ml of regular culture medium and incubated at normal conditions for 5-7 days. Because the hanging drop procedure sometimes resulted in spheroids that were non-uniform depending on location on tissue culture lid, Perfecta3D Hanging Drop Plates (3D Biomatrix) were also utilized to form spheroids. In both cases, droplets were held in place by surface tension and cells accumulated at the bottom of each droplet to form the MTS. The Perfecta3D Hanging Drop system required PBS to be added to the outermost wells and to the reservoir along the rim of the hanging drop plate and tray below to provide moisture, and the liquid was replaced every other day. This method produced a greater number of uniform spheroids and was used for drug studies with blebbistatin.

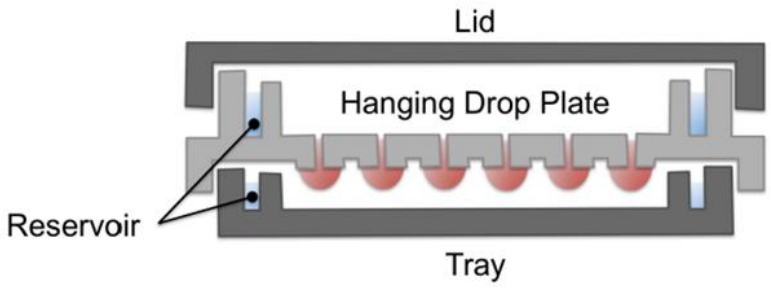

Figure 2.6: Perfecta3D Hanging Drop Plate (from 3D Biomatrix website)

When spheroids were ready to be harvested, 0.5, 1.0, and 3.0 mg/ml collagen I gels were prepared for the implantation process. Gels were made with pepsin-treated bovine collagen I (Nutragen, Advanced BioMatrix), 1X DMEM (Sigma Aldrich), 2.5% HEPES, 2.5% sodium

bicarbonate, and distilled water. For drug studies, blebbistatin dissolved in DMSO was added directly to the gel solutions at the desired concentrations. Gels were neutralized to pH 7.4, initiating fibrillogenesis, and 200 µl gels were transferred to glass cylinders glued to Fluorodish culture plates with glass bottoms (World Precision Instruments). One MTS per gel was implanted in as little excess cell media as possible immediately after neutralizing, and gels were incubated at 37°C under normal conditions. After 2 hrs, gels were overlaid with cell culture media, including blebbistatin for drug studies.

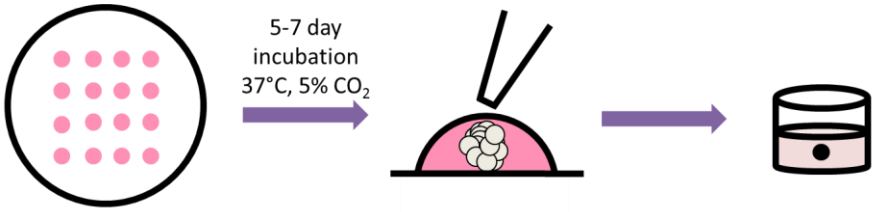

Figure 2.7: Hanging drop protocol for making multicellular tumor spheroids

MTS invasion was imaged using transmittance microscopy at 2, 24, 48, and 72 hrs post-implantation with a 10X objective. Transmittance 10X images were used to determine MTS size and invasion distance. The invasion front was defined as a circle that circumscribed 90% of cells, and the invasive distance was defined as the difference between the periphery of the spheroid and the invasion front.

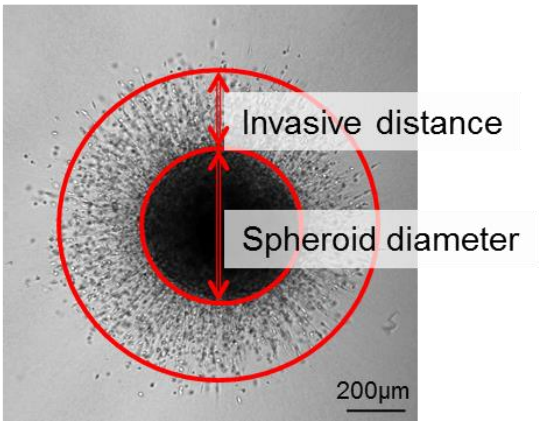

Figure 2.8: Representative spheroid image showing invasive distance and spheroid circles

CyQuant cell proliferation assays were performed measure cell viability (> 95%) at the blebbistatin concentrations used.

3 Collagen I self-assembly: revealing the developing structures that generate turbidity

Reprinted from *Biophysical Journal* (Volume 106, Issue 8, 15 April 2014, Pages 1822-1831)

3.1 Introduction

Collagen I is the most abundant protein in mammalian extracellular matrix where it is present primarily as fibrils, organized differently in different tissues (118). Given its physiological relevance, fibrillar collagen I matrices have been used both as scaffolds in tissue engineering and as three-dimensional environments for biophysical studies, especially those concerned with cell-matrix interactions (31, 34, 119-125). An appealing feature of collagen I matrices is their tunability. Both in vivo and in vitro, collagen I monomers self-assemble into fibrillar structures that may cross-link and/or entangle to form viscoelastic gels with varied network structures and mechanical properties. In vivo, diversity in these properties is realized through differences in monomer concentration, presence of various enzymes including those that cross-link collagen, and presence of additional extracellular matrix components that may intercalate with or otherwise affect the collagen matrix or assembly thereof (126). In vitro, network structural and mechanical properties may also be tuned through introducing cross-linkers and secondary gel components, as well as through varying temperature, pH, and ionic strength during self-assembly. Indeed, rather significant changes in both gel network structure and stiffness have been shown to result from changes in these parameters (107, 127-130). This control opens the door to independently varying collagen I network topology and mechanical properties, allowing for studies in which cell response to these variables is probed in physiologically relevant three-dimensional environments.

Collagen network properties are sensitive to temperature, pH, and ionic strength because these conditions affect the self-assembly of collagen monomers into fibrils. Thus, a fuller understanding of fibrillogenesis will enhance matrix design. Further clarification of the self-assembly of collagen may also inform discussion of the self-assembly of other fibrillar proteins, including pathological ones (131). To date, studies investigating the mechanism and kinetics of the collagen I self-assembly process in vitro have primarily monitored turbidity, an approach first employed more than a half century ago (132). During collagen I gelation, turbidity increases as a nearly transparent solution of monomers develops into fibrils that scatter significant amounts of light. Early studies showed that the increase in turbidity during gelation tracked precipitation of collagen into fibrils (82, 132). These studies and others also supported the hypothesis that collagen fibrillogenesis was a nucleation and growth process, as the turbidity curves were sigmoidal, displaying distinct lag and growth phases (82, 132-136).

Although turbidity has been and continues to be the method of choice to monitor developing collagen networks, imaging techniques are commonly employed to reveal structure of fully developed collagen and other biopolymer gels. Collagen I networks have been visualized using confocal fluorescence microscopy (CFM) of exogenously labeled collagen (98, 107, 137). Unlabeled collagen fibrils can also be imaged with two-photon fluorescence and second harmonic generation microscopy (127, 128, 138, 139). Confocal reflectance microscopy (CRM), with contrast emerging from light backscattering from collagen fibrils, has been the most commonly employed technique to image collagen gels (31, 34, 95, 119, 120, 124, 125, 140). The primary advantage of CRM relative to other techniques is that it requires neither the presence of potentially perturbative fluorophores nor the use of high power lasers.

Despite the growing popularity of imaging to reveal details of collagen network structure, imaging techniques have only rarely been used to visualize developing networks (95, 106, 140), and turbidity studies continue to be the dominant method used to investigate the time course of collagen gelation (88, 130, 141, 142). In this study, we simultaneously performed scanning transmittance microscopy (yielding in situ turbidity, IST), CRM, and CFM during self-assembly of collagen I networks of 0.5 mg/ml, 1.0 mg/ml, and 2.0 mg/ml at 27°C, 32°C, and 37°C. To our knowledge, these measurements represent the first direct visualization of the macromolecular entities responsible for the growing turbidity during collagen self-assembly. Increasing turbidity may result from increasing number and/or increasing size of collagen fibrils, and simultaneous IST measurements and confocal imaging revealed which of these processes dominate changes in turbidity at given times and under given conditions. Beyond elucidating the entities that give rise to turbidity, collapsing data from CRM into single variables revealed that IST and CRM are similarly sensitive to the number and dimension of fibrils and report similar information on the time course of collagen self-assembly.

3.2 Results and discussion

3.2.1 Qualitative description of gelation as revealed by CRM

Time-lapse images of unlabeled 0.5 mg/ml, 1.0 mg/ml, and 2.0 mg/ml acid-solubilized collagen I solutions during gelation at 27°C, 32°C, and 37°C were collected in confocal reflectance and scanning transmittance mode simultaneously. Representative time-lapse CRM imaging of the

gelation process of 1.0 mg/ml collagen at each of these temperatures is presented in Video S2 (110).

Following gelation in CRM revealed similarities across all collagen concentrations and gelation temperatures. In all cases, no structures were seen in the initial images. Later, fibrils became visible. When fibrils were first visualized, they were not locked into a network structure but instead moved relative to one another. During this phase of self-assembly, the network became denser: fibrils grew longer and more fibrils were visualized. At the same time, early visualized fibers became brighter. At arrest, fibrils were locked into position. Following arrest, previously visualized fibrils increased in brightness. Although there was no clear separation between the time scales on which fibrils became visualizable with CRM and grew in length and width, the late steps in collagen I self-assembly appeared dominated by fibrils increasing in width, as suggested by the increasing fibril brightness that continued throughout the majority of the visualized process.

Representative CRM images at the plateau time, t_{PL}, and at the arrest time, t_{ARR}, of label-free collagen formed at each concentration and temperature investigated are shown in Figure 3.1. As expected, the number of fibrils increased and mesh size decreased with increasing collagen content at each temperature. At the lower temperatures, fully formed gels were distinct from those prepared at high temperature, with fewer, longer, and thicker structures visualized. The structures may be fibrils, bundles of fibrils—termed fibers—or a combination thereof, the majority of which are expected to be < 200 nm in width (107, 128) and thus below the diffraction limit for optical wavelengths.

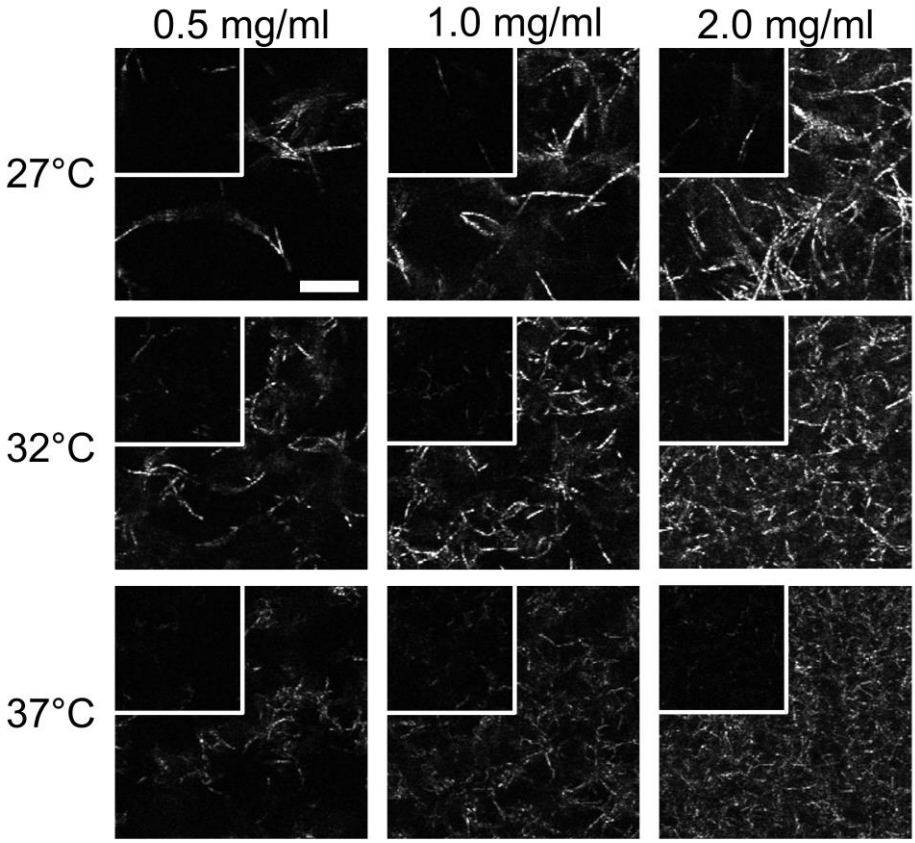

Figure 3.1: CRM images of collagen gels at plateau and arrest

Overlaid insets are images at arrest. Scale bar is 10 μm and is the same for all images. CRM images are unprocessed but are cropped, and each shows a representative portion of the full image.

The characteristics of the gels at plateau were also present at arrest, the time at which a spanning network structure is established (Figure 3.1, insets). As at plateau, at arrest lower concentration gels and those formed at lower temperatures showed sparser networks composed of fewer, longer fibrils than those of higher concentration and/or prepared at higher temperature. Although arrest and plateau gels mirrored each other, arrest images appeared more similar than did fully developed gels in terms of number of structures present and brightness of those structures, as will be discussed more fully below.

3.2.2 Early events of gelation as visualized by CFM

Because time-lapse CRM cannot visualize collagen monomers, oligomers, and perhaps early fibrils, its use in describing early events of collagen self-assembly is limited. To enhance understanding of these early events, time-lapse CFM images during self-assembly of FITC-labeled collagen were collected. Performed with commonly employed fluorescent tags, CFM is a more sensitive technique than CRM, under certain circumstances requiring as little as one fluorophore in the focal volume for signal to be discriminated from background. Furthermore, CFM can detect fibrils at all orientations, whereas CRM has limited sensitivity to out-of-plane oriented fibrils (143, 144). CFM does have disadvantages compared to CRM for imaging collagen self-assembly: first, bleaching limits the proportion of the gelation process that can be followed in a given movie; additionally, labeling has been shown to inhibit fibril thickening and bundling in low temperature gelation (107).

At all concentrations and gelation temperatures investigated, CFM time-lapse images displayed more structure at early time points than did CRM images (Figure 3.2). The earliest images revealed small isotropic features of moderate intensity against a lower intensity homogeneous background. Figure 3.2A shows the first image collected for a FITC-labeled collagen solution of 1.0 mg/ml at 32°C. At this time, the corresponding CRM image (Figure 3.2B) shows no structures. In CFM images, accretion into brighter spots on a darker background occurred within tens of seconds. At first, the bright structures were isotropic and mobile, and as their number increased they became anisotropic and fixed in position. By the arrest time (Figure 3.2C), at 5.6 min for the sample shown here, fibrils were evident. CRM images collected at this time also showed fibrils, though they appeared quite dim (Figure 3.2D).

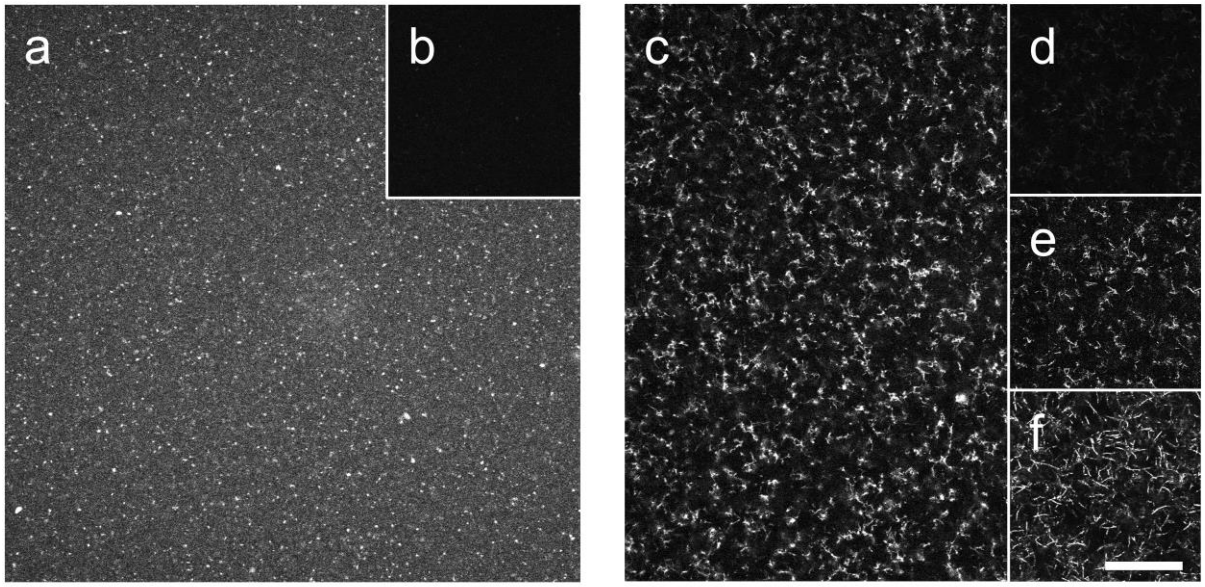

Figure 3.2: Comparison of CFM and CRM images at time points of interest

Images are from a representative 1.0 mg/ml collagen sample gelled at 32°C also shown in Video S1 (110). Left panel: The first images collected, 88 s after neutralization. **A** The initial CFM image reveals small isotropic features of moderate intensity against a lower intensity homogeneous background, whereas **B** the earliest CRM image reveals no structures. Right panel: Images at arrest and plateau. **C** The CFM image at t_{ARR} (5.6 min) reveals many structures. **D** The CRM image at arrest displays structures of low intensity that can be better visualized when **E** contrast is enhanced. **F** The CRM image at plateau (12.5 min) reveals that many structures in the fully developed gel can already be visualized at arrest (as in **C** and **E**). Scale bar is 25 μm for all images.

Compared to CRM, CFM is expected to be relatively insensitive to fibril width. As such, complementary analysis of CFM and CRM time-lapse images of collagen self-assembly can clarify the timescales of early fibril formation and fibril thickening. At arrest, CFM images revealed more structures than CRM images. After arrest, CFM images showed very little change except for overall photobleaching. CRM images, however, appeared to have increasing numbers

of fibrils and increasingly bright fibrils. Overlaying the CFM image at arrest (Figure 3.2C) with the CRM image at arrest (Figure 3.2D) shows the difference in visualized structures at that time, though enhancing contrast of the CRM image reveals a substantial number of fibrils (Figure 3.2E). Overlaying the CFM image at arrest (Figure 3.2C) with the CRM image at plateau (Figure 3.2F) shows strong colocalization. Video S1 (110) shows time-lapse CFM and CRM imaging of the sample depicted in Figure 3.2. Taken together, these images show that most fibrils are already present at arrest. Most of the change in CRM images after arrest must therefore be due to increasing width of fibrils that are already present.

3.2.3 CRM reveals structures responsible for turbidity

The sequence of events revealed by CRM and CFM of collagen I self-assembly—as well as the structure of the fully developed gels, with fewer and thicker fibrils at lower temperature—is broadly consistent with the nucleation and growth model of collagen self-assembly. Such a model was first proposed based on turbidity measurements showing a sigmoidal increase in turbidity during collagen self-assembly, with a lag phase of near zero turbidity followed by a growth phase with quickly increasing turbidity (82, 134). In this picture, during the lag phase nucleating structures are formed, after which the growth phase—characterized by quickly increasing turbidity—begins. During the growth phase, monomers self-assemble into fibrils anchored on the nucleating structures in an entropically driven self-assembly (80). As monomers are depleted, the growths phase ends and turbidity plateaus. Implicit in this understanding of the nucleation and growth model for collagen gelation is that no large structures are present in the lag phase, though a few early studies suggested otherwise (133, 145).

CRM and CFM report details of collagen gelation that can only be inferred from turbidity measurements. However, turbidity continues to be the method of choice to monitor the dynamics of biopolymer self-assembly. To compare the sequence of events revealed by CRM to those inferred from turbidity, CRM images were directly compared to turbidity measurements performed simultaneously using the multimodal microscopy set-up depicted in Figure 2.1. First, traditional turbidity measurements monitoring collagen gelation in a spectrophotometer were compared to results from IST measurements. For comparison with traditional turbidity measurements, scanning transmittance images were reduced to the single variable of IST, as described in the Materials and Methods. Differences between the IST measurement and the traditional turbidity measurement as performed here include that the IST measurement used a polarized light source, a high NA objective lens, a thinner sample, and a different apparatus for temperature control. Figure 3.3 shows a standard turbidity measurement and IST as measured via scanning transmittance microscopy of 1.0 mg/ml collagen samples undergoing gelation at 37°C. Although k_g was very similar in these measurements, time points of interest occurred approximately a minute later in standard turbidity than in IST. The discrepancy resolved when performing IST on a thicker sample, and we suggest the time difference is due to differences in heat transfer in the two set-ups. Once corrected for this time difference, turbidity and IST curves overlapped very well, as is also evident in the wavelength dependent scans (discussed in more detail later, see Figure 3.10). These measurements validated the use of IST as a measure of turbidity in a collagen solution undergoing gelation.

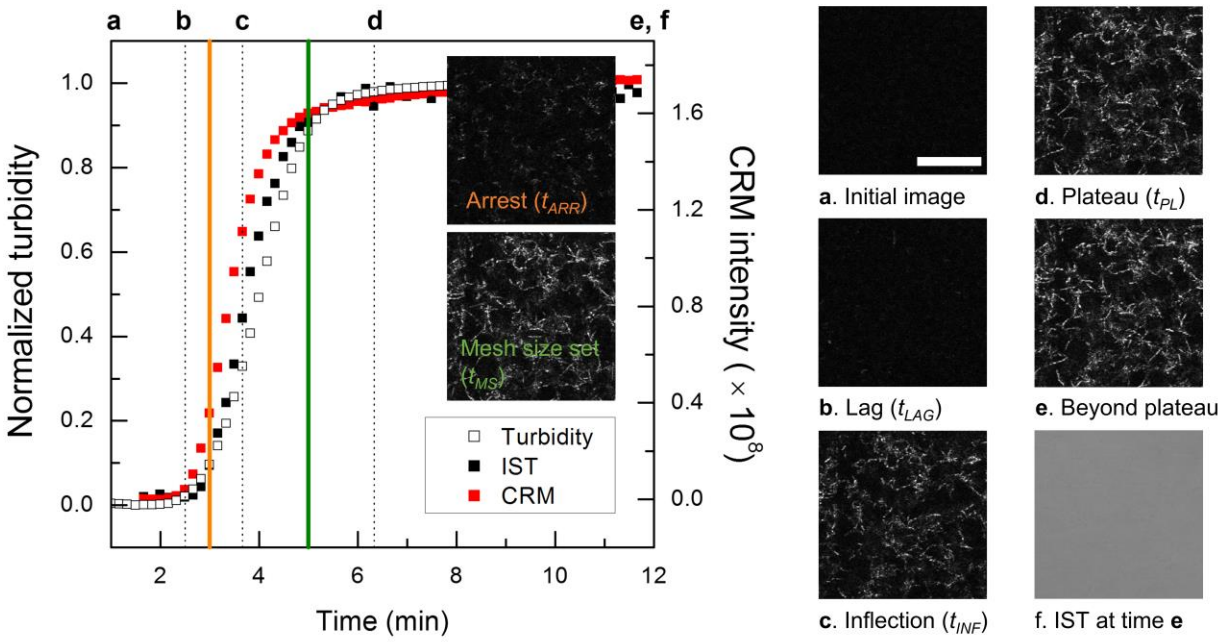

Figure 3.3: Traditional turbidity measurements track IST and CRM intensity evolution

At left, turbidity as measured with a spectrophotometer (black open squares), IST (black solid squares), and CRM intensity (red squares) from representative 1.0 mg/ml collagen samples gelled at 37ºC. The standard turbidity curve was shifted by one minute as described in the text. At right, images corresponding to dotted lines at time points of interest extracted from the IST curve: **A** initial CRM image, **B** CRM image at t_{LAG}, **C** CRM image at t_{INF}, **D** CRM image at t_{PL}, **E** CRM image beyond plateau, and **F** IST image beyond plateau. Images corresponding to t_{ARR} (orange line) and t_{MS} (green line) are shown as insets at left. Scale bar is 25 μm for all images. All images are unprocessed but cropped and show the same representative portion of the full image.

Having validated the IST measurement, CRM images were compared to key time points along the development of the turbidity curve during collagen self-assembly (Figure 3.3). In Figure 3.3, select CRM (and in one case, IST) images from the gelation of a 1.0 mg/ml collagen solution at 37°C are shown together with the corresponding time points on the IST curve, which was used

to assign t_{LAG}, t_{INF}, and t_{PL}. CRM images at these times revealed that at t_{LAG} very few structures were visualized but by t_{INF} many structures were present; in fact, most of the fibers present at t_{PL} as well as at the end of the measurement colocalized with those present at t_{INF}, though the structures were brighter at the later time points.

To complement information from time points obtained from turbidity, t_{ARR} and t_{MS}, which can only be identified from CRM, were also determined. Arrest was found to occur shortly after t_{LAG} determined from CRM for gels of all concentrations formed at all temperatures. From analysis of CRM and CFM images, it appears that most of the fibrils in the final network were already present at the arrest time even though < 10% of the final turbidity was established by this time. As such, most of the increase in turbidity must be due to thickening of fibrils that were already present.

This observation is reinforced by the image at t_{MS}, the time at which mesh size is no longer evolving. Mesh (or pore) size has emerged as a principal reporter of network structure in biopolymer gels because this quantity can be determined with ease and figures prominently in theories predicting how network structure sets material properties (107, 137, 146). Mesh size analysis yielded values for the fully developed gels consistent with earlier reports (107, 127, 147) though alternate approaches have yielded smaller mesh sizes (125, 137, 144). Because relative mesh size was of interest here, differences in absolute mesh size would not alter any conclusions of this study.

At early time points, when no or few fibrils were visible, mesh size could not be accurately determined, and therefore discussion of mesh size is limited to times beyond t_{ARR}. At the earliest time points assessed, between t_{ARR} and t_{INF}, there was a steep decay in mesh size (Figure 3.4A). Indeed, the great majority of mesh size evolution—from the dimensions of the sample to tens of

microns—occurred before t_{INF}, even though this point defines the time at which only half of the final turbidity had been established. This is consistent with the idea that mesh size is primarily sensitive to existence of fibrils but not their width, so long as mesh size is significantly greater than fibril width. Beyond the inflection time, CRM imaging suggested fibrils continue to thicken. This continued increase of fibril diameter resulted in slow evolution of mesh size even as turbidity continued to increase quickly, as increasing fibril width has a greater effect on turbidity than on mesh size.

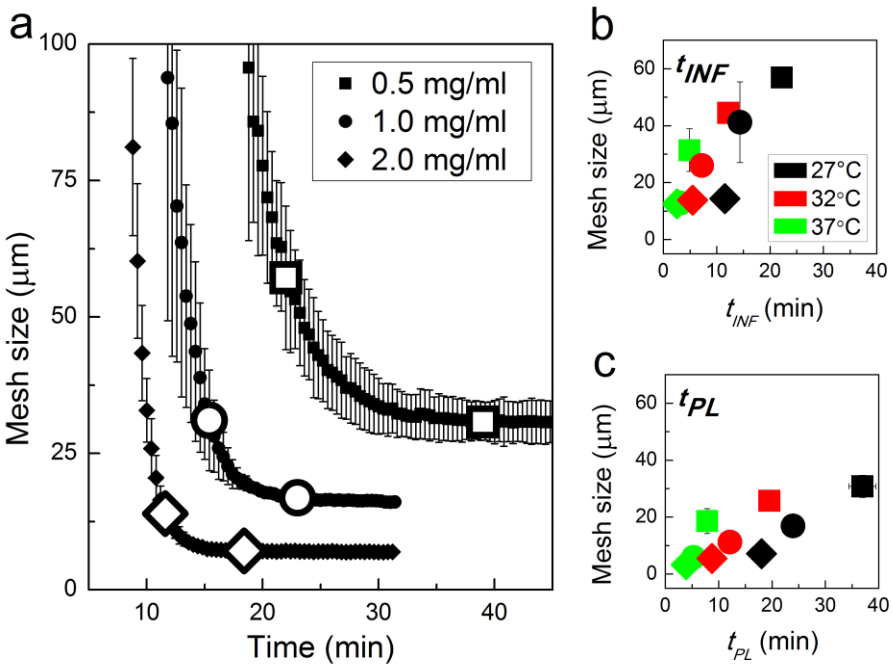

Figure 3.4: Mesh size evolution during fibrillogenesis

A Mesh size during gelation of 0.5 mg/ml (squares), 1.0 mg/ml (circles), and 2.0 mg/ml (diamonds) at 27ºC. Every other point is shown for clarity. Large symbols indicate t_{INF} and t_{PL} as determined from CRM intensity curves. Mesh size at **B** t_{INF} and **C** t_{PL} vs. **B** t_{INF} and **C** t_{PL} for all gels. Error bars represent standard deviations and are shown when larger than the symbols.

Plotting mesh size at t_{INF} and t_{PL} against time showed that time to inflection and plateau were only correlated with mesh size at a given temperature (Figure 3.4B and C). Figure 3.4C reveals that at t_{PL}, when mesh size is no longer evolving, mesh size varied more strongly with concentration for gels formed at higher temperature than lower temperature. This is consistent with the idea that increased collagen primarily leads to more fibrils at high temperatures and supports, instead, thicker fibrils at low temperatures. The evolution of mesh size from t_{INF} to t_{PL} revealed a similar decrease in mesh size across gel concentrations and gelation temperatures, with mesh size of all gels decreasing by a factor of ≈ 2 between these time points (Figure 3.4B and C). This trend indicates that the differential in fibril thickness present at plateau was already present at t_{INF}. CRM results at t_{INF}—though not those earlier, at t_{ARR}—also support that conclusion, as will be discussed below.

3.2.4 Quantitative comparison of turbidity and CRM intensity

Comparing CRM images to points along the IST curve revealed how the number and dimension of the developing structures lead to increased turbidity. A second key goal of this study was investigating whether CRM images could be reduced to a single variable that 1) tracked turbidity development in time and 2) reflected relative turbidity of a set of gels of different collagen content and network structure. A straightforward single variable for such comparison is CRM total intensity. CRM intensity and IST curves for all gels investigated are shown in Figure 3.5. It is apparent that all CRM intensity curves displayed sigmoidal shapes like the turbidity curves and that relative values of CRM and IST of the fully formed gels were similar for samples at all concentrations and gelation temperatures.

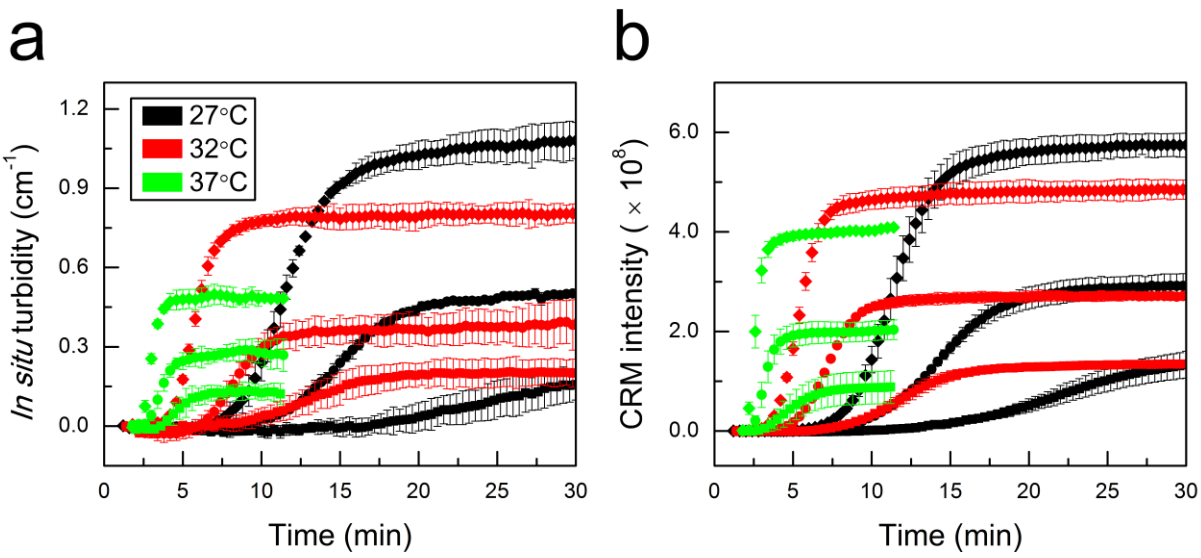

Figure 3.5: Average IST and CRM curves over time

Average **A** IST and **B** CRM curves for 0.5 mg/ml (squares), 1.0 mg/ml (circles), and 2.0 mg/ml (diamonds) collagen solutions gelled at 27ºC (black), 32ºC (red), and 37ºC (green). Every other point is shown for clarity. Error bars represent standard deviations.

3.2.4.1 Turbidity and CRM intensity report similar gelation time course

Although turbidity and CRM both rely on scattering from collagen fibrils, whether turbidity and CRM intensity would reveal the same information over the full course of the self-assembly process was not immediately clear. A standard turbidity measurement and IST as performed here monitor light in the forward direction, and the decrease of that light represents the scattering in all directions excepting a small cone in the forward direction. CRM, by contrast, directly monitors only the light scattered backward that can be collected by the objective lens. For the measurements presented here, an oil objective with NA = 1.42 was employed, and light emerging in the epi-direction in a cone of ≈ 140° was collected. Over time, the scattering entities in a developing collagen gel change size and shape, becoming larger and more anisotropic. This is expected to

alter the angular distribution of scattering over the course of gelation (148-150), potentially impacting the relative sensitivity of IST and CRM. Indeed, the proportion of scattering detected by CRM may be expected to be highest relative to that detected by turbidity measurements early in the gelation process (85, 149, 150). Similar arguments have been invoked when considering fibrin gelation as assessed by angle-dependent scattering compared to turbidity (151).

To quantitatively compare the time course of the development of IST and CRM intensity, t_{LAG}, t_{INF}, t_{PL}, and k_G were obtained from each curve. Figure 3.6 reveals that there was clear correlation between each of the time points as defined through IST and CRM intensity at all collagen concentrations and gelation temperatures. Similarly, k_G was strongly correlated between these measurements. Linear fits to the data in Figure 3.6A-C, described the data very well ($R^2 > 0.98$) with slopes of 0.81, 0.94, and 0.96 for t_{LAG}, t_{INF}, and t_{PL}, respectively. The fact that the slopes were somewhat < 1 shows that the time points of interest occur earlier in CRM than IST, as is also evident in Figure 3.3 (left panel). This was most obvious at the early time points, consistent with the idea that changes in angular distribution of scattering intensity during fibril development may lead to enhanced sensitivity of CRM relative to IST early in the gelation process. Indeed, we found that the full network structure was in place (t_{ARR}) shortly after t_{LAG} as defined by CRM, when very little turbidity had developed.

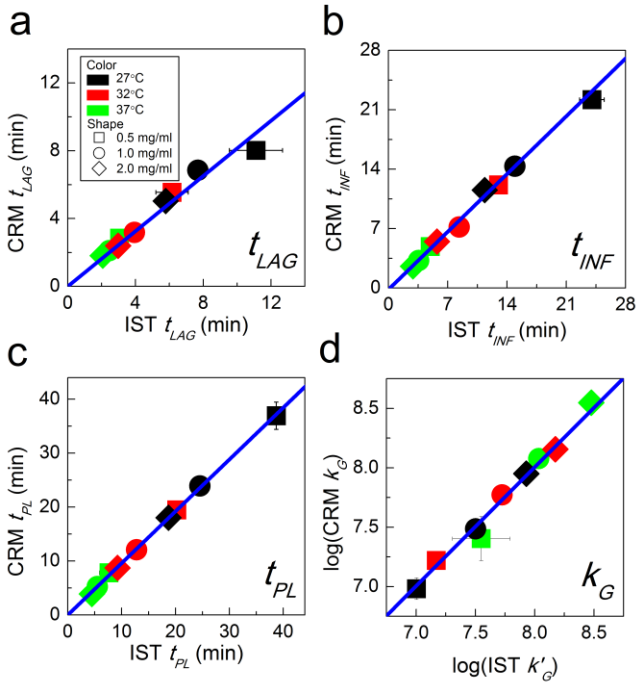

Figure 3.6: Time points of interest and slope of growth phase from CRM versus IST

A t_{LAG}, **B** t_{INF}, **C** t_{PL}, and **D** k_G obtained from CRM versus those obtained from IST. Linear regression was performed with the y-intercept set to zero, yield slopes of 0.81, 0.94, and 0.96 with $R^2 \geq 0.98$. In **A**, if the 27ºC 0.5 mg/ml point is excluded from the fit, the slope of the best-fit line is 0.88 and all $R^2 > 0.998$. In **D**, IST k_G values were normalized by multiplying by final CRM intensity over final IST, yielding k'_G. Error bars are standard deviations and are shown only when larger than symbols. Colors and symbols for **A**-**D** are as shown in the legend in **A**.

3.2.4.2 Turbidity and CRM intensity are similarly sensitive to fibril number and dimension

As highlighted by Figure 3.3, although CRM intensity and IST tracked each other in time, CRM contains direct information about the fibrillar structures that give rise to scattering. To investigate whether CRM and IST were similarly sensitive to fibril number and dimension, IST and CRM intensity values at particular time points during gelation were considered.

Previously, it was shown that at specific gelation conditions the ratio of turbidity to concentration of the fully developed gel, $A_\infty = \tau_\infty/c$, is constant (82). IST measurements at plateau were consistent with this finding, as shown in Figure 3.7 and Table 3.1. The values of A_{PL} = IST_{PL}/c, with plateau time determined from the IST curve, for a given temperature varied by no more than 15%, though IST data showed significant variation across samples of given concentration. Similar results were seen at the inflection time (A_{INF} = IST_{INF}/c), when all fibrils are expected to be present but only half of the final turbidity has developed, as the fibrils have not yet reached their ultimate thickness (Figure 3.7). Although gelation at a given temperature led to *A* values that were nearly constant across concentration, these values increased with decreasing gelation temperature, consistent with the idea that greater fibril width leads to increased scattering. The values of A_{PL} and A_{INF} averaged over concentrations show A_{INF} varied with gelation temperature to the same degree as A_{PL} (Table 3.1). This again indicates that differential in fibril width between structures formed at different temperatures was fully established by the inflection time, halfway through the growth phase of the turbidity curve.

Table 3.1: Ratio of A *to* W *at* t_{INF} *and* t_{PL} *across temperatures*

The ratio of IST to concentration ($A = IST/c$) and that of CRM intensity to concentration (W = CRM_{int}/c) at t_{INF} and t_{PL} averaged across temperatures. Time points evaluated were determined from the CRM intensity curve for *W* and the IST curve for *A*.

Temperature (°C)	Inflection		Plateau	
	A × 10^{-1} ± SD	**W × 10^{8}** ± SD	**A × 10^{-1}** ± SD	**W × 10^{8}** ± SD
27	2.1 ± 0.3	1.5 ± 0.1	4.5 ± 0.5	2.9 ± 0.2
32	1.9 ± 0.3	1.3 ± 0.1	3.8 ± 0.4	2.5 ± 0.1
37	1.2 ± 0.1	0.9 ± 0.1	2.5 ± 0.2	1.8 ± 0.2

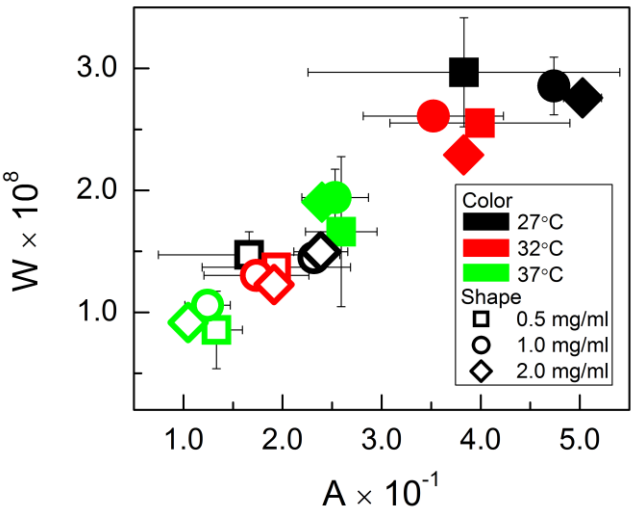

Figure 3.7: Ratio of W *vs.* A *at* t_{INF} *and* t_{PL}

Y-axis is $W = CRM_{int}/c$ and x-axis is $A = IST/c$ at t_{INF} (open symbols) and t_{PL} (solid symbols). Time points evaluated were determined from the CRM intensity curve for W and the IST curve for A. Error bars indicate standard deviations and are shown only when larger than the symbols.

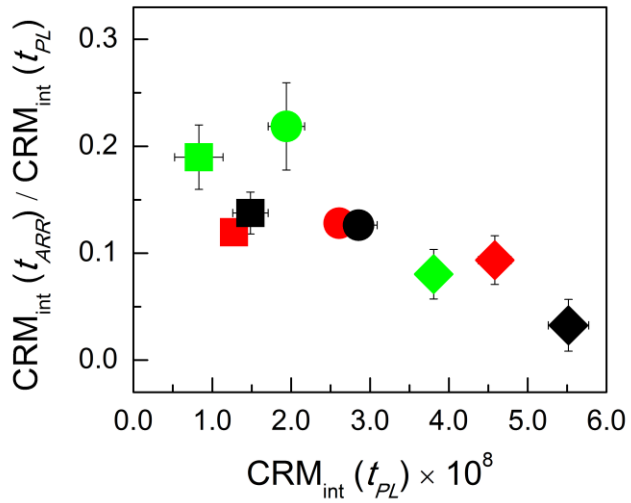

Figure 3.8: Ratio of CRM intensity at t_{ARR} *to that at* t_{PL} *versus CRM intensity at* t_{PL}

Symbols and colors are shown as in Figure 3.7. Error bars indicate standard deviations and are shown only when larger than the symbols.

The results for CRM intensity (CRM_{int}) mirrored those of IST, as shown in Figure 3.7 and Table 3.1. Indeed the values of $W = CRM_{int}/c$ varied slightly less for a given temperature across concentrations at both plateau and inflection than did the corresponding A values. Averaged over all samples at a given temperature, to within error W decreased with increasing gelation temperature in the same proportion as did A. Although W_{PL} and W_{INF} were constant at a given temperature across concentrations and decreased as a function of increasing gelation temperature, neither of these trends held at the arrest time. Indeed, CRM intensities at arrest varied little with concentration for gelation at a given temperature, consistent with arrest time being defined by the presence of a minimum spanning network. Additionally, the quantity $W_{ARR} = CRM_{int,ARR}/c$ showed no trend with gelation temperature, supporting the idea that fibril width differential as a function of temperature is not yet established by the arrest time, whereas it is established by the inflection time. These conclusions were strengthened by examining the proportion of plateau intensity that was present at arrest (Figure 3.8). At a given temperature, a decreasing proportion of CRM plateau intensity was established at arrest as gel concentration increased. Additionally, for a given concentration, with decreasing gelation temperature a decreasing proportion of plateau intensity was present at arrest, consistent with the idea that most fibril thickening occurs after arrest. Figure 3.8 reveals that the fully developed gels that scattered the most, due to a large number of fibrils and/or thick fibrils, had the smallest proportion of their ultimate scattering present at arrest. This is consistent with the presence of a minimal spanning structure in which ultimate fibril diameter differential is not yet established at arrest.

To further test the hypothesis that the putative network consists of thin rods regardless of gel conditions and fully formed gel structure and to assess the relative sensitivity of the techniques employed in this study, fibril diameter during gelation was assessed using wavelength-dependent

measurements and analysis based on the theory of scattering from long rods (83-85, 109). Equation 4 was applied to both standard turbidity and IST data, performed on 1.0 mg/ml collagen gels formed at 37ºC. First, standard turbidity assays of these gels were performed at 400, 458, 488, 515, 543, and 633 nm (Figure 3.9). From these time scans, wavelength scans were constructed at each time point.

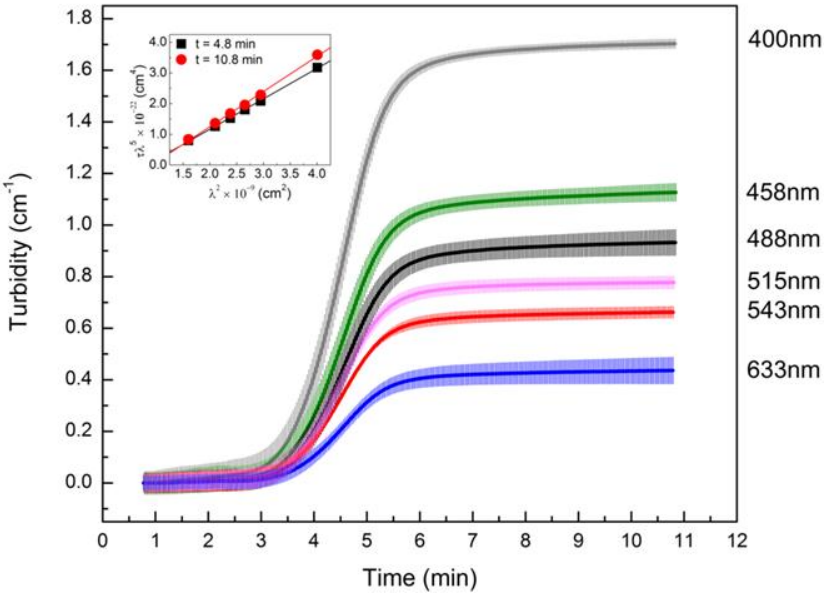

Figure 3.9: Standard turbidity curves using different wavelengths

Turbidity curves obtained from 1.0 mg/ml collagen samples gelling at 37ºC. No time shifts of standard turbidity measurements were performed to account for possible differences in heat transfer between the measurements as described in the main text. Average curves were constructed from two or three measurements and error bars are standard deviations. Insets show $\tau\lambda^5$ vs. λ^2 and least squares linear fits for the data reconstructed at t = 4.8 and 10.8 minutes.

Equation 4 assumes the scattering entities are monodisperse rods that are much longer and thinner than the wavelength of light employed (114). These assumptions may break down late in the gelation process at low temperature where fiber bundles are present as well as early in the gelation process at any temperature, particularly before arrest, where long fibers may not be present. Despite these potential problems, analyses of fully formed collagen gels as well as those undergoing disassembly have been undertaken previously (88, 108). In those measurements, as in ours, while Equation 4 resulted in reasonable mass to length ratios (μ) that changed smoothly during the gelation process, obtained diameter values appeared sensitive to noise and prone to artifacts (88). As such, fibril width was estimated from the mass to length ratio using geometric arguments, with number of molecules in a cross section given by $N = \mu/(M/4.6D)$ with M the molecular mass of the collagen I monomer (290 kDa) and D the axial periodicity seen in banded collagen fibrils (67 nm) (88, 108, 152). Given a circular cross-section and measured packing in hydrated fibrils, fibril diameter can be approximated as $d = 1.83\sqrt{N}$ (152). This set of calculations assumes monomer packing that is constant as a function of gelation temperature and throughout the gelation process.

The approach described above was employed on standard turbidity measurements of 1.0 mg/ml collagen gelling at 37ºC (Figure 3.9). Plots of $\tau\lambda^5$ vs. λ^2 were well fit by lines both at the end of gelation as well as during the growth phase, as shown in the inset of Figure 3.9. Similar fits were obtained for times as early as 2.5 min.

Absolute values of $\mu = 8.2 \times 10^{12}$ Da/cm and d = 54 nm were obtained for fully formed 1.0 mg/ml collagen gelled at 37ºC using the data shown in Figure 3.9. The value obtained for mass to length ratio is consistent with that measured previously using wavelength dependent turbidity (88, 108) and the diameter estimate is also in range of other reports (82, 88, 107, 108, 128, 153).

IST and CRM measurements of 1.0 mg/ml collagen gelling at 37°C were also performed at 488, 543, and 633 nm (Figure 3.10). It is apparent that the relative values of IST and CRM intensity were similar as a function of wavelength to those measured via standard turbidity. We note that as at 488 nm (Figure 3.3 and Figure 3.6), CRM preceded IST at early time points, with arrest occurring when a greater proportion of CRM than IST had developed. This was also true at the other wavelengths studied, and no clear trend was found with wavelength.

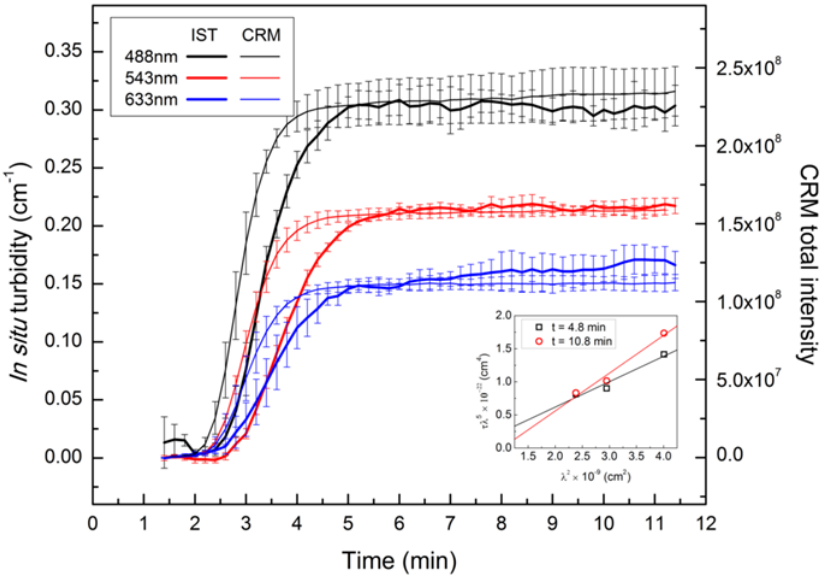

Figure 3.10: IST and CRM curves using different wavelengths

IST (thick) and CRM intensity (thin) curves obtained from 1.0 mg/ml collagen samples gelling at 37°C at 488, 543, and 633 nm, from top to bottom. No time shifts of CRM/IST measurements were performed to account for possible differences in heat transfer between the measurements as described in the main text. Average curves were constructed from two or three measurements and error bars are standard deviations. Insets show $\tau\lambda^5$ vs. λ^2 and least squares linear fits for the data reconstructed at t = 4.8 and 10.8 minutes.

IST data can be analyzed using Equation 4 in the same manner as standard turbidity data (Figure 3.10, inset). Wavelength dependent IST measurements yielded a somewhat lower value of $\mu = 4 \times 10^{12}$ Da/cm. If an effective pathlength of 0.2 mm (compared to the expected pathlength of ≈ 0.4 mm based on sample volume and sample cell shape) was employed in converting measured absorption to turbidity, μ obtained from IST was the same as that obtained from standard turbidity measurements. The use of such an effective pathlength may be warranted because a concave meniscus formed in the sample cell creating a smaller effective pathlength (≈ 0.3 mm). The further correction may be warranted due to the tightly focused light used in IST.

Given the relative values of CRM intensity to IST as a function of wavelength (Figure 3.10), it appears that much the same information is present in the CRM intensity and IST results. While no analytical method has been developed to convert CRM intensity to mass to length ratio and diameter, this is in principle possible. Moreover, if CRM intensity is normalized to IST, the analysis described by Equation 4 can be performed on the normalized CRM intensity measurements and will yield the same results.

Performing analysis of wavelength-dependent measurements as a function of time during gelation suggested that at arrest fibrils in 1.0 mg/ml gels forming at 37°C were ≈ 20 nm. The same measurement and analysis was then employed on 1.0 mg/ml gels forming at 27°C and also showed that fibrils at arrest were ≈ 20 nm even though this approach suggests they were nearly 100 nm in the fully formed gel (Figure 3.11). Taken together, this data further supports the conclusion that the initial network spanning structure is composed of thin fibrils that are relatively insensitive to gelation conditions and that fibril thickening is the chief activity of the turbidimetric growth phase. These measurements and analysis also suggest that CRM can be employed to visualize collagen fibrils as thin as 20 nm.

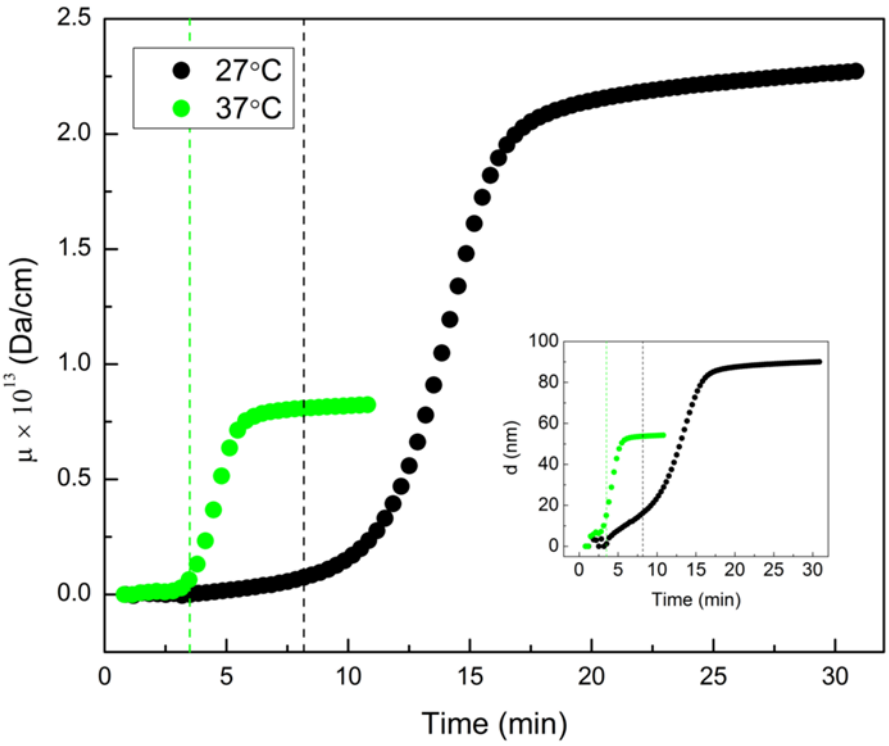

Figure 3.11: Mass to length ratio and fibril diameter from wavelength dependent turbidity

Measurements are of 1.0 mg/ml collagen gelled at 37ºC and 27ºC. Dashed lines indicate expected arrest times based on CRM imaging and 1 minute shift of standard turbidity measurement compared to CRM/IST measurements as described in Figure 3.3.

3.3 Conclusion

IST measurements of collagen self-assembly performed simultaneously with confocal imaging were employed to reveal the structures that underlie the development of turbidity during collagen self-assembly. All trends seen in IST measurements across fully developed collagen gels of different concentrations and gelation temperatures were also present when evaluating CRM intensity, showing the two techniques are similarly sensitive to fibril number and dimension. The time course of IST and CRM development was also similar, with CRM revealing increased sensitivity to early scatterers. Despite the similarity of turbidity and CRM intensity measurements,

taken together CRM and CFM support a somewhat different picture of the lag and growth phases of collagen self-assembly compared to that inferred from turbidity measurements alone. Our findings exclude the possibility that no large structures are present in the lag phase and that turbidity tracks precipitation through the entirety of the gelation process, demonstrate that a minimal spanning structure that is relatively insensitive to gelation conditions is present before turbidity develops, and show that the majority of the increase in turbidity is attributable to fibril thickening. In addition to clarifying details on the time course of collagen gelation, given scattering cross sections reported from different biopolymer fibers (154), we suggest that simultaneous CRM and IST measurements may also be applied to the study of gelation of a wide range of intracellular and extracellular biopolymers.

3.4 Description of supporting movies

Both supporting movies are available online (110).

3.4.1 Supporting movie 1

Fibrillogenesis of 1.0 mg/ml collagen at 32°C recorded by simultaneous time-lapse CFM, CRM, and IST. The channels from left to right are fluorescence, reflectance, and transmittance. Scan speed was 3.26 s/scan, and the interval between images was 10 s. Movies are shown at a frame rate of 10 frames/s. The first 100 images (16.7 min) are shown although the movies were collected for 30 minutes. The movie has been cropped and each image is 91 x 91 μm.

3.4.2 Supporting movie 2

Fibrillogenesis of 1.0 mg/ml collagen at 27°C, 32°C, and 37°C recorded by time-lapse CRM. The channels from left to right are in order of increasing temperature. Scan speed was 3.26 s/scan, and the interval between images was 10 s (shown at a frame rate of 10 frames/s). The first 150 images are shown for 27°C and 32°C, while 60 images are shown for 37°C since gelation occurred on a much quicker time scale at that temperature. The movie has been cropped and each image is 91 x 91 μm.

4 Simultaneous microscopy and rheology of type I acid-solubilized collagen fibrillogenesis

4.1 Introduction

Type I collagen is prominently used in research and is one of the most widely-occurring collagens, in particular for its abundance in extracellular matrix that is useful for studying cell-matrix interactions in three-dimensional in vitro environments (31-33). Collagen I is present mainly in fibrillar form, providing connective structure and support for tendons, skin, ligaments, cornea, and other non-cartilaginous tissues. In the lab, collagen I fibrillar networks can be made from solutions of monomers purified from animal tissues. *In vitro* fibrillogenesis is affected by many factors including concentration, temperature, pH, ionic strength, and the introduction of cross-linkers and secondary gel components (82, 108, 133), which result in collagen gels with tunable structural and mechanical properties.

Initial studies from more than half a century ago used turbidity to monitor type I collagen self-assembly and showed that fibrillogenesis follows a nucleation-and-growth pattern, where monomers assemble with little change in turbidity in the lag phase followed by a period of exponential growth and eventual plateau as the gel reaches an equilibrium state (82). However, the main disadvantage to turbidity is that there is no direct corresponding image of gel network structure, especially at non-equilibrium times where assumptions in applying light scattering theory are no longer valid (86, 88). Dynamic (quasi-elastic) light scattering (DLS) has also been used for measuring the size of particles dispersed in liquid, in particular collagen monomers or small aggregates kept in acidic solution to prevent fibrillogenesis (90, 91). These and other light

scattering studies are usually coupled with some microscopy (most often SEM or TEM) to provide visual accompaniment.

In more recent literature, the collagen I self-assembly process continues to be monitored with turbidity or DLS but also has been studied using imaging techniques and rheology. Non-invasive imaging methods such as confocal microscopy (reflectance, fluorescence) provide a direct image narrative for how gel structure develops but is limited by poor resolution of early aggregates immediately after gelation has been initiated (86). However, confocal reflectance microscopy in particular is simple to perform and does not contain fluorophores that disrupt the normal gelation process or require the use of high power lasers like with two-photon fluorescence or second harmonic generation microscopy. The previous chapter showed that monitoring gelation with confocal microscopy can be a proxy for traditional turbidity measurements, highlighting the importance of performing microscopy simultaneously with other types of measurements to assess gelation behavior (86).

Additionally, rheology has been used in collagen literature primarily to assess the mechanical properties of equilibrium gels, with few studies focused on the properties of the gel during the self-assembly process (95-97). Although some studies have attempted to characterize collagen gelation with traditional sol-gel transition theories (106, 107), this approach is made difficult by the complexity of biopolymer gelation that cannot be fully described with traditional polymer theories. Furthermore, only a few studies have ever characterized collagen gelation with both imaging and rheological studies (95, 104, 106-108). The ability to perform simultaneous measurements would enhance fundamental biopolymer studies by allowing for the visualization of a developing network while also monitoring the gel mechanical development; a direct correlation of the observables from these two methodologies would avoid encountering issues like

non-uniform sample size and gelation conditions that may be present when these methodologies are employed alone. Also, using both techniques at the same time would allow for further insights into how structural development affects mechanical development and vice versa.

In vivo and *in vitro* applications of type I collagen require a more thorough understanding of gelation conditions and corresponding gel properties. In this study, collagen self-assembly was monitored with oscillatory rheology and simultaneously imaged with confocal reflectance microscopy at different collagen concentrations and temperatures. The dual methodology employed here provides a detailed description of the timescale for the development of mechanical and structural properties of collagen gels formed under near-physiological conditions. This study examines gelation in the context of percolation and semiflexible polymer theories. Combining the two methodologies is an important tool for the study of how the structural and mechanical properties are coupled during collagen gel self-assembly.

4.2 Results and discussion

Thus far, the modified Anton Paar rheomicroscope set-up used by the authors has allowed for the simultaneous imaging of collagen fibrils as they form *in vitro* with monitoring mechanical property development in the form of oscillatory rheology. The ability to simultaneously monitor gelation visually and mechanically provides the ability to assess whether mechanical definitions are the same as structural definitions.

4.2.1 Rheological and visual description of gelation

Simultaneous confocal imaging and oscillatory rheology time sweeps were performed on 2.0 mg/ml and 3.0 mg/ml type I collagen gels formed at 24ºC and 32ºC. An example of observables

obtained from this dual method for a representative 2.0 mg/ml sample formed at 24ºC is shown in Figure 4.1. Confocal reflectance images showed contrast from back-scattered light from fibrillar components during the collagen self-assembly process, reported as the total intensity per image over time, a valid observable for tracking gelation progress (86). Oscillatory rheology reported the development of storage and loss modulus during this process. Following the gelation process with both imaging and rheological measurements allowed for the direct comparison between the development of structural and mechanical properties in each sample.

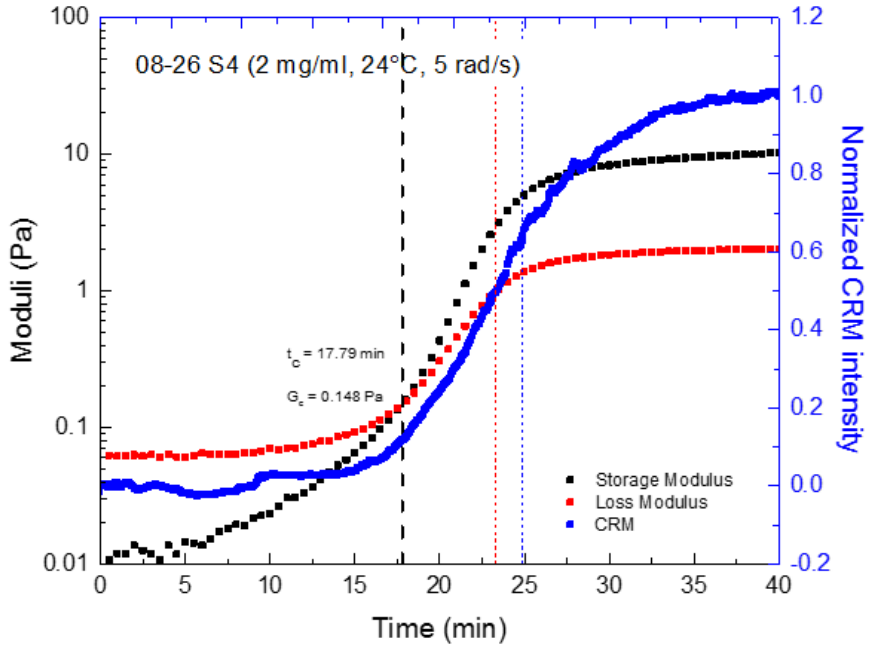

Figure 4.1: CRM and rheological development of collagen during gelation

Gelation was initiated with the addition of NaOH to the liquid sample of 2.0 mg/ml collagen. Within ~ 1.5 min, the sample was mixed, placed on the rheometer cover slip pre-equilibrated to 24ºC, and both confocal reflectance imaging and oscillatory rheology began. The collagen gelation process showed the characteristic S-shaped curve in accordance with nucleation

and growth theory. Initially, at time 0 (defined as the time at which rheology starts), as is often the case with many gelling solutions, the storage modulus G' and loss modulus G'' were very low (< 1 Pa), with the storage modulus approximately an order of magnitude smaller than the loss modulus. The solution consisted of collagen monomers that underwent Brownian motion and assembled into nuclei as they came into contact with other monomers, so it was mostly liquid at this time point and stored little to no elastic energy. The CRM total intensity was background-corrected and normalized, and no fibers were seen in initial images.

As the solution gelled, white pixels appeared in the CRM images, which seemed to be the earliest nuclei that became large enough to reflect light; these nuclei were not fixed within view, and they appeared and disappeared from image to image. During this time, G'' held very steady (G'' ~ 0.06 Pa), while G' started to slowly increase. Arrest time, t_{ARR}, was called at ~ 5 min as thin long fibrils begin to appear between 5 and 15 minutes; although new fibrils became visible until t_{INF} (~ 24 min) and the gel continued to become more dense, the fibrils were fixed within the field of view and fixed relative to each other immediately following their first appearance at 5 min. CRM total intensity stayed very low despite the appearance of few fibrils; the mesh size at arrest could not be accurately determined because so few fibrils were present and intense enough to be seen after thresholding.

Following arrest, the storage and loss moduli increased quickly, with the G' increasing at a faster rate than G'', eventually leading to a crossover point at time t_C ~ 18 min, with G_C = 0.15 Pa. At t_C, the normalized CRM total intensity was ~ 12% of the equilibrium gel intensity. The characteristic bundling of collagen gelled at lower-than-physiological temperatures was seen around this time. ξ_{char} at crossover was found to be 80 μm, but this may have been overestimated because the threshold level removed pixels that were fibers in addition to background noise. Upon

enhancing the brightness and contrast of the image, the majority of fibrils in the equilibrium gel were already present by rheological crossover time t_C; however, often the entirety of the fibril was not seen (likely because it had not grown thick enough to reflect light picked up by the PMT), so that would have contributed to the much larger mesh size obtained at t_C than at t_{PL}. As gelation progressed, a substantial number of dangling ends to fibrils were seen until well after $t_{PL,R}$, where they appear to become fixed.

After t_C, G' continued to increase at a faster rate than G'' until they both plateaued around $t_{PL,R} \sim 27$ min, with the G' value approximately an order of magnitude greater than that of G''. Although a plateau was clearly seen when logarithmically scaled, the values for G' and G'' continued to increase but did so at a very low rate, potentially due to unavoidable evaporation effects. Also, graphing both moduli and CRM intensity on logarithmic scales resulted in adequate overlap of $t_{PL,CRM}$ and $t_{PL,R}$ (not shown). All fibrils seen at equilibrium could be seen shortly after t_C with no image manipulation, and the fibrils continued to thicken, resulting in a normalized CRM total intensity that increased even as the moduli values leveled off. At $t_{PL,CRM} \sim 34$ min, the CRM intensity also completely plateaued. The mesh size at $t_{PL,R}$ and $t_{PL,CRM}$ were 18 μm and 16 μm, respectively.

These rheological gelation curves were in agreement with the two step nucleation and growth model of collagen fibrillogenesis. According to this model, nuclei formation dominates during the lag phase and does not result in major rheological changes until some critical percentage of monomer aggregation takes place, after which the majority of moduli increase is characterized by fibril formation. However, fibril formation can take place in two distinct ways: a) collagen monomers (triple helices) assembling end-to-end creating longer fibrils or b) collagen monomers assembling laterally and resulting in thicker fibrils. Prior studies from our lab have shown that

some minimum spanning network is present relatively early on in the gelation process, with gels becoming arrested quickly after t_{LAG}. Such studies have indicated that the majority of fibril assembly post-arrest occurs through the lateral assembly mechanism, where fibrils are growing thicker and few additional connections are made to the network so mesh size stays consistent.

4.2.2 Trends across temperatures and concentrations

4.2.2.1 Structural changes

The structural and mechanical properties of collagen gels are dependent on the conditions under which gelation occurs, including factors such as concentration, temperature, ionic strength, and pH. In this case, gels of different concentration and temperatures were formed to compare the change in gel properties (Figure 4.2). Overall, 3.0 mg/ml gels were denser than 2.0 mg/ml gels formed at the same temperature, and gels formed at 32ºC displayed much shorter, thinner fibers and a denser network than those formed at 24ºC. Furthermore, gels formed at 24ºC displayed fibril bundling that is not typically seen in gels formed at 32ºC. These temperatures were chosen to maximize differences in gelation structure; although 32ºC is not physiologically relevant for humans, it was the highest temperature at which gelation occurred slowly enough to capture crossover times.

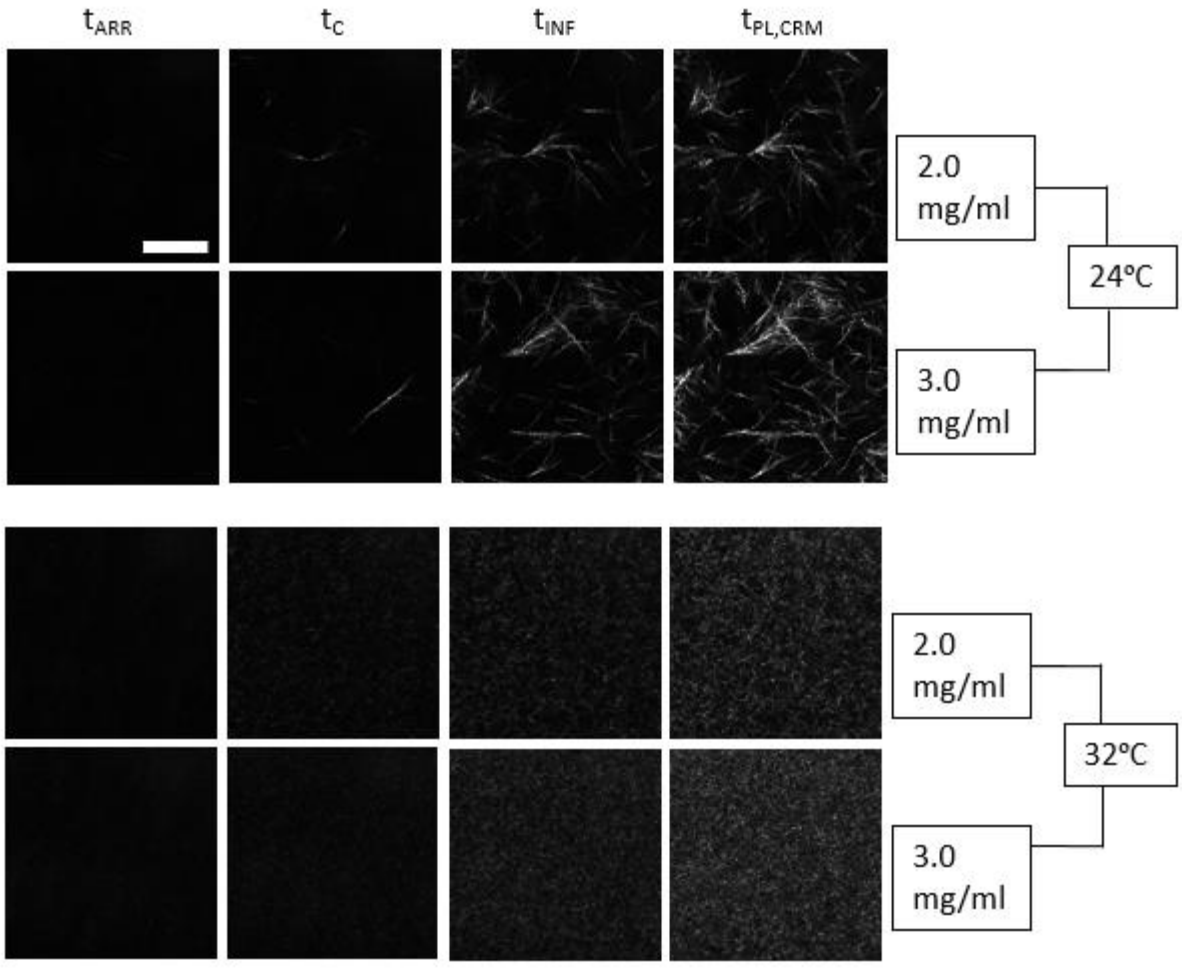

Figure 4.2: Comparison of 2.0 and 3.0 mg/ml collagen gelled at 24ºC and 32ºC

4.2.2.2 Time points of interest

Table 4.1 shows the time points of interest for all samples. Gelation times for 2.0 mg/ml were slower than that for 3.0 mg/ml. The difference in gelation progression between different concentrations was much smaller than that at different temperatures – while gelation at 24ºC occurred slowly enough to capture the entire nucleation and growth process, gelation at 32ºC occurred so rapidly that it was difficult to capture any images prior to arrest, with gels fully formed within a few minutes. From these results, gels were structurally and visually defined much earlier

than what was seen rheologically, and also a spanning structure was present well before any rheological development was observed. Additionally, the relative time course for gelation across all sample types was similar at early time points (for example, t_C / t_{ARR} ~ 3), but relative time from t_C to t_{INF} and from t_{INF} to t_{ARR} started to differ in 24ºC and 32ºC samples. Arrival at t_{PL} occurred much later for 32ºC than for 24ºC, which may reflect different gelation mechanisms that resulted in the very different equilibrium structures.

Table 4.1: Time points of interest across all gel conditions

mg/ml, ºC	t_{ARR}	t_C	t_{INF}	$t_{PL,R}$ (log)	$t_{PL,CRM}$ (linear)
2.0, 24	5.8 ± 0.8	18 ± 2	22 ± 2	27.4 ± 0.8	32.4 ± 1.6
3.0, 24	4.6 ± 0.7	12 ± 1	19 ± 2	20 ± 1	27 ± 3
2.0, 32	0.3 ± 0.1	1.0 ± 0.2	1.5 ± 0.2	3.2 ± 0.2	3.4 ± 0.3
3.0, 32	0.19 ± 0.06	0.48 ± 0.07	1.2 ± 0.2	2.2 ± 0.1	2.8 ± 0.2

Although cross-correlation analysis had been used in the past to validate t_{ARR} (86), this analyses was not used to identify t_{ARR} in this instance because t_{ARR} often appeared very early on in the gelation process where only a few fibrils were seen. However, the few fibrils seen were did not change positions within the field of view and grew thicker and brighter over time. Unlike in the previous study, there was very little to no unidirectional flow even at low gelation temperature, which may be due to the thinness of the samples (with a truncation gap of 100 μm, the thickest part of the sample would be ~ 400 μm at the edges of the tool) and the quick heating produced by the dual Peltier temperature controls. At the objective focal point in the x-y plane of the sample, the gap size was approximately 140 μm. According to (155), a gap size should be at least ~ 150

μm to not cause a magnified stress or strain response, but a gap size just short of that should be acceptable and the bulk moduli values were within range of that of other studies. More interestingly, results from the microscopy seem to contradict prior studies using CRM/IST to some extent because there appeared to be significant lengthening of network simultaneous with thickening of fibrils, especially in the minute immediately after t_{ARR}. This discrepancy could be due to the much thinner sample used in these studies as compared to the thicker gels used in previous studies. One possibility is that the samples were so thin that heat transfer occurred more rapidly and resulted in fibrils in closer contact to the tool acting as nucleators for gelation.

4.2.2.3 Moduli at time points of interest

Storage and loss moduli at time points of interest are shown in Table 4.2, except at t_C where $G_C = G' = G''$ so only one modulus is shown. At t_{ARR}, for the samples at 24ºC, G'' was more consistent than G' because G' was initially very low or sometimes not detected until a few minutes had passed after gel initiation, and in general, G at earlier time points was more variable than at later time points. Moduli values for gels at 32ºC were overestimated because arrest likely occurred earlier than what was visualized, both because of the required set-up time in getting each sample mixed and properly situated before imaging (~ 1.5 min) and because very small fibrils did not scatter enough light to be detected.

Table 4.2: Moduli at time points of interest

mg/ml, ºC	G at t_{ARR}	G_C at t_C	G at t_{INF}	G at $t_{PL,R}$ (log)	G at $t_{PL,CRM}$ (linear)
2.0, 24	0.03 ± 0.03 0.13 ± 0.05	0.4 ± 0.2	3 ± 2 1.2 ± 0.4	10 ± 2 2.3 ± 0.4	12 ± 3 2.5 ± 0.5
3.0, 24	0.04 ± 0.02 0.18 ± 0.08	0.7 ± 0.2	22 ± 8 5 ± 1	27 ± 5 5.6 ± 0.8	35 ± 4 6.6 ± 0.7
2.0, 32	0.03 ± 0.04 0.10 ± 0.04	0.23 ± 0.07	1.8 ± 0.6 0.55 ± 0.05	8.2 ± 0.7 1.6 ± 0.1	8.4 ± 0.7 1.6 ± 0.1
3.0, 32	0.09 ± 0.07 0.02 ± 0.01	0.4 ± 0.2	7 ± 2 1.7 ± 0.4	20 ± 3 4.0 ± 0.5	22 ± 3 4.2 ± 0.4

As expected, equilibrium gels with higher concentrations of collagen and denser networks had higher G' and G''. Equilibrium gels at the same concentration are more similar rheologically than gels of different concentrations formed at the same temperature, so concentration is more important in determining the final moduli than the temperature at which gelation took place. For both concentrations, gels formed at 24ºC were slightly stiffer than their counterpart at 32ºC; this trend is observed because the fibrils formed at 24ºC are significantly thicker, more bundled, and store more elastic energy, so the storage moduli are more different than the loss moduli in absolute pascals. The ratio of storage and loss moduli for a 2.0 mg/ml gel formed at 24ºC compared to that formed at 32ºC is consistently greater than 1, as shown in Table 3, and the same applies for 3.0 mg/ml gels at both temperatures (ratio at t_{ARR} only shows this sometimes because there is significant variation in moduli measured at early time points. In fact, for gels at the same concentration but formed at different temperatures, the rheological gelation curves are extremely similar and overlap well when the 32ºC curve is stretched out in time to match that of the 24ºC curve. This seems to indicate that either the rheological curve cannot give direct information about

gelation mechanism or that the gelation mechanism is the same at both temperatures, supporting the claim that it is nucleation that sets the ultimate gel structure.

For gels at the same temperature, their moduli at t_C was much more similar than moduli at later time points t_{INF}, $t_{PL,R}$, and $t_{PL,CRM}$, as shown in Table 4.3. This observation was supported by the imaging, which showed that at crossover, gels at a particular temperature were very similarly structured in terms of fibril properties (number, length, and width) which started to differ more by the end of gelation. In other words, it was not possible to predict the conditions under which gelation occurs by looking at the structure of the gel at t_C. Ratios obtained at t_{ARR} were not reliable enough to come to any conclusions, since there was a lot of fluctuation in absolute and relative moduli during the lag phase in rheology. Ratios for t_{INF} were especially high—since t_{INF} was extracted from the CRM intensity curve, it appeared that the CRM intensity inflection point for 2.0 mg/ml occurred when the rheological development was two-thirds complete (at 24°C, average $G_{INF}' \sim 22$ Pa, compared to $G_{PL}' \sim 27$ Pa, and at 32°C, average $G_{INF}' \sim 7$ Pa, compared to $G_{PL}' \sim 8.2$ Pa), whereas for 3.0 mg/ml the CRM inflection point occurred relatively early as compared to the rheological development (at 24°C, average $G_{INF}' \sim 3$ Pa, compared to $G_{PL}' \sim 10$ Pa, and at 32°C, average $G_{INF}' \sim 1.8$ Pa, compared to $G_{PL}' \sim 20$ Pa). The higher concentration gels were less mechanically developed by CRM inflection even though structurally they looked very similar to equilibrium gels at t_{PL}. Mechanical stiffness was accounted for as fibers grow thicker from t_{INF} until t_{PL}. At early time points, rheology was less sensitive to structural changes observed, but at later time points when fibrils appear to thicken, CRM changes are very low as compared to rheological changes.

Table 4.3: Ratios of moduli for 2.0 / 3.0 mg/ml collagen at time points of interest

Ratio for G'	t_{ARR}	t_c	t_{INF}	$t_{Pl,R}$	$t_{PL,CRM}$
24°C	1.30	1.64	6.64	2.78	3.00
32°C	3.21	1.97	3.76	2.49	2.61
Ratio for G"	t_{ARR}	t_c	t_{INF}	$t_{Pl,R}$	$t_{PL,CRM}$
24°C	1.40	1.64	3.96	2.45	2.63
32°C	2.44	1.97	3.14	2.54	2.63

Because taking the direct ratio can be somewhat misleading since the moduli were plotted on a logarithmic scale, taking the ratio of log(G for 2.0 mg/ml) to log(G for 3.0 mg/ml) was done and also produced similar results (not shown). Patterns seen for G' were also present for G''.

4.2.2.4 Mesh size at time points of interest

At 24ºC, both 2.0 mg/ml and 3.0 mg/ml gels displayed long and thick fibrils with a high degree of bundling. This bundling results in relatively large pore sizes for the equilibrium gels, ξ_{char} = 15 ± 6 μm and 7 ± 3 μm, as compared with gels at 32ºC, ξ_{char} = 3.0 ± 0.3 μm and 2.5 ± 0.1 μm, for 2.0 mg/ml and 3.0 mg/ml respectively. The evolution of mesh size for gels of different concentrations or different temperatures all follow the same pattern, where mesh sizes are very large initially (if calculated at all) and exponentially decrease until reaching some plateau. The errors associated with gels at lower temperature are much larger due to the heterogeneity of the gels. Because the imaging objective is in a fixed location, images taken of multiple fields of view per sample are unfortunately not possible with the setup used. Confocal reflectance imaging limits the view to a thin z slice of the gel so that explains why interconnectedness of the fibril network at lower temperatures is not seen in each slice (there is significantly more "empty space" at 24ºC

than at 32ºC). Using the ξ_{char} method, trustworthy mesh sizes from t_{INF} and later could be determined by thresholding using the image at t_{PL}.

Table 4.4: Mesh size evolution

mg/ml, ºC	ξ_{char}* at t_c	ξ_{char}[1] at t_{INF}	ξ_{char}[1] at $t_{PL,R}$ (log)	ξ_{char}[1] at $t_{PL,CRM}$ (linear)
2.0, 24	33 ± 3	24 ± 9	16 ± 6	15 ± 6
3.0, 24	44 ± 20	13 ± 5	11 ± 6	7 ± 3
2.0, 32	Threshold not reliable	8.2 ± 0.8	3.1 ± 0.3	3.0 ± 0.3
3.0, 32		8.3 ± 0.6	3.0 ± 0.3	2.5 ± 0.1

[1]Used threshold from image at $t_{PL,CRM}$
*Used threshold from image at t_C

However, at earlier time points like at t_C, using the threshold obtained from iterative methods on the gel image at t_{PL} did not work well because very few fiber pixels remained after applying the threshold. This result was especially true for images at 32ºC since the fiber networks were already too dense as soon as any fibers were visible or distinguished from background intensity. At 24ºC, for images at t_C, thresholding was done by applying iterative methods directly to that image and then calculating ξ_{char}. At 24ºC, the difference between ξ_{char} at t_C and t_{INF} was much bigger than the difference between ξ_{char} at either $t_{PL(R, CRM)}$ and t_{INF}. Although fibrils reached arrest very early on during the course of gelation, the network fills in as more fibrils become visible between t_C and $t_{INF,}$ which explains the large decrease in ξ_{char} during this period. Between t_{INF} and either t_{PL}, very few new fibrils become visible as the structure is completely set but fibrils increase in intensity as they thicken, accounting for the smaller decrease in ξ_{char}.

4.2.2.5 Critical gel point

Historically, the gel point has been defined as a phase transition from a liquid to a solid, caused by the growth of a network structure to infinite molecular weight (156). In well-studied cross-linking polymers, this is a well-defined point during polymerization: the polymer is at the gel point if its steady shear viscosity is infinite and its equilibrium modulus is zero (112). Physically, the gel point occurs when one of the molecules has grown large enough to reach the length scale of the sample (112). Typically, the gel point has been observed in rheological measurements when G' increases faster than G'' and crosses over, resulting in a cross-linked gel that has a G' value larger than G''. This is the same definition as the t_C discussed previously. However, the gel point should be a physical characteristic of gels independent of measurement frequency, so some studies utilized percolation theory as another approach to understanding gelation in a frequency-independent manner. This approach assumes monomers to occupy sites in a lattice, with some probability p that two neighboring lattice sites will form a bond. There exists some probability p_c at which all the lattice sites become an interconnected network structure, which can be calculated for lattices of different dimensions. Solutions above the percolation threshold become critical gels (157). Attempts have been made to fit collagen gelation into the percolation model (95, 106), with varying degrees of success, and was also performed below, using Equations 1-3 described earlier.

Tan δ (= G'' / G') values were used to identify t_G for gels at the same temperature and concentration but different frequencies and Equations 1-3 were applied. Unlike typical critical gels, the tan δ did not crossover at a specific time to give a distinct t_G value, but instead, t_G was determined to be the time at which tan δ converged both by eye and analytically. The precise convergence time for the tan δ of the 3.0 mg/ml gels technically occurred prior to starting rheological measurements, so the calculated value of Δ was presumed to be inaccurate and higher

than the actual value. Unfortunately, this method of obtaining Δ was limited by the speed of sample set-up on the rheomicroscope. However, this limitation did not account for the complete overlap of tan δ for 3.0 mg/ml gels. If the methodology allowed for earlier measurements immediately after initiating gelation, tan δ would have been very large and the time at which tan δ overlapped across frequencies would have been a time very shortly after initiation, which would have occurred much earlier than t_C. That would indicate that the gel itself reached a frequency-independent gel point very quickly, and that fibrils formed within a short amount of time after gelation initiation. Speculation was difficult here because no imaging was available to determine what occurred this early during gelation.

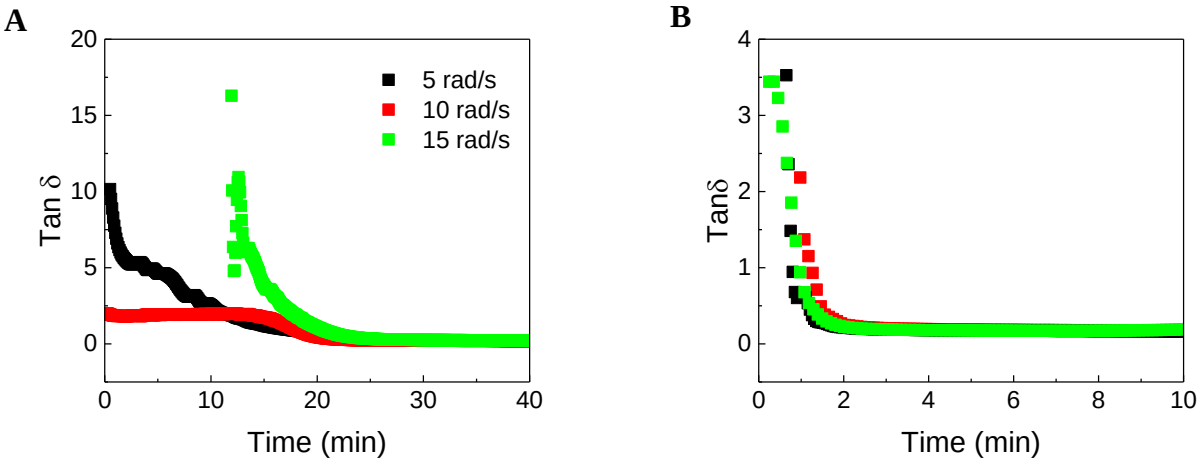

Figure 4.3: Tan δ convergence curves for 2.0 mg/ml gels

Tan δ = G'' / G' shown at **A** 24ºC and **B** 32ºC. Curve convergence does not occur until relatively late in the gelation process; this point was identified by eye and also analytically using the method described in Chapter 2.5.1.

Values for Δ are shown in Table 4.5 and in general were much lower than previously calculated values for Δ, except for Δ ~ 0.7 for 3.0 mg/ml gels formed at 32ºC (already known to be inaccurate). It is unclear what exactly a critical exponent value Δ ≈ 0.1 – 0.2 represents. This value was much lower than those typically seen in physical, chemical, and some biopolymer gels (95, 106, 158, 159). Δ ≈ 0.2 has been seen in vulcanized polyethylene and crystalline polypropylene (160). Additionally, these results showed a t_G that occurred far later than t_C and was much closer to t_{PL}. This result was contrary to many studies indicating an early gel point and was not supported by simultaneous imaging, so biopolymer gelation does not fall within the framework of percolation theory. The significance, if any, of a frequency-independent gelation time t_G was not apparent, and percolation theory did not fit well with the gelation process observed in imaging.

Table 4.5: Frequency-independent gel point and critical exponent

Conc	Temp	t_g (eye)	Δ (eye)	t_g (analytical)	Δ (analytical)
2 mg/ml	24°C	23.34 min	0.203	24.91 min	0.171
2 mg/ml	32°C	2.31 min	0.131	1.53 min	0.206
3 mg/ml	24°C	15.39 min	0.200	14.89 min	0.223
3 mg/ml	32°C	0.35 min	0.710	Excellent overlap	0.710

4.2.3 Frequency dependent gelation behavior

Oscillatory tests for materials usually include testing at variable frequencies to probe the material's time-dependent deformation behavior. High frequencies simulate rapid motion and probe short time behavior, whereas low frequencies probe long term behavior (111). Although frequency sweeps for equilibrium collagen gels are frequently reported in the literature (128, 161-

164), frequency sweeps for collagen during the gelation process are rarely seen, likely due to technical difficulties with pausing the gelation process in a non-disruptive manner.

From Figure 4, crossover modulus showed some increase with increased frequency across all conditions. However, the trend for modulus increase was relatively small and categorizes these collagen gels as materials that show frequency independent responses to oscillatory shear. This result showed that these gels had fixed structures that did not require much structural rearrangement to respond to deformations from oscillatory shear, in contrast to viscoelastic frequency-dependent materials that have too little internal structure and are easily disturbed. The slight increase in G' and G'' with increasing frequency was explained by the material becoming slightly stronger/more stiff as the speed of deformation increases (typical response for gels/materials with G' higher than G'' in general).

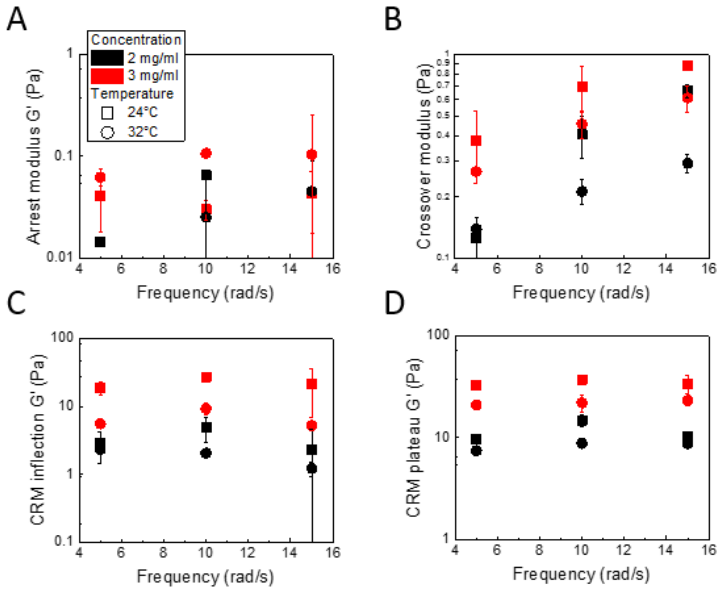

Figure 4.4: Storage modulus as a function of frequency

A t_{ARR} **B** t_C **C** t_{INF} **D** $t_{PL,CRM}$

In a previous publication, frequency sweeps of gels from 0.5 to 2 mg/ml at 22°C and 37°C displayed the same frequency dependence, $G' \sim \omega^{0.17\text{-}0.18}$ (107). The set of experiments reported here, using storage modulus measurements at $t_{PL,CRM,}$ showed a frequency dependence of $G' \sim \omega^{0.12}$, which was comparable to that from the previous publication and still demonstrated relative frequency independence. This observation also held true using storage modulus measurements at t_{INF}, with $G' \sim \omega^{0.04}$. However, at t_{ARR} and t_C, the storage moduli demonstrated noticeable frequency dependence ($G' \sim \omega^{0.90}$ and $G' \sim \omega^{0.91}$, respectively). During the early gelation periods, the solution was more sensitive to frequency and responded more like an entangled network or quasi-gel and behaved more like a high viscosity liquid rather than a fully formed gel. Typically, according to literature values, these entanglement networks displayed a frequency dependence of $G' \sim \omega^2$ and $G'' \sim \omega^1$ (165), so these collagen solutions had medium relaxation times shorter than that of chemical gels and longer than that of entangled networks.

A more careful examination of frequency dependence at crossover time is shown in Figure 4.5A and B. As frequency increased, slightly slower t_C's and higher CRM intensities at t_C were seen, which was more obvious at 24°C but less noticeable at 32°C since the values were more spread out for 24°C samples. When t_C was normalized to $t_{PL,CRM}$, the data points for 32°C became more spread out but were still too clustered together to fit the trends at 24°C. Figure 4.5C and D show the frequency dependence of modulus at t_C and actual crossover time, both with and without normalization of modulus to modulus at $t_{PL,R}$. It appears that smaller length scale solutions became gels later than ones at larger length scales; we therefore propose that imaging is the zero-frequency limit of rheology (the longest length scale probed).

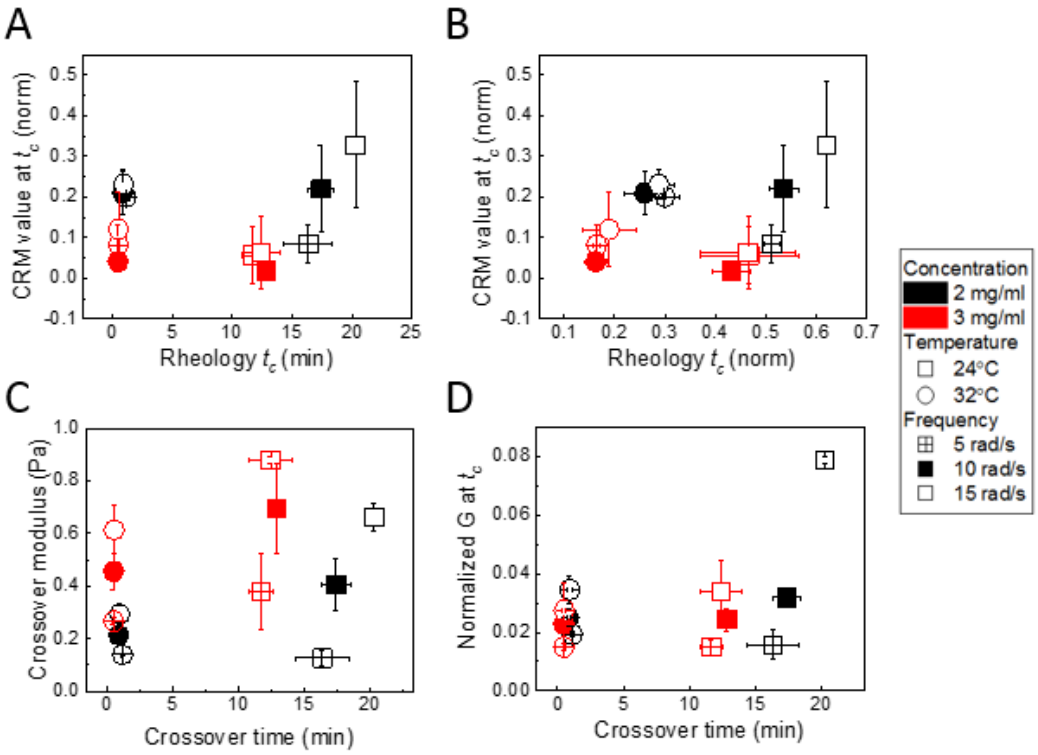

Figure 4.5: Frequency dependent trends

A t_C vs. CRM value at t_C
B t_C (normalized to $t_{PL,CRM}$) vs. CRM value at t_C
C t_C vs. G at t_C
D t_C vs. G at t_C (normalized to modulus at $t_{PL,R}$)

4.2.4 Application of MacKintosh semiflexible polymer theory

A previous publication discussed the application of two models that can, to various extents, account for aspects of collagen elasticity as semiflexible polymers. According to the model developed by MacKintosh, originally used to describe chemically cross-linked networks of worm-like chains, G' is expected to be proportional to $\xi^{-22/5}d^{28/5}$, where ξ is mesh size and d is diameter of the fibril (see derivation in (107)). This relationship holds true for semiflexible polymers where $d << \xi < l_p$, l_p being persistence length, and assumes affine deformation. For collagen fibrils formed in vitro in this study, $d \sim$ 25-100 nm, $\xi \sim$ 1-50 μm, and $l_p \sim$ 1 cm (69, 98). A similar model developed

by Morse to describe tightly entangled solutions of semiflexible polymers without accounting for cross-links predicts the relationship $G' \sim \xi^{-14/5}d^{-4/5}$ (166, 167). Because the previous publication found the MacKintosh to be a better fit across all temperature ranges, the MacKintosh model was also used with the G' and ξ obtained from this study. Proportionality constants from the previous publication were used with the current data to extrapolate fibril diameter at time points of interest prior to complete gelation.

Shown in Figure 4.6 are the fibril diameter calculations using $\log(G') = m*\log(\xi^{-22/5}d^{28/5}) + b$, where m = 0.8313 or 0.6613 and b = 9.0801 or 7.7008 (these proportionality constants were taken from (107), the first set of constants fit $d_{fiber,\ mixed}$ and ξ_{avg} data, and the second set of constants fit $d_{fiber,\ mixed}$ and ξ_{char} data). Both equations produced fibril diameters that were very close, although the second set of constants used was technically more appropriate for this data since ξ_{char} was used. For time t_C and t_{INF}, the mesh size at $t_{PL,CRM}$ was used because using respective mesh sizes at t_C and t_{INF} produced fibril diameters that did not fit what was seen during structural development through microscopy, like negative values or much larger values at earlier time points than at later ones. The fibril diameter at 24°C was about 2-3 times larger than at 32°C across time points of interest t_C, t_{INF}, and $t_{PL,CRM}$. Plotting the time point of interest and fibril diameter and using a power fit revealed the following relationships between fibril diameter through time: at 24°C, $d \sim t^{1.1\ to\ 1.2}$ and at 32°C, $d \sim t^{0.5\ to\ 0.6}$.

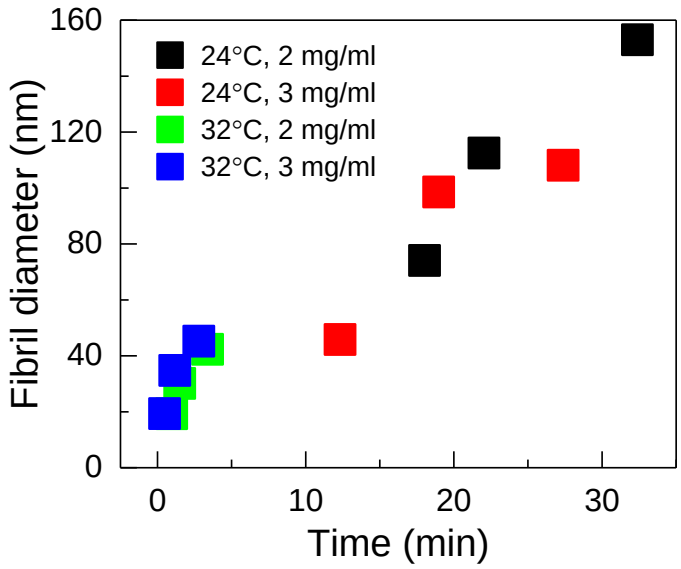

Figure 4.6: Fibril diameter over time using MacKintosh equation

4.3 Conclusion

This work focused on evaluating collagen gelation from simultaneous rheological and microscopy measurements, which provided interesting connections between structural and mechanical development for gels formed at two concentrations and temperatures. This study also examined gelation in the context of percolation and semiflexible polymer theories. Combining the two methodologies is an important tool for the study of how the structural and mechanical properties are coupled during collagen gel self-assembly.

5 Understanding mechanisms of glioma invasion in multi-dimensional environments

5.1 Introduction

Gliomas are the most common brain tumors in adults and are classified into four grades as defined by the World Health Organization, characterized by cytological atypia, mitotic activity, microvascular proliferation, and/or necrosis, as seen in biopsies (168). Glioblastoma multiforme (GBM) is the most aggressive and malignant form of glioma (Grade IV) in humans and has an especially poor prognosis. Even with the optimal treatment protocol of surgery, radiation, and chemotherapy, the median survival time for GBM patients is 1 year after diagnosis (168, 169). This poor prognosis is due to the particularly aggressive invasion achieved by GBM cells, which are often spread diffusely through the brain and makes complete surgical resection of the tumor difficult—more than 80% of tumors will reoccur within 2-3 cm of the original lesion (169). Current chemotherapeutic treatments such as anti-angiogenic compounds are marginally effective at prolonging survival but come with many adverse side effects, including neuronal cytotoxicity and inducing resistance to therapy (170). Developing more effective treatment strategies for these tumors requires, at minimum, a fuller understanding of the molecular mechanisms underlying this aggressive cell invasion.

The interaction between glioma cells and their extracellular environment is not well understood, but studies have shown that these interactions are important in driving tumor invasion into the brain parenchyma (171). The two competing theories for how high grade gliomas invade so efficiently in the crowded environment of the brain are that glioma cells effectively change their

shape and size to squeeze through small pores in the environment, and/or glioma cells use matrix metalloproteinases (MMPs) to degrade and remodel structural proteins in their surroundings to set up paths permissive of invasion (172). Glioma cell motion as visualized through brain slices from a mouse model is characterized by intermittent migratory bursts with nuclear deformation, separated by periods of little or no movement, which is consistent with the schematic depiction in Figure 5.1 (173). The migratory phenotype seen in the mouse model, together with the known dearth of extracellular space in the brain (174, 175), suggest that the glioma cells may possess the ability to change their shape and/or generate strong forces to propel the cell body forward through small pores. Both activities are expected to depend on the activity of myosin II, a molecule that is a major source of cytoplasmic and nuclear contractile force (173).

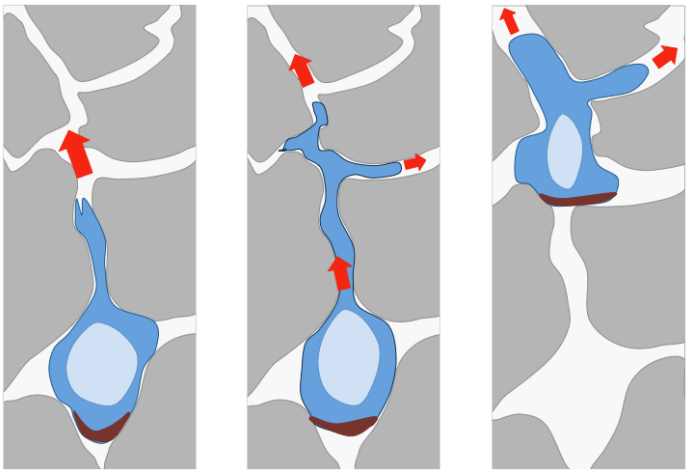

Figure 5.1: Schematic of glioma migratory phenotype

The cell nucleus (light blue), with the aid of myosin II (maroon), must change shape quickly in order to squeeze through the small spaces in the surrounding environment. This figure is adapted from (173).

In this study, type I collagen was chosen for three-dimensional cell studies of GBM invasion. Collagen, while one of the most prevalent forms of protein in the body and a dominant component in the ECM of many interstitial tissues, is not normally present in high quantities in the brain ECM (39, 176, 177). However, glioma cells have interesting associations to collagen that are not well understood. The major form of collagen in brain is collagen IV, present in the basement membranes of vascular endothelial cells. In glioma, collagen IV levels are upregulated and can be found in the basement membrane lining the tumor (39). Additionally, there is controversy about whether fibrillar collagens are found in GBM tumors; some groups reported that a subset of glioma tissues contain significant levels of fibrillar collagens like type I (176), while others reported an absence of all fibrillar collagens (178, 179). A subset of glioma cell lines express collagen-binding integrins and blocking integrin function with antibodies has been shown to reduce cancer cell invasion in rat brains (180-182). Furthermore, there is evidence that knockdown of Endo180, a receptor that mediates the degradation of collagen and is upregulated in GBM tumors, in glioma cells results in dramatic decrease in cell motility and invasion (176, 183, 184). These studies implicate collagen in the regulation and progression of GBM invasion.

In order to better understand the invasive properties of glioma invasion, it is crucial to investigate migration in well-controlled two dimensional and three-dimensional environments *in vitro* because gliomas move differently depending on the dimensionality of their environment. Glioma cells were challenged with myosin II inhibitor blebbistatin (Figure 5.2) to characterize its effects on different types of cell motility. First, glioma migration was characterized in two-dimensional gap closure assays, where cell squeezing is not required for cells to move across surfaces. Next, Transwell assays were used to evaluate the ability of cells to move through a pseudo-three-dimensional environment through pore sizes smaller and larger than nuclear size.

Finally, glioma invasion in varied pore-size type I collagen gels were characterized using the multicellular tumor spheroid model. Spheroids are used frequently for invasion studies because there exists a natural gradient for cells to invade outward, as nutrients likely have a harder time reaching the center of the spheroid. Blebbistatin did not inhibit cellular movement in two-dimensions, but did have marked effects on assays in pseudo-3D and 3D environments. Further studies will investigate other factors affecting cell shape change and/or the importance of MMP inhibition in glioma invasion.

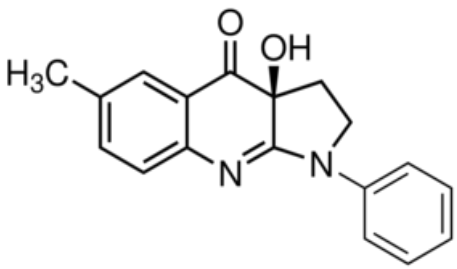

Figure 5.2: Blebbistatin

5.2 Results

A range of assays with different dimensionalities were chosen in order to assess whether the saltatory movement with cell squeezing behavior described in glioma studies was unique to C6 cells in 3D environments.

5.2.1 Gap closure assays

Gap closure assays were performed to assess C6 migration on a completely two-dimensional landscape. Cells plated on tissue culture plates were allowed to migrate into the gap for 8 hrs with or without blebbistatin treatment. Cells moving to close the gap appeared to be at constant velocity, within error, across control and drug-treated samples (Figure 5.3A). They did not display saltatory movement, rather employing a slow crawl into the gap. Individually cells would occasionally move beyond the gap front, but the majority of cells stayed in contact with other cells. Blebbistatin did not affect the 2D migration rate of C6 cells. However, blebbistatin did appear to cause cell morphology change that was not seen in the control DMEM or DMSO cells—cells exposed to blebbistatin appeared more rounded and three-dimensional (Figure 5.3B), although this morphology change did not affect migration speed.

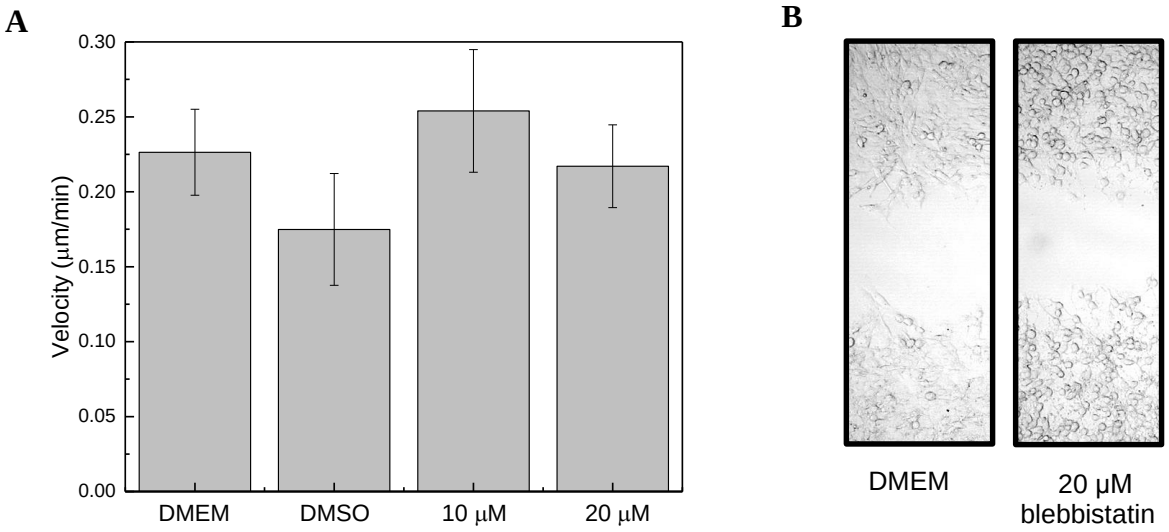

Figure 5.3: Results of gap closure assays

A Cell velocity did not change with the addition of blebbistatin. **B** Cells exposed to 20 μM blebbistatin show rounding compared to control cells.

5.2.2 Transwell migration assays

Transwell results were normalized against the migration in DMSO control samples, per field of view (Figure 5.4A). For 8 μm Transwell pores, C6 migration was the same within error across blebbistatin concentrations, and for 3 μm pores, migration decreased dramatically with increasing blebbistatin concentration. Cell viability and proliferation was the same compared to controls. The images in Figure 5.4B were processed using the Find Edges function in ImageJ, and show that the nuclei of cells that passed through 3 μm pores have distorted nuclei, appearing oblong and deformed, while nuclei that passed through 8 μm pores were mostly circular, as would be expected for cells that did not have to squeeze much to traverse through the Transwell membranes.

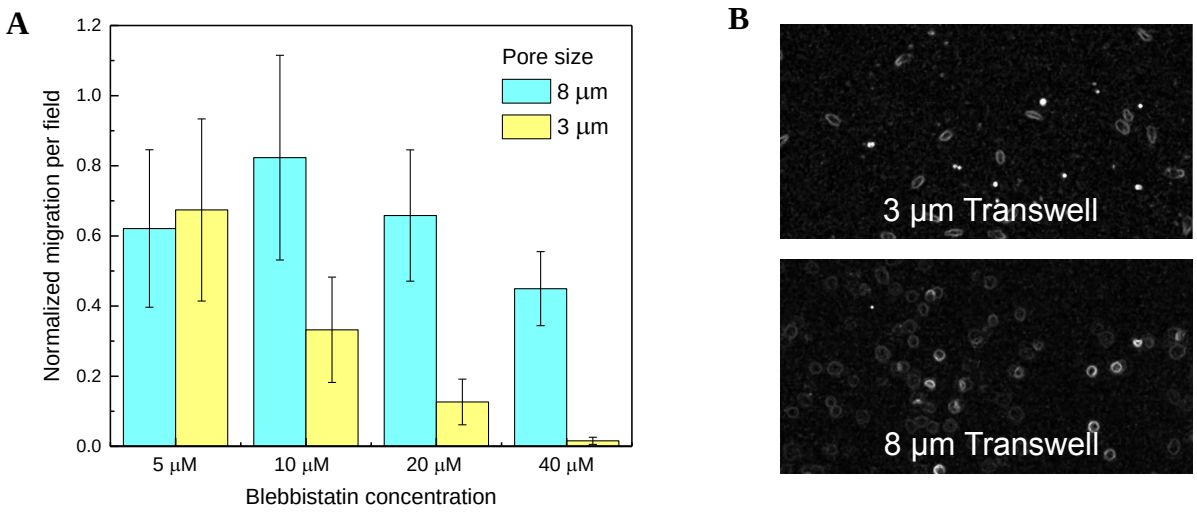

Figure 5.4: Results of Transwell assays

A Migration through 8 μm pores did not change when exposed to blebbistatin, whereas migration through 3 μm pores decreased with increasing blebbistatin. **B** Cell nuclei appear deformed when passing through 3 μm pores that are smaller than nuclear size.

5.2.3 3D collagen gel invasion assays

MTS were implanted into 0.5, 1.0, and 3.0 mg/ml type I collagen gels. These concentrations were chosen following some preliminary experiments to identify gels with different pore sizes to investigate the effect of pore size on cell invasion. The lowest concentration used, 0.5 mg/ml, has pore sizes that are comparable to being bigger than cell size, while the highest concentration of 3.0 mg/ml has pore sizes that are smaller than cell size and will require cells to engage nuclear contraction to invade. Figure 5.5 shows representative images of collagen fibrils at the collagen concentrations used:

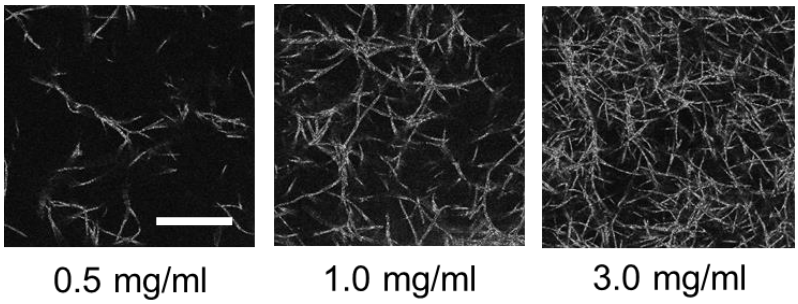

Figure 5.5: Reflectance images of pepsin-solubilized type I collagen fibrils

As collagen concentration increases, the collagen network becomes denser with smaller pore sizes, and fibrils become shorter and slightly thinner. Scale bar is 50 μm.

Spheroids were implanted into these gels and invasive distance was measured at 2, 24, 48, and 72 hrs. Invasive distance is the distance between a circle circumscribing ~90% of the outermost cells and the size of the spheroid at that time point, which accounts for spheroid expansion and proliferation that is not considered to be part of the invasion. Results from several MTS invasion assays were pooled and show the increase in invasive distance over time when implanted into

different collagen concentrations (Figure 5.6A). Differences in invasive distance between spheroids in 3.0 mg/ml gels and spheroids in 0.5 or 1.0 mg/ml gels was statistically significant across all time points, despite having large error bars. This result remained intact when the invasive distance was normalized by spheroid diameter (Figure 5.6B). Early invasion from 2 hrs to 24 hrs of spheroids in 3.0 mg/ml gels lagged behind that of spheroids in 0.5 or 1.0 mg/ml gels, but the rate of invasion catches up at later time points (Figure 5.6C). Although additional culture media with dissolved blebbistatin was overlaid on top of gels after every imaging time point, it was unclear whether spheroids were in contact with the same concentration of blebbistatin throughout the duration of the experiment.

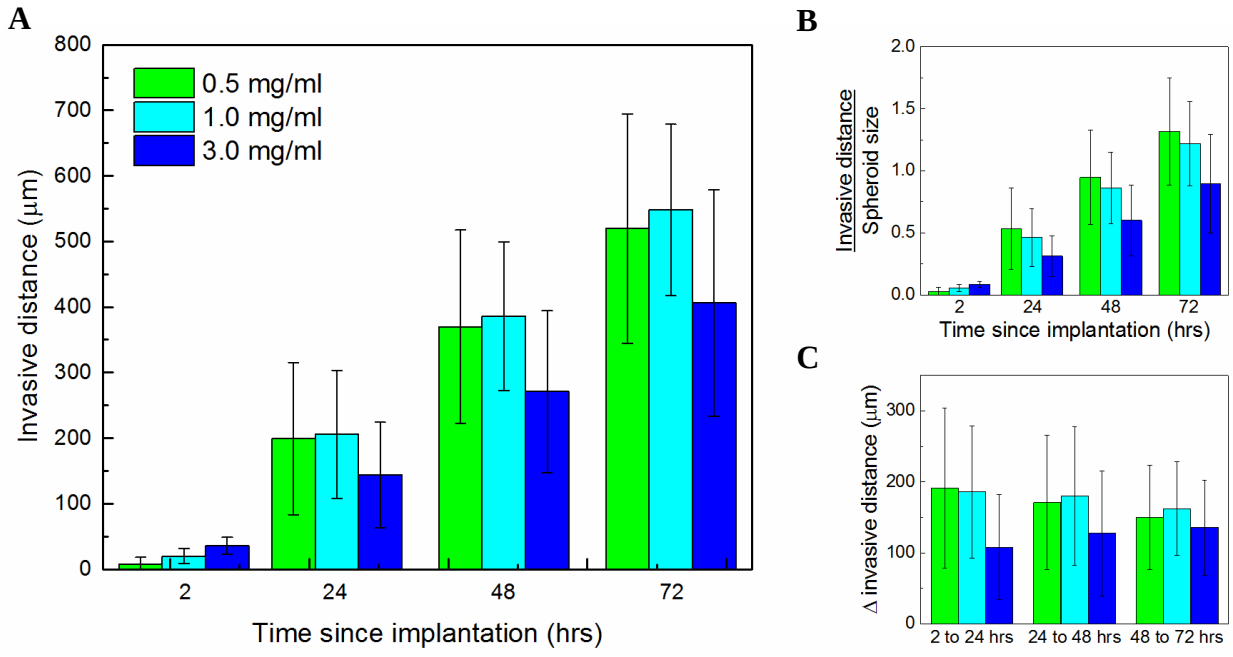

Figure 5.6: Results of MTS invasion assays

A Pooled results for spheroid invasion in different concentrations of collagen (N = 32, 36, 35 for 0.5, 1.0, and 3.0 mg/ml gels respectively). **B** Normalized invasion by spheroid size. **C** Change in invasive distance between time points.

It was likely that the local environment experienced by cells in the 0.5 and 1.0 mg/ml gels were very similar, and/or that these cells have a high capacity for rearranging their surroundings with the aid of MMPs and other digestive enzymes. The environment experienced by cells in 3.0 mg/ml gels was more challenging since pore sizes were smaller, therefore requiring more cell shape change in order to for cells to invade. Recorded invasion videos provide supporting evidence that glioma cells have the unique ability to efficiently change their cell and nuclei shapes to traverse through small spaces (Figure 5.7). Cells invading in 3.0 mg/ml gels displayed saltatory movement with significant cell shape change but such behavior was seen much less frequently in lower concentration gels.

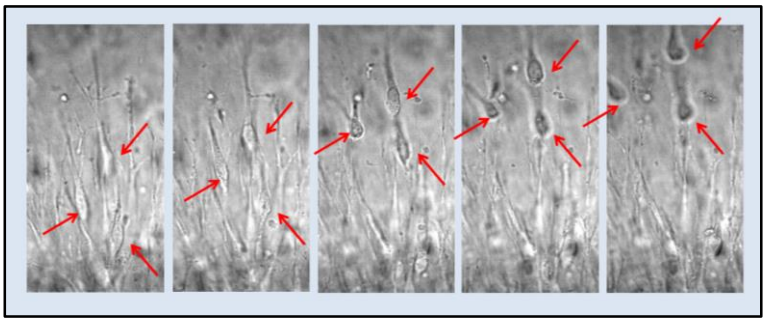

Figure 5.7: Time-lapse images of C6 migratory phenotype from video

5.2.4 Preliminary spheroid studies with blebbistatin

Blebbistatin decreased the invasive distances of spheroids without affecting their growth in 3.0 mg/ml collagen (Figure 5.8). These initial experiments were done in order to find the drug concentration that would decrease invasion without affecting cell viability. Density of cells beyond the spheroid boundary increased over the course of the experiment. Similar to in 2D assays, changes in cell morphology were observed—cells appeared more rounded (Figure 5.9).

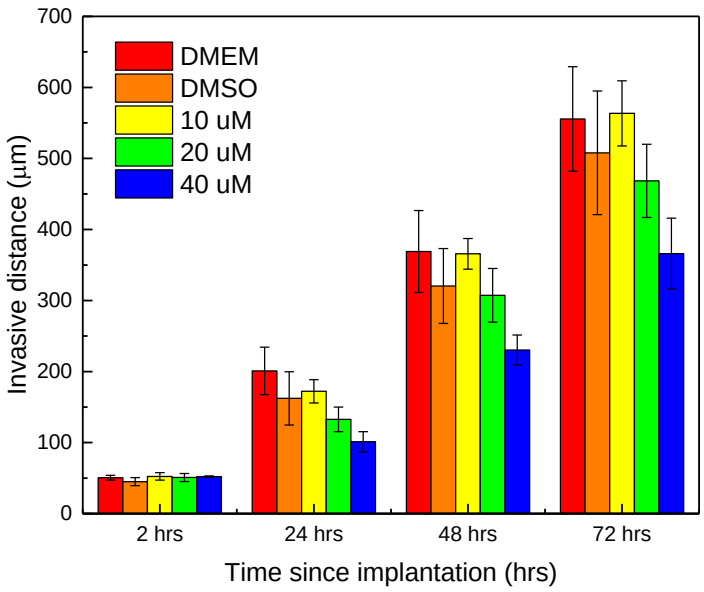

Figure 5.8: Invasive distance for blebbistatin-treated MTS

Spheroids implanted into 3.0 mg/ml collagen gels show decreased invasion with increasing blebbistatin concentration.

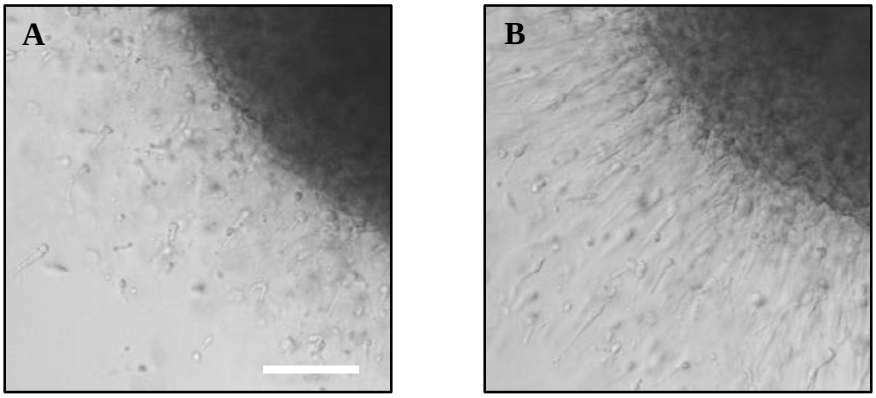

Figure 5.9: Cell invasive phenotype changes when exposed to blebbistatin

A Spheroid at 48 hrs post-implantation in 40 µM blebbistatin; cells are rounded and invade less densely than **B**, a DMSO control spheroid at the same time point. Scale bar is 200 µm.

5.3 Discussion

Glioma migration depends on a complex interplay between biophysical and biochemical factors that are not well understood, most obviously demonstrated by the lack of safe and effective therapies available to patients. A fundamental investigation aimed at a better understanding of glioma invasion mechanisms is necessary to develop more targeted treatments.

In this study, blebbistatin inhibited the ability of glioma cells to contract their nuclei, which affected invasion in three-dimensional environments that require significant cell shape change to traverse through small pore sizes. Cell migration in 2D did not require myosin II, since blebbistatin did not change gap closure rates at any concentration, and saltatory movements with cell and/or nuclear squeezing were not observed. Previous studies have proposed that the unique movement of glioma cells in 3D are an adaptation to cellular invasion in spatially constrained environments (173, 185); myosin II specifically provides nuclear contraction to allow cells to squeeze effectively through small pore sizes, but perhaps there are also other mechanisms for cell shape change involved as well. Additionally, myosin II is involved in regulating the formation of cell protrusions through its interaction with actin (186-188), so blebbistatin may also affect the cell's ability to polarize by inhibiting actin bundling and thus cellular remodeling. Across environments of different dimensionalities, cells exposed to blebbistatin caused changes in cell shape, where cells appeared more rounded and demonstrated limited ability to invade in a mesenchymal manner, characterized by cells that polarize and develop actin-driven protrusions that engage in interactions with ECM typically via integrin receptors and through the formation of dynamic focal adhesion complexes (189-193). Interestingly, some studies also report that blebbistatin slightly enhanced the speed and range of nuclear movements in two-dimensional environments (194, 195), because

inhibiting myosin II destabilized focal adhesions and was compensated for by another migration mechanism utilizing microtubule-associated motors (195).

One consideration of these MTS invasion studies is that it is possible that MTS cells were affected by the different stiffness in gels of varying pore size and concentration. 3.0 mg/ml gels are stiffer than 0.5 mg/ml and 1.0 mg/ml gels by approximately one order of magnitude difference in storage modulus. However, in a previous study, no correlation was found between bulk gel stiffness and invasion preference at such low moduli values (31). Additionally, it is well documented that glioma and other cancerous as well as non-cancerous cells preferentially invade stiffer environment (196-198), so the expected result that invasion in denser environments would be enhanced if stiffness was the dominating factor was not observed here. Also, increasing blebbistatin concentration showed increased effects on invasion, so it is more likely that cell shape change is limiting rather than a preference for stiffer substrates.

Further experiments are required to fully investigate the role of cell shape change and/or extracellular matrix remodeling in glioma invasion, and it is possible that both of these mechanisms are used simultaneously. First, the drug studies must be repeated in 0.5 mg/ml gels; expected results would show that blebbistatin does not inhibit cell invasion in low concentration gels. In addition to blebbistatin, there are other drugs that limit other forms of cell shape change, including 5-nitro-2,3-phenylpropylamino benzoic acid (NPPB) and chlorotoxin, both chloride ion channel inhibitors (199); it is also possible to knockdown myosin II isoforms in cells with RNAi and observe effects on invasion, or to target other proteins involved in migration pathways upstream of myosin II activation. Biochemical pathways involved in invasion are very complex, but some studies targeting Rho kinase in the signaling cascade have already shown potential in blocking glioma migration in Transwell assays and through brain tissue sections (185).

Glioma cells have the ability to extensively remodel their local environment through the secretion of MMPs, a family of zinc-dependent that are able to degrade various collagens (172, 200, 201). MMP-2 and MMP-9 have been shown directly to facilitate glioma progression and invasion (202-204), and other up-regulated MMPs in gliomas have been shown to be correlated with poor prognosis and shorter survival times (200, 205, 206). Although blocking MMP activity with inhibitors reduces glioma cell invasion (202), clinical trials with such inhibitors have failed and more studies are needed to fully investigate the role of MMPs in disease progression (207, 208). Additionally, other studies report that some tumor cells compensate for MMP inactivity by changing their migration mode, from classic mesenchymal migration to amoeboid migration, where cells are rounded and traverse collagen networks by squeezing through pores without substantial remodeling of the network (209, 210). Further studies require the use of specific MMP inhibitors on glioma cells to investigate whether gliomas also have the ability to shift their migration mechanism when extensive ECM remodeling is not available; visualization of MMP degradation can also be done with DQ^{TM} collagen (Life Technologies), which becomes fluorescently de-quenched when digested.

Another area where research efforts are currently underway is in the role of integrins as regulators of glioma invasion, often in conjunction with MMP activity. Integrins are found throughout cell membranes and are especially clustered in focal adhesions, large protein complexes that serve as points of contact between cells and the extracellular environment (189, 211). As mentioned earlier, focal adhesions are dynamic structures critical to mesenchymal behavior, as they are found on the tip of cellular protrusions and link the actin cytoskeleton to ECM components such as collagen, fibronectin, and laminin (212). Several integrins are highly expressed in gliomas, such as $\alpha v\beta 3$, an attachment site for the popular arginine-glycine-aspartic

acid (RGD) motif in certain ECM proteins, often found concentrated in focal adhesions at the leading edge of migrating cells (213-215). Some studies even implicate collagen-binding integrins in the β1 family as regulators of glioma invasion (216), so integrin antibodies should be used to investigate their effect on glioma invasion in collagen gel environments. Because specific integrin activation also varies with migration mode (217), additional studies targeting integrins should be completed to elucidate their role in migration in multiple dimensions.

5.4 Conclusion

Understanding of the relationship between cancer cells and their microenvironment is critical to the development of better therapeutics. The experiments detailed in this study aimed to separately test the role of cell shape change and extracellular matrix remodeling and has made progress in establishing conditions for glioma MTS studies. The ability for cells to change their shape is at least one mechanism important for glioma, and more studies are needed to fully investigate other adaptations that glioma cells have developed to invade so efficiently into the densely-packed environment of the brain.

6 Bridging the gap between instructional and research laboratories: teaching data analysis software skills through the manipulation of original research data

6.1 Introduction

Competence in computing and data analysis has become increasingly important in preparing chemistry students for careers in industry and academic research. Problem solving, which includes the ability to "analyze data using appropriate statistical methods" and to "understand the fundamental uncertainties in experimental measurements," is included in the American Chemical Society's (ACS) "Guidelines for Bachelor's Degree Programs" list of skills that must be developed within an undergraduate chemistry program (218).

In this paper, we describe a study in which ongoing scientific research was adapted for a general chemistry laboratory course. The instructors and teaching assistants (TAs) for the course collaboratively developed an assignment for students with the authors of a paper published in *Biophysical Journal* (110). This research article provided an opportunity to introduce the analysis of spectroscopy data in the context of a recent study published by a graduate student in the Chemistry department. Using raw data provided by the research group and directions created by the paper's lead author, students analyzed the data, then wrote a summary and commentary paper. The activity description and directions, as provided to the students, are provided in the Supplemental Information (see section 6.6.1 of this thesis).

Several papers have been published describing the use of Microsoft Excel and other data analysis programs in teaching undergraduate chemistry and chemical engineering courses (219-

223). These activities have included examples where undergraduate chemistry students use linear and non-linear regression models to calculate solution enthalpies according to the van't Hoff equation to investigate solubility trends for various anhydrous salts, the temperature dependence of heat capacities, or investigating the kinetics of several chemical and radioactive decay reactions (219, 221, 223). Computational programs used in the data analysis activities have included Gaussian '09, Microsoft Excel, Excel Visual Basics Application, and MATLAB (220, 222, 223). Here, we designed an activity to teach data analysis using Excel or similar computational programs by selecting a journal article from a research lab in the home Chemistry department.

The activity was designed to teach undergraduates about statistics relevant to analytical chemistry as well as to introduce them to the primary literature in the field, another key skill identified in the ACS Guidelines. There have been many papers published that focus on teaching students to locate, analyze, evaluate, and cite scientific articles, usually utilizing database searches, outlining exercises, and student papers (224-229). Increasing student exposure to primary literature in an introductory chemistry course can benefit all students, including those who are not pursing an undergraduate chemistry degree.

Here, we describe a practice in undergraduate science education in which the students develop skills in computing and data analysis, as well as the ability to critically read and evaluate scientific literature. First, the process by which the authors of the research paper designed the instructions for the data analysis activity is described, with considerations for various adaptations explained. Next, the implementation of the assignment by the course instructors and TAs is discussed, along with the iterative process of improving this curriculum initiative. Finally, we evaluate student feedback received via anonymous surveys completed after carrying out the assignment in order to assess the success of the activity in achieving the initial aims.

This collaboration was motivated by the desire to symbiotically improve both undergraduate and graduate education. As in some previous studies, we sought to teach undergraduate students how to use Excel for data analysis within the context of real laboratory experiments. Excel was provided in the computer lab and students were welcome to bring other data analysis software as long as the software allowed for the necessary data analysis. Many students begin this course with little or no experience with any data analysis programs. Because several other assignments in the course require software to general graphs and analyze data, we first wished to give students an introduction to such software that goes beyond the use of tutorials and provides an authentic research context. Second, we wanted to introduce students to reading and evaluating primary literature. For many of them, this would be their first time reading a scientific research article. Third, we intended that the collaboration would give students the opportunity to learn more about departmental research and researchers.

This type of collaboration also facilitates graduate-level education, as it provides graduate students with the opportunity to gain pedagogical experience by becoming involved with course development. Constructing chemistry curricula has been identified as a skill that can benefit chemistry graduate students and helps move advanced graduate students beyond their role as TAs (230, 231). Engagement with teaching has been found to positively impact critical research skills, such as generating hypotheses and designing valid experiments, highlighting the importance of both research and teaching during the graduate experience (232, 233). Specifically, the graduate student involved helped identify learning objectives and then redesigned the activity based on achieved learning outcomes. Additionally, in adapting research for undergraduate education, the graduate student gained experience describing her research and making research problems accessible to introductory students and non-scientists.

6.2 Curriculum development

For the activity, it was important to specify which skills students would learn. The activity was used in a laboratory course designed for introductory level undergraduates, including students with widely diverging backgrounds and skill levels. For example, while the typical undergraduate was a student attending college directly out of high school, the course also included post-baccalaureate students considering a change in career who had been out of school for many years. Students in the course varied from having no experience to extensive expertise with data analysis software, so it was important for the activity to bring all students up to a similar level of competence so they could readily complete the three other experiments in the current curriculum that required students to use data analysis software. Students identified several skills developed in the activity as particularly useful in subsequent labs. These skills included using functions, referencing cells and workbooks, and making charts. This data analysis activity was strategically situated before the spectroscopy experiment, which was the first experiment in the course requiring students to generate a graph. In addition to orienting students to Excel and similar data analysis software, this timing introduced and contextualized terminology that was to be discussed in the next class session, specifically, wavelength, path length, and absorbance.

The article selected for the development of this exercise was deemed appropriate for several reasons: 1) the chemistry concepts related directly to material covered elsewhere in General Chemistry and General Chemistry Laboratory curricula, 2) the vocabulary introduced ideas to be discussed in the next lecture, thus providing context for the students when preparing for their next laboratory experiment, and 3) a subset of the experiments could be straightforwardly analyzed starting with the raw data collected.

The published article, whose lead author was a graduate student researcher, contained several sets of experiments, but only one was chosen for the data analysis activity. The researcher, after discussions with the course instructor, decided which type of analysis to incorporate into the activity. The particular analysis chosen was straightforward to implement, provided students the opportunity to analyze raw data, and connected to topics covered in the first weeks of the laboratory course (specifically, absorption, wavelength, and error analysis). Once a set of raw data was chosen, the researcher wrote a short introduction, tying in the research article topic to popular biomedical applications, and created an outline of steps that students would complete. The course instructor and researcher deliberated about how detailed these instructions would be. It was important for these instructions to provide a mix of technical skills and context for the researcher's data analysis decisions, e.g. the time required before beginning data collection was not identical for each sample, so the researcher tracked this time across samples and subsequently accounted for this in the data analysis.

The portion of this article selected for the data analysis activity related to turbidity increase during collagen fibrillogenesis. Turbidity measurements during the collagen self-assembly process were collected at six wavelengths to reveal fibril diameter over the course of fibrillogenesis (110). This biophysical experiment provided a link between the medical interests of many students and the visible spectroscopy experiment scheduled for the lab session following this data analysis activity. The General Chemistry Lab students carried out a portion of the full data analysis described in the publication. Students were first introduced to the article with a seventeen minute video recorded by the graduate researcher: this presentation (with audio) provided background on the role of collagen in the body, the research lab's interests, and an overview of the experimental design with data collection (see presentation slides, without audio, in section 6.6.2 of this thesis).

During the activity, students were provided with a handout that included an introduction and task-oriented directions that led them through each step in the data analysis with a focus on the researcher's goal and reasoning (section 6.6.1). The directions avoided specific instructions on what buttons to click. The first set of students who participated in this activity (during the Summer of 2014) were able to submit questions directly to the graduate student researcher (section 6.6.4). These questions and the researcher's response were provided to future students as an additional resource when writing a final paper that required both a summary and commentary section. The directions for the final paper placed emphasis on student reflection on their engagement with the data, and asked students to explicitly identify aspects of the article they found challenging as well as find links to the material studied in the laboratory course.

6.2.1 Researcher collaboration

The initial adaptation of the published journal article for this activity was completed by the primary author of the article. The goals from this perspective for adapting the research publication for a laboratory classroom setting were two-fold: first, to choose one out of several experiments presented in the article to adapt with the objective of introducing undergraduate students to basic data analysis skills; second, to develop the graduate student's own skills in curriculum development. In achieving these goals, the primary author of the article collaborated extensively with laboratory instructors and TAs to identify factors for a successful adaptation.

For the graduate student researcher, developing the article into a data analysis activity was an opportunity to be involved in curriculum development and approach teaching from a unique perspective. It was also an opportunity to explain the research to non-scientists. When the exercise was initially implemented with the small courses that ran over the summer, the researcher led a

session with students to answer questions after the exercise and also led a tour of laboratory where the research was conducted. In subsequent semesters, with more students completing the exercise, it was not possible to include a lab tour and an introductory video was utilized instead.

6.2.2 Curriculum implementation

With a draft of the instructions written by the graduate student preceptor, the instructors and undergraduate student TAs implemented the assignment as part of the curriculum of a six-week general chemistry laboratory course held during the summer session of 2014. The small class size, increased instructor to student ratio, and short course length with two six-week courses offered back to back provided an opportunity to pilot the activity twice with adaptations between. There were two TAs (in this case, fourth-year undergraduate chemistry majors) and one faculty instructor for each six-week course. The implementation of this assignment was an opportunity for these undergraduate TAs to gain experience in the iterative process of course design, implementation, and redesign.

We carried out the first implementation with 29 students, assigning mandatory time in the department's computer lab for the students to work on the activity for a two-hour period. Students were given and told to read the original article and the instructions and to complete the activity described in the instructions. Students were not required to complete the activity in that two-hour period, but instead instructed to complete as much as possible in class, with the understanding that there would be an additional dedicated drop-in office hour with the instructor and TA available to answer questions.

Because many students had little or no experience using Excel, and because the majority of them had never read a scientific journal article, there was initial resistance to carrying out the

assignment. The instructor and TAs had to convince students that struggling through reading the article and understanding the steps in the assignment was not only normal, but actually integral to the process of reading and understanding scientific literature and to processing data with data analysis software. However, their feedback was also used to clarify and modify the instructions. Although students still struggled during the second six-week course, they completed the assignment in less time than the first section, despite having no more experience with Excel. The first set of students completing the activity reported an average of 2.5 hours spent in-class and 6.8 hours spent out of class, as compared with the second set of students who reported an average of 3.9 hours in class and 2.8 hours out of class.

The next implementation of the assignment occurred during the fall semester offering of the general chemistry laboratory course and included 124 students. Several logistical changes were made to compensate for the larger class size. Time was reserved in the department's computer lab during every lab section for two weeks. After students completed the week's experiment, they were encouraged to go to the computer lab and work on the data analysis assignment. Because there was not enough space to accommodate the full class size, this was not mandatory. The number of steps in the assignment was also reduced from 11 to 6, removing the creation of analogous graphs that were critical for the researchers but did not introduce new skills to the students. In addition to the undergraduate and graduate TAs assigned to each section, either the instructor or a TA familiar with the assignment from the initial summer sessions was available to answer student questions. Students were provided with modified instructions and the original article as well as the newly produced instructional videos. In these videos, certain steps of the assignment were demonstrated. To avoid student's copying the numbers they saw in each video, care was taken to provide details on working with Excel and using specific commands without

displaying the numbers in the sheet. The videos were crafted without audio to facilitate multiple students viewing them concurrently in a single computer lab.

At the start of the activity, students directed their questions to instructors and TAs, and one-on-one help was provided for many of the initial steps requiring basic software techniques, e.g. inserting formulas or linking data between sheets in the same file. However, as students became more comfortable with the language of the program, they began to teach each other how to complete steps and trouble-shoot difficulties they encountered. Student understanding of the data was deepened by this peer teaching, and students developed a deeper understanding of the content of the *Biophysical Journal* paper itself. Students also discussed the content of the article (for example, the relationship between turbidity and absorbance), as the last step of the experiment required the recreation of a single graph with multiple data sets, showing relationship between absorbance and time for each of the wavelengths investigated. This graph included custom error bars using the standard deviation of multiple trials and provided an opportunity for students to determine an appropriate title for their graph. Both of these skills were mentioned by students as new skills they had no previously used when generating scientific graphs.

After performing the computer laboratory assignment described above, students were assigned two writing assignments. The goal of both was to encourage students to become more comfortable tackling complex journal articles that require multiple readings and resulted in a valuable (though incomplete) understanding of the content. Students were encouraged to explicitly identify aspects of the research and article reading process they found challenging, with an emphasis placed on their reflection and engagement. The first writing assignment related to reflecting on the process of analyzing the data from the *Biophysical Journal* article and situating the data analysis activity within the context of this journal article. The second assignment required

each student to select and write about another journal article form a research lab in the department. Each student chose a unique article and no class time was dedicated to discussion of the article or data analysis therein. Both writing assignments required a one page summary followed by a one page commentary where students reflected on the process of engaging in complex and technical scientific literature.

6.3 Curriculum assessment and redesign

After completing the data analysis activity, students were asked to complete an anonymous, voluntary survey (for which IRB approval was obtained) that took approximately 6 minutes (section 6.6.3). The survey was administered over each of the four semesters in which the activity was performed (Summer 2014, Fall 2014, Spring 2015, and Summer 2015), and 190 of the 545 enrolled students completed the survey. The students surveyed were undergraduate science, post-baccalaureate, and engineering students enrolled in the General Chemistry Laboratory course. In addition to survey data, the course instructors read the two-page papers written by each student. These papers provided insight into student engagement with both the article and the data analysis activity.

Initial survey data indicated that Summer 2014 students were frustrated by lack of specificity in the directions and spent an average of 3.4 in-class hours and an additional 4.2 hours outside of class to complete the eleven steps. Subsequently, the directions were edited to provide additional tips, and an introductory video was recorded by the researcher. Following this, the Fall 2014 students spent an average of 2.0 in-class hours followed by 2.0 hours out of class completing the activity. Students in the Spring 2015 and Summer 2015 semesters reported the activity required two or fewer hours in and out of class to complete (

Table 6.1). The goal was to streamline the activity so it could be completed within two hours by the majority of the students (with additional help provided during office hours). By clarifying the directions, training the TAs, and removing redundant skills, the time required for the activity was reduced while critical components of the activity were maintained as assessed by the self reports of skills and the quality of the written papers.

Table 6.1: Implementation of data analysis activity per semester

	Summer 2014	Fall 2014	Spring 2015	Summer 2015
Number of students	29	125	272	125
Number of steps	11	5	7	7
In class support	4 hrs	2 hrs	2 hrs	2 hrs
Additional support	3 hrs	2 hrs	Office hrs only	Office hrs only
Average student report hrs spent on activity (in class/out of class)	3.4/4.2 hrs	2.0/2.0 hrs	1.8/1.1 hrs	1.7/2.1 hrs

The main change between the first two iterations of this activity was the number of steps required. Specifically, the activity was decreased from eleven to six steps by removing data processing that repeated data analysis skills already covered. After implementing this activity with the full Fall 2014 cohort, the number of steps was then increased to seven by providing more detailed instructions for steps that students found confusing.

6.4 Survey results and discussion

An overwhelming majority of students (75%) suggested this activity be maintained in the course curriculum citing a long list of skills gained by engaging with data analysis software in this way. Specifically, students mentioned linking between sheets, entering equations, and adding custom error bars to a graph as new skills they had developed.

Students in the first iteration of the activity, who had an opportunity to meet and discuss directly with the graduate student who performed the research, commented very positively on this experience. In survey responses, students indicated that they particularly liked that the module humanized the research experience and demonstrated that the graduate student was a "regular person." These responses highlighted the importance of students meeting and talking to someone who is engaged in research.

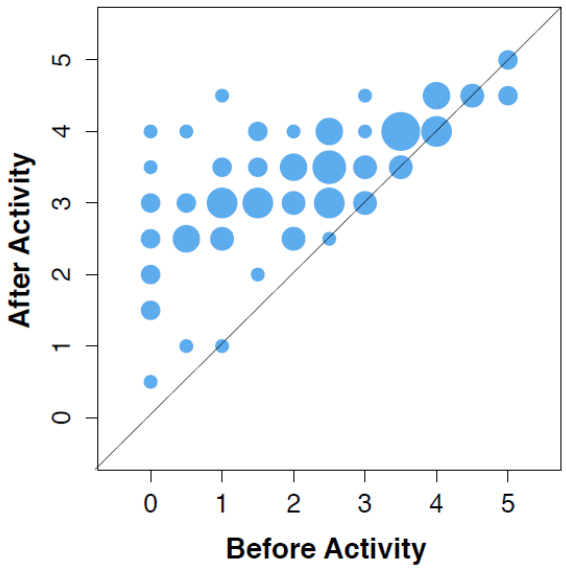

Figure 6.1: Self-reported Excel ability

Points to the left of the 1:1 line indicate a greater reported ability after the activity. The size of each point represents the relative number of responses with the largest data point having N = 6.

Table 6.2 Self-reported Excel skill before and after participating in activity

	Before activity	**After activity**
Mean	2.239	3.321
Standard deviation	1.409	0.890
N	176	176

Students t-test: $t = 14.117$; $p < 0.01$; degrees of freedom = 175

Nearly all students who completed the survey reported that their confidence and skills using Excel increased or remained the same after completing this data analysis activity (Figure 6.1 and Table 6.2). A significant difference was observed in the self-reported before-and-after Excel skills between the students who suggested we maintain this activity in the course and the students who suggested we remove it (Table 6.3); both populations showed an average reported gain in their Excel skills. Because a self-reported measure of gain was used, it is possible student frustration impacted how they reported their skills. Moving forward, it would be useful to develop an independent measure of Excel skills to address this possible issue.

Table 6.3: Gain in self-reported Excel skills by the students who suggested we maintain this activity in the course versus students who suggested we remove the activity for future semesters

Self-reported gain among students suggesting…	Activity be maintained	Activity be removed
Mean self-reported gain	1.197	0.739
Standard deviation	1.066	0.766
N	132	44

Welch's t-test: $t = 3.093$; $p < 0.01$; degrees of freedom = 102

Because the activity was intended to provide structured support for learning to face the challenges of troubleshooting data analysis software, the researchers felt it was important to avoid step-by-step instructions. How the activity was presented to students, group dynamics, and TA buy-in were key aspects in making this activity a success. These were achieved by explicitly discussing the pedagogical goals of the activity, focusing on the skills acquired in the process, and stressing the importance of these skills when seeking to join a research laboratory. Most students struggled with the initial steps (particularly if they are new to Excel) but quickly moved into helping each other and problem solving—this attitudinal shift was most notable when the TAs offered encouragement.

Analysis of the writing assignments suggested students struggled to paraphrase the research when writing their summaries. In Summer 2015, the writing assignment was redesigned to decrease the summary section to half a page, providing a page and a half of space for the commentary section. This change decreased student paraphrasing of the original article and offered more opportunity for reflection on the reading and data analysis process.

6.5 Conclusions

A collaborative approach to curriculum design provides a learning experience for the curriculum designers and the students in the course. By pairing with a research lab to share data analysis techniques, we found an opportunity to discuss pedagogical decisions with a researcher and authentic research considerations with undergraduates. Challenging students to read complex literature and supporting them through the data analysis provided to be a successful approach to teaching data analysis techniques. Moving forward in the course, little or no support was needed in subsequent laboratory and data analysis activities for the spectroscopy, acid-base, and kinetics labs. After incorporating this data analysis activity, some students asked whether they could include more advanced components in their graphs, such as error bars. Reading the second research paper (individually selecting articles about research in the Chemistry department) was also less challenging for students; they would read and re-read the article several times before looking up words and bringing questions to the instructors.

The authors would suggest the following be taken into consideration when adapting a similar exercise for a course:

1. Articles should be based on research that is appropriate for students at their particular level. The subject matter will be foreign but should build upon concepts that the

students are familiar with from the course itself. Students will be intimidated by the depth of information from the article, but their interaction with the article will be a more realistic representation of how young researchers (in contrast to experts) achieve science literacy.

2. Articles must contain an experiment (or portion thereof) amenable to an exercise that allows students to manipulate raw data. Having students interact with experimental data is an important component of the exercise, since real data will require students to use critical thinking to analyze the data and prioritize results.
3. The authors strongly encourage the practice of choosing articles that come from research laboratories within the department or the same academic institution. This connection is meaningful and has the consequence of encouraging graduate student involvement, as was the case for this study, as well as allowing students to immerse themselves in local graduate-level research.

Overall, our experience leads us to strongly recommend integration of ongoing research into instructional laboratory courses in the context of teaching basic data analysis skills for the benefit of both undergraduate students and graduate researchers. Given sufficiently clear instructions, the students will be appreciative of the opportunity, and whenever possible, face-to-face interactions between the researchers and the students are encouraged to maximize the positive elements of the exposure to the research environment.

6.6 Supporting materials

Included in this section are the activity instructions and screenshots of background slides given to the undergraduate students participating in the Excel activity. Also included are the post-activity survey given to students and a sample list of questions and answers to student questions to demonstrate their engagement in the activity. Supporting videos and raw data will be available online upon publication.

6.6.1 Activity directions

DRY LAB: EXCEL DATA ANALYSES

Introduction:

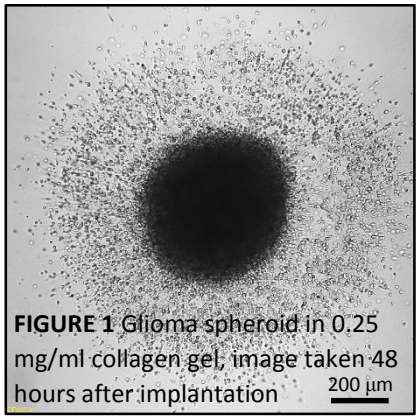

FIGURE 1 Glioma spheroid in 0.25 mg/ml collagen gel, image taken 48 hours after implantation

Collagen I is the most abundant protein in the connective tissues of mammals, present in fibrils and found in parts of the body such as tendons, ligaments, skin, corneas, cartilage, and bones. It is produced by fibroblast cells, which are responsible for making much of the extracellular matrix that gives structure to animal tissues. In research, because of its physiological relevance, collagen has been used as scaffolds in tissue engineering and as three-dimensional environments for cell studies. In the Kaufman lab, we use collagen gels to study cancer cell migration within the context of a crowded environment (1-3). **Fig. 1** shows a multicellular tumor spheroid implanted into a collagen gel, where the dark center is the original shape of the spheroid and the cells have clearly invaded radially outward. We have found that the extent of cellular invasion is dependent on the properties of the gels, which is why it is important for our lab to have control over making gels with different structural and mechanical properties. For example, a recent article from our lab (3) reported that breast cancer spheroids were much more invasive when implanted in 1.0 mg/ml collagen gels than in 4.0 mg/ml gels. It is suggested that the limited invasive behavior is due to the physical constraints of the system imposed by the increased number of collagen fibers and resulting dense meshwork.

Experimentally, collagen gels are typically prepared by diluting a commercially available stock solution of collagen monomers (extracted in our case from the tails of rats) in a buffer that provides all the necessary nutrients for cells to survive. The solution is neutralized to pH 7.4, which activates the gelation process, immediately transferred to a sample cell and placed at the appropriate temperature to allow *fibrillogenesis* to occur. During this process, collagen monomers self-assemble into fibrillar structures with network properties that are highly dependent on concentration and temperature. In general, increasing collagen concentrations will produce gels with shorter fibrils, whereas lower temperature gelation produces thicker and more bundled fibrils. See Figure 1 in reference (4) for confocal reflectance images of what fibrils look like when the self-assembly process takes place at different concentration and temperatures.

A better understanding of fibrillogenesis will allow researchers to control for these properties. To date, there have been many studies investigating the mechanism and kinetics of the self-assembly process, which have primarily monitored turbidity. During collagen I gelation, turbidity increases as a nearly transparent solution of monomers develops into fibrils that scatter significant amounts of light, resulting in a sigmoidal curve similar to that seen in **Fig. 3** below. Our studies and others support the hypothesis that collagen fibrillogenesis is a nucleation and growth process, as the sigmoidal curves have distinct lag and growth phases. Imaging techniques can also be employed to reveal the structure of the developing gel. In this lab, you will be using actual data from turbidity measurements and microscopy taken during gelation to reveal information about the collagen self-assembly process. The data and

suggested analyses comes from a recent publication (4) and has been simplified for the purpose of this exercise.

The majority of the publication deals with reconciling information from traditional turbidity measurements and modern imaging techniques like confocal reflectance microscopy by collapsing the reflectance images into a single variable that tracks traditional turbidity fairly well. Along the way, we developed a new way to simultaneously obtain *in situ* turbidity from scanning transmittance images. These measurements helped us conclude that fibril and network formation occurred before substantial turbidity was present, and the majority of increasing turbidity during collagen self-assembly was due to increasing fibril thickness (lateral assembly of monomers and small fibrils) rather than due to branching that increases overall network density (**Fig. 2**).

FIGURE 2

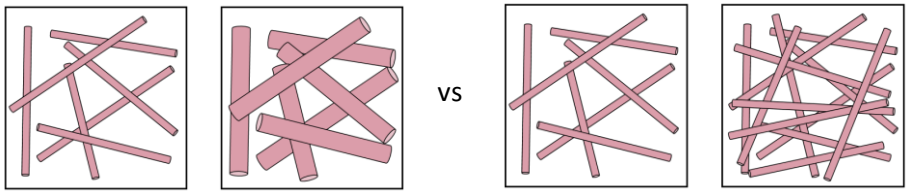

References

(1) Kaufman, L.J., C.P. Brangwynne, …, D.A. Weitz. 2005. Glioma expansion in collagen I matrices: analyzing collagen concentration-dependent growth and motility patterns. *Biophys. J.* 89:635-650.

(2) Yang, Y.L., S. Motte, and L.J. Kaufman. 2010. Pore size variable type I collagen gels and their interaction with glioma cells. *Biomaterials.* 31:5678-5688.

(3) Guzman, A., M.J. Ziperstein, and L.J. Kaufman. 2014. The effects of fibrillar matrix architecture on tumor cell invasion of physically challenging environments. *Biomaterials*. In press, available online.

(4) Zhu, J. and L.J. Kaufman. 2014. Collagen I self-assembly: Revealing the developing structures that generate turbidity. *Biophys. J.* 106:1822-1831.

Relevant Definitions

Turbidity Cloudiness of a solution caused by individual particles scattering light; can be measured using a spectrophotometer. Limited because measurement only gives a value of how much light has not passed through

Confocal reflectance microscopy (CRM) Imaging technique dependent on contrast emerging from backscattered light; we use the total intensity of these images as a measure of the gelation process. Monomers and small fibrils are diffraction-limited, so "size" is much bigger in images than in reality

***In situ* turbidity (IST)** Measure of forward scattering light calculated from intensity of scanning transmittance microscopy images. Essentially same as regular turbidity, except this has the advantage of being performed simultaneously with CRM

Goals:

Use Excel comfortably to:

1. Perform typical calculations using large amounts of data, including background subtraction, and averaging
2. Linearize data to extract slope and y-intercept
3. Interpret data in the context of a research problem

Experimental Approach:

Traditional turbidity measurements

FIGURE 3 UV spectrophotometer set-up

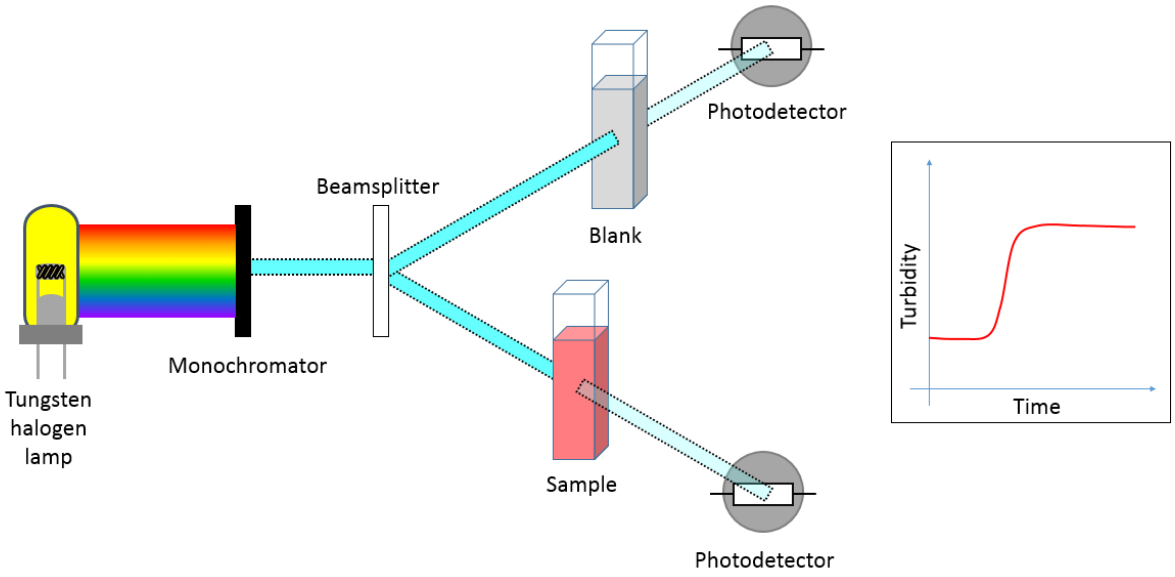

The collagen solution was made, neutralized with the appropriate amount of NaOH, then immediately transferred to a cuvette and placed into the cuvette holder. Gelation occured rapidly with the addition of NaOH, so this step was completed very quickly. The reference solution consisted of everything that normally goes into the collagen solution except for the collagen itself, which includes cell-friendly medium (even though no cells were used in these experiments, but normally we implant cells into gels), buffers, and distilled water.

For these experiments, standard turbidity measurements were performed using a dual-beam Cary 5000 spectrophotometer, which reported absorbance *A*

$$A = -log\frac{I}{I_0} = \alpha p \qquad (1)$$

with *I* the intensity of transmitted light, I_0 the intensity of transmitted light in the reference solution (the solution without collagen), α the absorption coefficient (cm^{-1}), and *p* the pathlength in cm. Turbidity τ was calculated via

$$\tau = \frac{A}{p} ln10 \quad (2)$$

These measurements were completed at certain wavelengths: 400, 458, 488, 515, 543, and 633 nm. 400nm is the standard wavelength used for collagen turbidity, while the other five wavelengths were chosen because they match with the lasers that we have in lab. Both the sample and reference were held in 1 cm quartz cuvettes, and measurements were taken every 10 s.

In situ *turbidity measurements*

FIGURE 4 Microscopy set-up

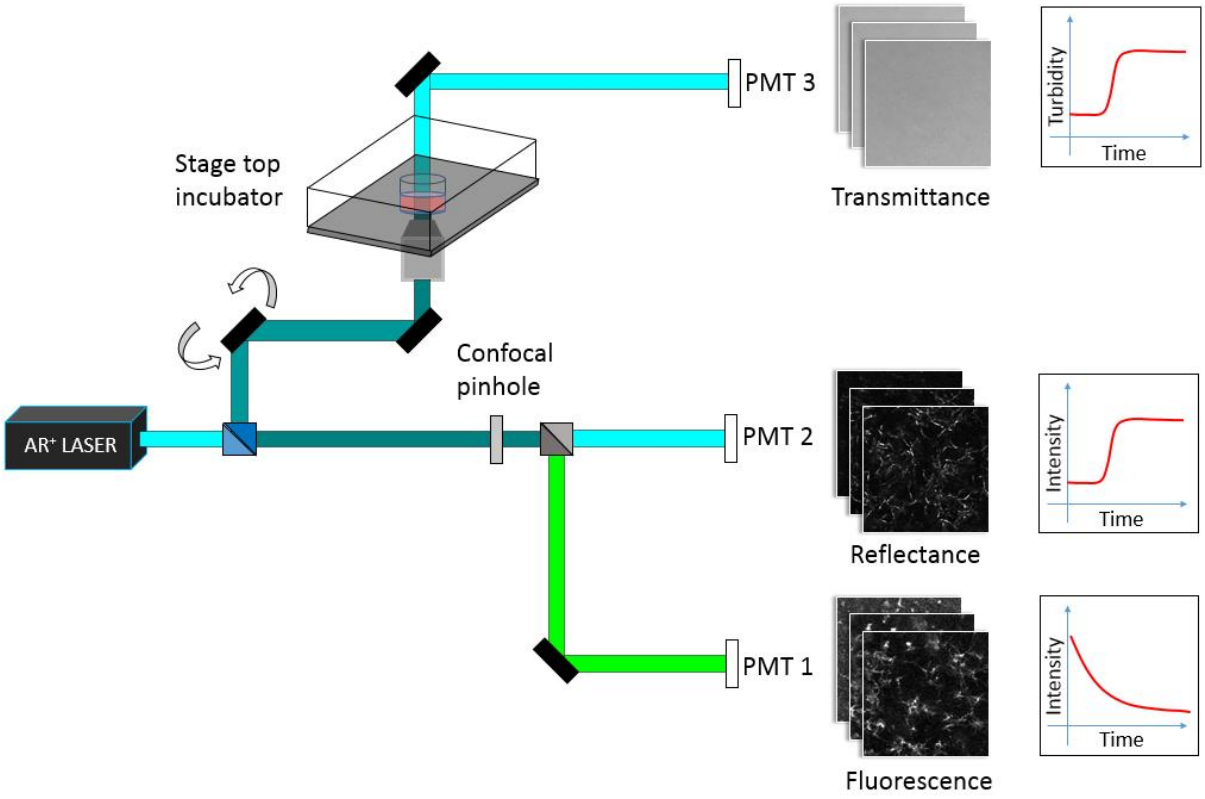

For these measurements, collagen solutions were made in the same way as above. Instead of transferring the solution to a cuvette post-neutralization, we transferred a smaller volume of the solution into a homemade cylinder that was epoxied to a glass coverslip bottom. The coverslip bottom is made of thin enough glass so that we can image using a 60x oil immersion objective, which has a small working distance of only ~50 μm into the sample. In the publication, we imaged collagen gelation using three different channels, but for the data below, we will be focusing only on the scanning transmittance channel. Laser light passes through the sample and is collected using a photomultiplier tube, producing images that get gradually darker as gelation occurs since less light is able to pass through the sample due to scattering. The total intensity of these images (sum of all pixels) is then extracted and translated into turbidity, also using Eqs. (1) and (2) and with the total intensity of the first image in the series as I_0.

There is some discussion about what the pathlength should be for this particular set-up. This is important because of the *p* to use in Eq. 2. Based on the actual volume of the solution used and the dimensions of the cylinder, *p* would be 0.4 cm. However, due to the presence of a meniscus, the actual pathlength when measured with a ruler is more like 0.3 cm. Furthermore, because we use a confocal microscope with laser, the light is actually focused into a tiny spot so that potentially changes the pathlength as well. We attempt to correct for this in the data analyses.

Data analyses:

Wavelength dependent measurements of turbidity and in situ *turbidity for 1.0 mg/ml collagen at 37°C*

Purpose Use light scattering equations to extract information about fibrillogenesis.

The data here is mostly presented in the supplementary info. You will effectively be reproducing Figures S3/S4 from the paper.

There exists a known relationship between wavelength of light and turbidity:

$$\tau\lambda^5 = A\mu(\lambda^2 - Bd^2) \text{ with } A = \frac{88}{15}\frac{\pi^3 cn\left(\frac{dn}{dc}\right)^2}{N_A} \text{ and } B = \frac{92}{77}\pi^2 n^2 \quad (3)$$

with τ turbidity, λ wavelength of light, μ mass per unit length, *c* mass concentration of collagen, *n* the refractive index of the solvent, *dn/dc* the refractive index increment, N_A Avogadro's number, and *d* the fibril diameter. For collagen in water, *n* = 1.33 and *dn/dc* = 0.186 cm^3/g. Plotting $\tau\lambda^5$ vs. λ^2 yields a slope of $A\mu$ and a y-intercept of $-A\mu Br^2$.

0. Your first exercise will be to figure out the units for all of the components that go into Eq. 3.
   HINTS:
   - From Eq. 2, absorbance has no units, but τ has units of cm^{-1}.
   - *c*, concentration, has units of g/ml.

ANSWER:

$[\tau] = cm^{-1}$
$[\lambda] = cm$
$[A] = cm^3 \times mol/g$
$[c] = g/ml = g/cm^3$
$[n]$ = unitless
$[dn/dc] = cm^3/g$
$[N_A] = mol^{-1}$
$[\mu] = g/mol \times cm^{-1} = Da/cm$
[B] = unitless
[*d*] = cm

Quantitative information on fiber dimensions may be assessed through wavelength dependent turbidity measurements. Standard turbidity assays of these gels were performed at 400, 458, 488, 515, 543, and 633 nm. From these measurements, wavelength scans were constructed at each time point (every 10 s for 10 min). We will use this data in this section to tell us about the mass/length ratio and fibril diameter throughout gelation.

1. We'll start with the absorbance data from the UV spectrophotometer. Make a new sheet and label it 'Step 1'. (It is recommended that you create a new sheet for every step in this lab.) Notice that at time ≈ 0, slightly different absorbances are obtained across the trials. This might be due to not zeroing the instrument after every trial. Let's call this background and subtract the initial value for each trial.

EXCEL TIP #1: When you copy over the columns from the original data, do NOT just copy and paste the columns. The way to reference a cell from another sheet is by starting a formula by typing '=', clicking on the sheet tab, clicking on the cell you wish to reference, and hitting 'ENTER'. This should produce a formula of the form ='Sheet X'A1 (in this example, "A1" is the cell on 'Sheet X', where "A" is the column and "1" is the row). Reference the original data so that if changes are made to this original data, these changes are applied throughout the workbook. The video below will show you how to do this. Once you link the first cell to the corresponding cell in the original data you can fill in the remaining cells in your new sheet. By placing your cursor on the bottom right corner of the cell you should notice that the cursor changes to a black cross, now drag down to the last row of data. To apply this formula to every column, highlight the column of data you just linked and drag across.

EXCEL TIP #2: The format =A$1 may be useful, the "$" tells Excel to keep the row number constant. Once you enter your formula for background subtraction you can apply this calculation to an entire column. Now drag down to fill in the background subtracted data for the rest of the cells. To fill in the background subtracted data for the remaining columns, highlight the column and drag across.

Need help? Here is a link to a video tutorial specific to this step:
Step 1 Excel lab: https://www.youtube.com/watch?v=hC0Twv6kB0I

2. Make a new sheet. Link over the columns for the time and the background-subtract absorbance values. For all the trials, calculate the turbidity from this absorbance using Eq. 2.

EXCEL TIP #3: Set-up your turbidity calculations in a new space, to the right of your absorbance data. This will make step 5 *much* easier.

Need help? Here is a link to a video tutorial specific to this step:
Reference data: https://www.youtube.com/watch?v=UjWhNq68yhM

3. Change the time from s to min by inserting a new column to the right of your data in s, then enter an equation that will convert your s to min.

4. Although measurements were taken every 10 s, remember that some time elapses after the solution is neutralized and transferred to a cuvette before measurements are started. You are given the time corrections in s – convert the time delays to minutes, add them up for each trial, then take the average and standard deviation. Now divide the standard deviation by the average to estimate the difference in the shifts.

EXCEL TIP #4: Excel has many built in formulas, i.e. for calculating averages and standard deviations. To calculate the average, type in "=AVERAGE()" and select the range of cells; to calculate the standard deviation, type in "=STDEV()" and select the range of cells.

Because the shifts differ by less than 2%, it is likely ok to ignore this correction to the time of measurements.

5. Obtain average turbidities (and the standard deviation) for the 2 or 3 trials at each wavelength (at each time by selecting across). Use Excel Tip #4 for the first formula and then drag down to the last row of data to repeat calculations at every time point.

6. Make a scatterplot of these six curves. The graph should be on a separate sheet, and should include: title, axes labels, appropriate scales for axes, and a legend. Additionally, use y-axis error bars to indicate the standard deviation of the turbidity values

EXCEL TIP #5: Insert empty scatterplot. Create a new sheet, right click on any cell, and go to Select Data. Click "Add", then select the x and y columns. Do this for each curve separately, and label the data according to the wavelength. To add the error bars, click on a curve, go to Design → Add Chart Element → Error Bars → Custom → Specify Value and select the standard deviation for both positive and negative error values. Make sure that these are vertical error bars; if horizontal error bars show up, just delete them. Repeat for each curve.

Need help? Here is the link to a video tutorial specific to this step:
Graphs and error bars: https://www.youtube.com/watch?v=c7oFwRi4iH0

6.6.2 Background slides

A PowerPoint file with audio narration for each slide was provided to students prior to the in-class computer time so that they could have additional background information for the raw data they received. These slides covered the following topics:

- Overview of Kaufman lab biophysical chemistry research
- Relevance of collagen in the human body
- Collagen self-assembly and traditional studies using UV/VIS spectrophotometry
- Experimental set-up and sample confocal reflectance/transmittance video of gelation
- Wavelength-dependent turbidity equation and results

These slides and the audio narration will be available online upon publication.

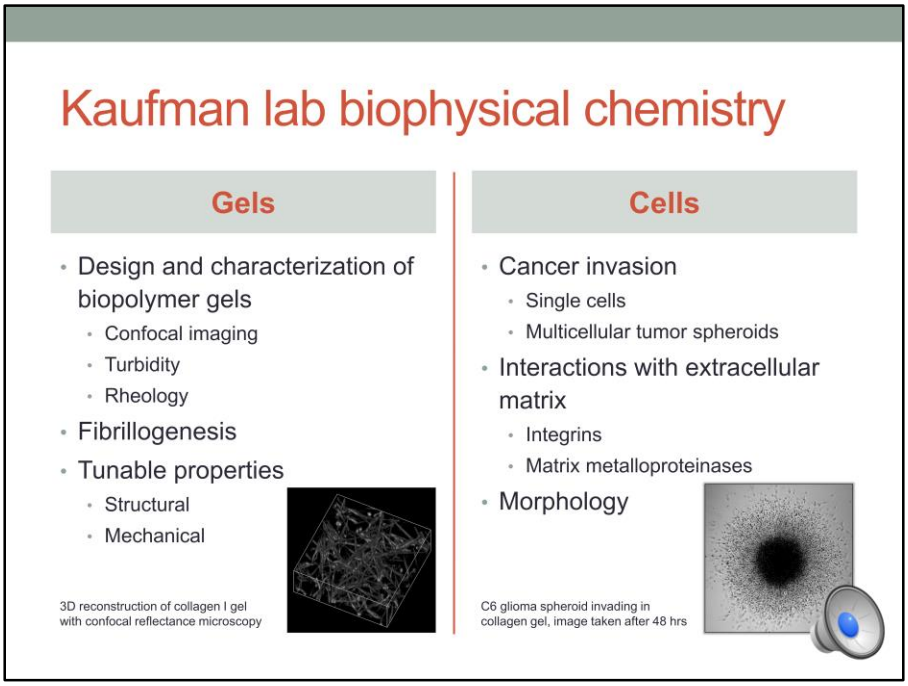

Collagen in the body

- Most abundant protein
- Structural support
- Many different types of collagen

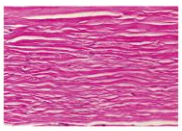

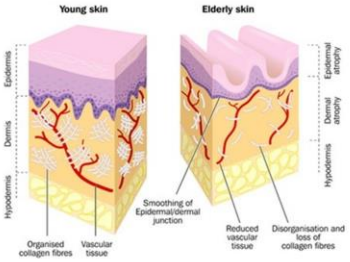

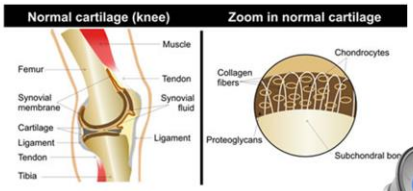

Collagen in the body

- Most abundant protein
- Structural support
- Many different types of collagen

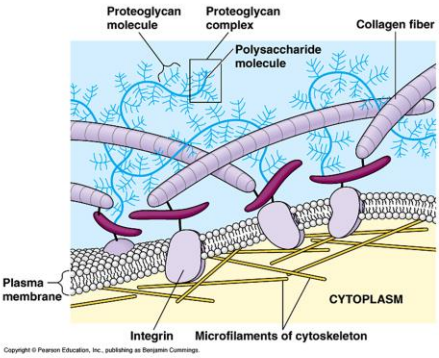

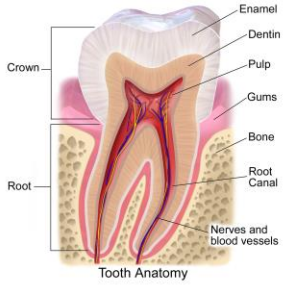

Tooth Anatomy

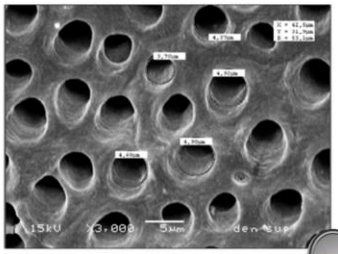

Figure 1. SEM micrograph showing dentinal tubules an
area measured under in bovine dentin.

Collagen in the body

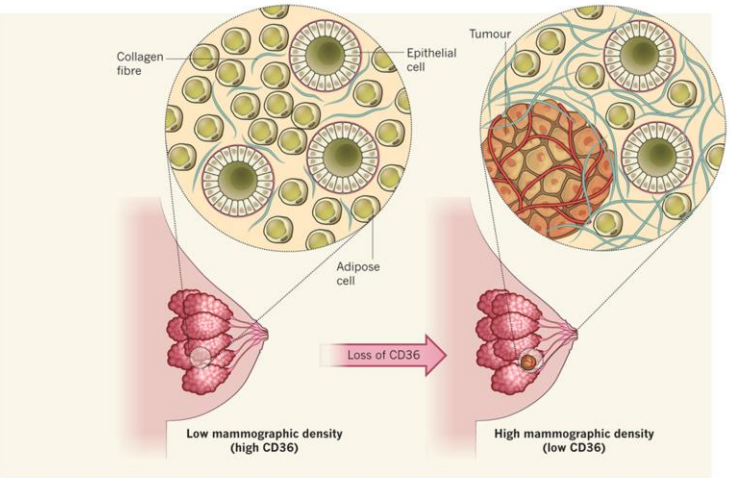

Nature **490**, 490-491 (2012)

Fibrillogenesis

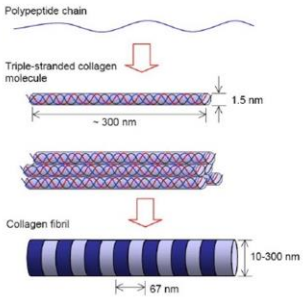

Type I collagen

- Self-assembly process
- Gelation parameters
- Structural and mechanical properties

Traditionally (since the 1960s), collagen gelation has been studied using turbidity:

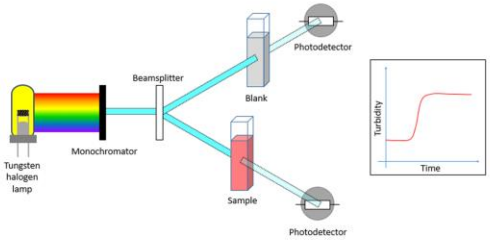

What information can we get from imaging the gelation process? How is this information similar to and different from what we get from turbidity?

Experimental set-up

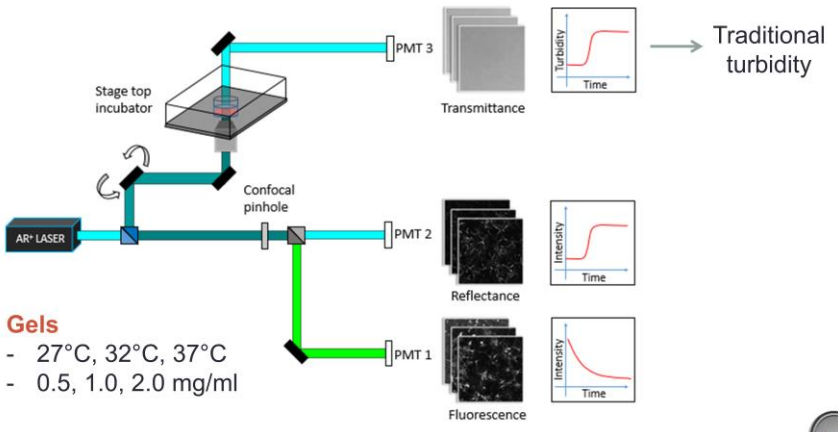

Gels

- 27°C, 32°C, 37°C
- 0.5, 1.0, 2.0 mg/ml

Sample video: 2.0 mg/ml, 37°C

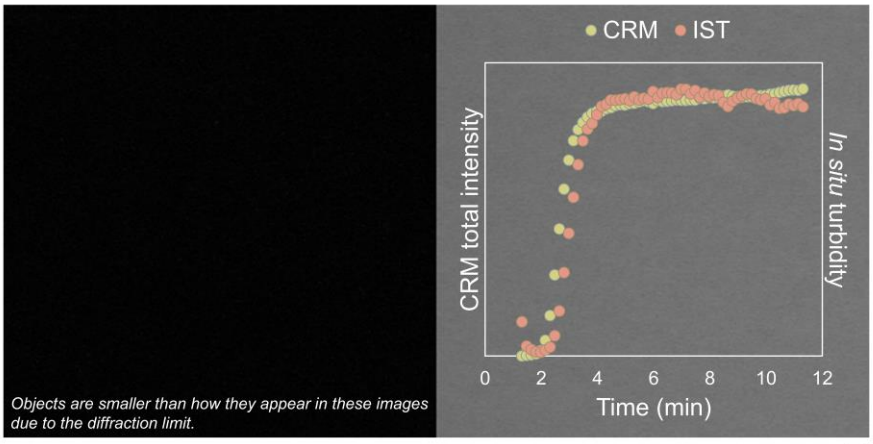

Reflectance Transmittance

Wavelength-dependent turbidity

- Specific research goals
  - Apply classic light scattering equations to turbidity and imaging data to extract fibril mass/length ratio μ and fibril diameter
  - Compare results from turbidity and imaging methods
- Identified this part of the publication as most appropriate for students
  - Spectroscopy
  - Excel-appropriate tasks

$$\tau\lambda^5 = A\mu(\lambda^2 - Bd^2)$$

Relationship between turbidity τ and wavelength λ

Experimental data gathering

- 1.0 mg/ml gels
- Turbidity
- Reflectance and transmittance images
- Light/lasers at different wavelengths

Wavelength-dependent turbidity

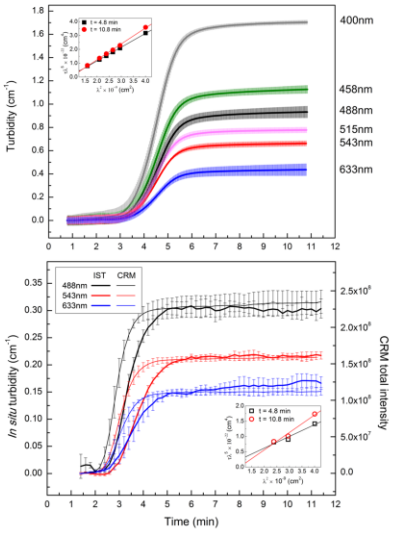

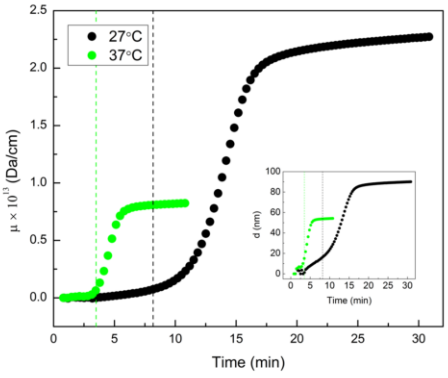

6.6.3 Post-activity survey

After students turned in the activity, they were emailed a link for this survey.

Research Purpose: The purpose of this study is to investigate the impact of an Excel activity in a General Chemistry Laboratory course. You are being asked to participate in this study because you are registered for the General Chemistry Laboratory course and have completed the Excel activity. The study consists of a single survey that is both voluntary and anonymous. The results of this study will be used for research publication and presented at conferences. If you decide to participate in this study, your part in the research will involve a survey that will take approximately 6 minutes to complete.

Risks: No foreseeable risk. To the best of our knowledge, taking part in this study will not hurt you.

Benefits: No direct benefit. You will not receive personal (direct) benefit from taking part in this research study. However, the information collected from this research may help others taking this course in the future.

Confidentiality: No identifiable information will be collected during this study. This survey is anonymous.

Compensation: No compensation is provided for your participation in this study. Participation in this study is voluntary. Refusal to participate will involve no penalty or loss of benefits to which you are otherwise entitled. You may discontinue participation at any time without penalty or loss of benefits to which you are otherwise entitled.

Additional information: If at any time you have comments or concerns regarding the conduct of the research or questions about my rights as a research subject, you should contact the Columbia University Institutional Review Board (IRB).

1. Do you agree to participate in this study?

   ☐ Yes, by selecting this box I agree to participate in this research study.

   ☐ No, I do not wish to participate in this research study.

2. Approximately how many hours did you spend <u>in class</u> working on the excel activity?

3. Approximately how many hours did you spend <u>outside of class</u> working on the excel activity?

4. Please rank your experience and knowledge of Excel BEFORE starting the Excel activity. (0 = no experience, 5 = expert)

5. Please rank your proficiency in using Excel AFTER starting the Excel activity. (0 = no experience, 5 = expert)

6. Did you find the video tutorials useful? (0 = didn't use them, 5 = extremely helpful)

7. Did you find the in-class computer lab sessions helpful? (0 = didn't use them, 5 = extremely helpful)

8. How comfortable are you using Excel to carry out your future data analysis on your own? (0 = not comfortable at all, 5 = extremely comfortable)

9. If you learned a new technique with Excel, please list at least one thing you learned doing this activity.

10. If you found the lab frustrating, please list at least one thing you found frustrating about this activity.

11. Do you recommend we include this lab in future semesters?

    ☐ Yes

    ☐ No

    ☐ Yes, if the following issues are addressed (please list issues in question 11)

12. Issues (if any) from question 10

13. Did you find the background material (provided with the Excel activity) helpful?

☐ Yes

☐ No

14. Have you read the original article yet?

☐ Yes

☐ No

15. Did you find that the Excel activity helped you better understand the original journal article? (0 = no, not at all, 5 = yes, the Excel activity was helpful)

16. Do you have any other feedback or considerations as we consider using this activity in future semesters?

6.6.4 Questions from students for the graduate student researcher

When this activity was first implemented in Summer 2014, students were required to submit three questions each after reading the research article to be answered by the graduate student researcher. The graduate student researcher used these questions as a starting point for an in-class discussion with students, but also provided written answers to students so that they could refer to them while writing a short paper reflecting on the activity. Presented here are a sample of the questions and answers given to demonstrate student and graduate researcher engagement in the activity. Student questions are in black and graduate student researcher answers are in blue.

- What prompted interest in this experiment/area of study?
- What were/are some of the largest "holes" in the research surrounding collagen before you conducted this experiment?

The biophysical chemistry side of the Kaufman lab studies how the microenvironment of cancer cells can affect their ability to invade, as a model for cancer metastasis. Often it is the secondary metastasized tumor that will kill a patient, not the primary tumor. We are interested in using collagen gels to simulate the 3D environment that cancer cells live in; but first, a better understanding of how collagen gels form will give us greater control over how we make these 3D environments.

The process of collagen fibrillogenesis has been debated over since a string of papers came out in the 60s-80s. The primary argument was over whether fibrillogenesis occurred in a nucleation-and-growth manner (as supported by the sigmoidal shape of the turbidity curve) or more like a multistep process with several intermediate fibril sizes. Our analyses supports the

nucleation-and-growth process.

- How was the moisture content in the gels maintained over the course of 30 minutes? Is moisture content in the collagen gels important to the experiment?

This is an excellent and very observant question. In the UV spectrophotometer setup, moisture is easily maintained because there were fitted lids for the cuvettes that we used. For the microscope setup, at first I tried using parafilm to cover the top of the cylinders but the parafilm was found to change shape over time, which greatly affected IST measurements (since light is transmitted through the parafilm). I eventually just kept it open to the air, and over 30 minutes, even at 37ºC, noticed that the gel was able to mostly maintain its moisture (done by eye, also could see if volume had decreased using a ruler). Moisture content is definitely important because you wouldn't want the gel to dry out too much, but there were also other constrains, such as the shape of the cylinder and making sure it all fit inside the microscope incubator system.

- Does turbidity generally stand as a one-variable measurement? Do you ever use color or hue change measurements to complement this approach?

Technically, monitoring turbidity at various wavelengths is identical to monitoring "color" developing at that wavelength. If you mean monitoring visually by eye, there is not anything that we can think of that would give collagen a particular color. Perhaps we could attach dyes that react in some way to change color when monomers come together, but this would be a chemical bond and not a physical bond and could also change the original structure.

- As a student in General Chemistry Lab, I have noticed that practice makes perfect or at least in my case, better than the previous attempt. My laboratory skills come with better results as I become more familiar with the equipment and gain experience in performing techniques. In the *Collagen I Self-Assembly* experiment, were there "dry runs" or practice attempts before performing the actual experiment in order to minimize chances of errors in technique and material preparations?

Absolutely. To give you some idea of that, I probably spent a year doing similar-ish experiments prior to doing the experiments that went directly into the paper. The experiments done for the paper took a total of maybe 1-2 weeks, but a lot of work was done prior to it all coming together.

- What are the pros and cons of using scanning transmittance microscopy as opposed to a more traditional spectrophotometer method?

The major pro is that it can be done simultaneously with imaging. We have published papers in the past that correlated traditional spectrophotometry with imaging, but it was hard to conclude much quantitatively because the samples are different since they had to be done separately.

- I was fascinated by your careful, quantitative comparison of turbidity and CRM intensity - particularly how you singled out CRM intensity as giving comparable sigmoidal shapes as those produced in turbidity curves. Perhaps this is obvious, but, did you know in advance that these two curves would be comparable, or was that experimentally determined? Also,

you mentioned that there were possible differences between the standard turbidity and the IST setups in terms of heat transfer. Earlier in the article, it was mentioned that the heating mechanisms were made in-house. Did this hiccup seem to make sense after the fact (i.e. do you think it might have been avoided), and how difficult was it to correct?

No, we did not know that CRM would be similar to turbidity for the reasons stated in the paper (monitoring different proportions of light in the forward direction for IST vs. reverse direction for CRM) and were surprised that the curves ended up being similar. In terms of differences in heat transfer, this is more due to the shape and size of the sample holders than to the fact that we made our heaters in house. Yes, we could potentially make both heating systems the same and control the degree of heating better, but we did the best with the equipment that we had.

- Is there a significant difference in cost, time, or work between the imaging techniques explored in the paper? Alternatively, if CRM imaging is more sensitive to early stages of self-assembly, are there other advantages to IST or traditional spectroscopic turbidity measurements? Two research methods are discussed in the article: turbidity and imaging. What are some of the specific advantages and disadvantages of each method in terms of what types of data they provide and what types of error each technique is prone to?

We are stressing the ability to simultaneously measure CRM and IST. IST is essentially the same as traditional turbidity; it's just that we are able to do both simultaneously and correlate the imaging with IST directly since the data comes from the same sample. Imaging gives us the ability to see the structure of the gel, whereas turbidity does not. IST is particularly sensitive to ambient conditions (can be affected by the lighting in the room, even) so that is a disadvantage.

- If CRM and IST analysis demonstrated similar results in regards to studying the turbidity in collagen I is there any formation advantage to employing one technique over the other in this regard?

CRM is more sensitive to the early stages of self-assembly, because smaller entities have a larger proportion of back-scattered to forward-scattered light.

- In the section entitled "CRM reveals structures responsible for turbidity", I am curious to know how "mesh size varied more strongly with concentration for gels formed at higher temperature than lower temperature". Wouldn't the increased temperature allow for greater vibrations to rearrange bonds and create more uniform mesh sizes?
- Why is greater variation in mesh size at t_{PL} for gels formed at higher temperatures supportive of the idea that greater temperatures lead to more fibrils relative to the fewer thicker fibrils present at lower temperatures?

This means that at the higher temperature (37ºC) the mesh sizes are more similar across concentrations than at the lower temperature. This is supportive that there are more fibrils at higher temperature (leading to decreased mesh sizes) and then less fibrils at lower temperatures (larger mesh sizes overall). There is no rearrangement of bonds.

- What causes the collagen to begin fibillogenesis? From what I understood, anything that was added to the stock collagen was either to dilute it or provide FITC for labeling purposes, so my comprehension is that it is a thermodynamic reaction - which is why the solutions had to be prepared in a room at 4°C (?). If this is the case, what is exactly going

on? Are there free form particles of collagen (monomers) floating around that start to self-assemble, creating longer and thicker polymers at a certain temperature and that beyond an ideal range of temperature, there is too much energy, too much movement and it is harder for them to colocalize? Is this what nucleation is? Also, I was surprised that longer, thicker fibrils formed at 27°C as opposed to 37°C – body temperature. Does the thickness and length of the fibril correspond to specific characteristics of cell matrix adhesions, etc. (this is related to my first line of questioning)? I apologize I feel like this line of questioning has less to do with the actual experiment and more to do with the concept behind it.

Fibrillogenesis is primarily an entropic process where water molecules are freed as monomers find each other. "Nucleation" occurs when a few monomers come together and then form that minimal spanning structure, where "growth" in our case is when the fibrils widen significantly from the interactions of the remaining free-floating monomers aggregate onto the minimal spanning structure. In the body, collagen can be present in many different forms, some fibrillar and some not, and the structure is very much dictated by its function in various body parts. We use our gels as the simplest system in which to study cancer invasion, so it is likely only representative of certain parts of the body where there is normally a lot of collagen present.

- For the arrest time of the fibrils, it could only be measured using the CRM images rather than the IST. The arrest time of the fibrils was confusing for me to understand because it was the time that the fibrils were fixed in location relative to one another and when the gel structure was fixed as well. These two times were different however, with the fibrils arresting before the gel. Would this time difference have any great impact on your data

involving arrest time and fibril development? Would the extended time from actual fibril (location) arrest alter your data in any way?

That's very a very observant comment. We heavily debated using various arrest times, especially for the experiments done at lower temperatures when there was still substantial flow after fibrils were locked into place relatively to each other. After trying it out both ways, we decided to use our definition of arrest because it did not seem to substantially affect that conclusions of the paper.

- Can you give an example where the extra information about lag and growth phases gleaned from CRM measurements, but not reflected in traditional turbidity measurements, may be important to experimental conclusions about a particular collagen self-assembly?

What we call arrest (minimal spanning structure) is clearly happening during the lag/early growth phase and we'd eventually like to extract image information to tell us about the dimensions of the early network.

References

1. Shoulders, M. D., and R. T. Raines. 2009. Collagen structure and stability. Annual review of biochemistry 78:929-958.

2. Kadler, K. E., C. Baldock, J. Bella, and R. P. Boot-Handford. 2007. Collagens at a glance. Journal of cell science 120:1955-1958.

3. Lodish, H. F. 2000. Molecular cell biology. W.H. Freeman, New York.

4. Ivarsson, M., A. McWhirter, T. K. Borg, and K. Rubin. 1998. Type I collagen synthesis in cultured human fibroblasts: Regulation by cell spreading, platelet-derived growth factor and interactions with collagen fibers. Matrix Biology 16:409-425.

5. Green, H., B. Goldberg, and G. J. Todaro. 1966. Differentiated Cell Types and Regulation of Collagen Synthesis. Nature 212:631-&.

6. Marinkovich, M. P., and V. Rocha. 1986. Collagen-Synthesis and Deposition during Mammary Epithelial-Cell Spreading on Collagen Gels. J Cell Physiol 128:61-70.

7. Ohji, M., N. Sundarraj, J. R. Hassell, and R. A. Thoft. 1994. Basement-Membrane Synthesis by Human Corneal Epithelial-Cells in-Vitro. Invest Ophth Vis Sci 35:479-485.

8. Liotta, L. A. 1993. Molecular and Cellular Aspects of Basement-Membranes - Rohrbach,Dh, Timpl,R. Science 261:1611-1613.

9. Fratzl, P. Collagen : structure and mechanics.

10. Liu, X., H. Wu, M. Byrne, S. Krane, and R. Jaenisch. 1997. Type III collagen is crucial for collagen I fibrillogenesis and for normal cardiovascular development. Proceedings of the National Academy of Sciences of the United States of America 94:1852-1856.

11. Wenstrup, R. J., J. B. Florer, E. W. Brunskill, S. M. Bell, I. Chervoneva, and D. E. Birk. 2004. Type V collagen controls the initiation of collagen fibril assembly. The Journal of biological chemistry 279:53331-53337.

12. Morton, R. W. 1990. Basic Biomechanics of the Musculoskeletal System, 2nd Edition - Nordin,M, Frankel,Vh. Am J Occup Ther 44:764-765.

13. Burdick, J. A., and R. L. Mauck. 2011. Biomaterials for Tissue Engineering Applications A Review of the Past and Future Trends Introduction. Biomaterials for Tissue Engineering Applications: A Review of the Past and Future Trends:1-5.

14. Kannus, P. 2000. Structure of the tendon connective tissue. Scand J Med Sci Spor 10:312-320.

15. Mouw, J. K., G. Ou, and V. M. Weaver. 2014. Extracellular matrix assembly: a multiscale deconstruction. Nature reviews. Molecular cell biology 15:771-785.

16. Kahn, C. J. F., X. O. Wang, and R. Rahouadj. 2010. Nonlinear Model for Viscoelastic Behavior of Achilles Tendon. J Biomech Eng-T Asme 132.

17. Myllyharju, J., and K. I. Kivirikko. 2001. Collagens and collagen-related diseases. Annals of medicine 33:7-21.

18. Gajko-Galicka, A. 2002. Mutations in type I collagen genes resulting in osteogenesis imperfecta in humans. Acta Biochim Pol 49:433-441.

19. Rauch, F., and F. H. Glorieux. 2004. Osteogenesis imperfecta. Lancet 363:1377-1385.

20. Callewaert, B., F. Malfait, B. Loeys, and A. De Paepe. 2008. Ehlers-Danlos syndromes and Marfan syndrome. Best practice & research. Clinical rheumatology 22:165-189.

21. Rombaut, L., F. Malfait, I. De Wandele, A. Cools, Y. Thijs, A. De Paepe, and P. Calders. 2011. Medication, surgery, and physiotherapy among patients with the hypermobility type of Ehlers-Danlos syndrome. Archives of physical medicine and rehabilitation 92:1106-1112.

22. Lee, C. H., A. Singla, and Y. Lee. 2001. Biomedical applications of collagen. Int J Pharm 221:1-22.

23. Ruszczak, Z. 2003. Effect of collagen matrices on dermal wound healing. Advanced drug delivery reviews 55:1595-1611.

24. Chattopadhyay, S., and R. T. Raines. 2014. Review collagen-based biomaterials for wound healing. Biopolymers 101:821-833.

25. Doillon, C. J., M. G. Dunn, E. Bender, and F. H. Silver. 1985. Collagen fiber formation in repair tissue: development of strength and toughness. Coll Relat Res 5:481-492.

26. Doillon, C. J., C. F. Whyne, S. Brandwein, and F. H. Silver. 1986. Collagen-based wound dressings: control of the pore structure and morphology. Journal of biomedical materials research 20:1219-1228.

27. Singh, O., S. S. Gupta, M. Soni, S. Moses, S. Shukla, and R. K. Mathur. 2011. Collagen dressing versus conventional dressings in burn and chronic wounds: a retrospective study. Journal of cutaneous and aesthetic surgery 4:12-16.

28. Meena, C., S. A. Mengi, and S. G. Deshpande. 1999. Biomedical and industrial applications of collagen. P Indian as-Chem Sci 111:319-329.

29. Alt, K. W. 1993. Structure, Function and Evolution of Teeth - Smith,P, Tchernov,E. Homo 44:98-98.

30. Chun, K., H. Choi, and J. Lee. 2014. Comparison of mechanical property and role between enamel and dentin in the human teeth. Journal of dental biomechanics 5:1758736014520809.

31. Yang, Y. L., S. Motte, and L. J. Kaufman. 2010. Pore size variable type I collagen gels and their interaction with glioma cells. Biomaterials 31:5678-5688.

32. Yang, Y. L., C. Sun, M. E. Wilhelm, L. J. Fox, J. L. Zhu, and L. J. Kaufman. 2011. Influence of chondroitin sulfate and hyaluronic acid on structure, mechanical properties, and glioma invasion of collagen I gels. Biomaterials 32:7932-7940.

33. Guzman, A., M. J. Ziperstein, and L. J. Kaufman. 2014. The effect of fibrillar matrix architecture on tumor cell invasion of physically challenging environments. Biomaterials 35:6954-6963.

34. Kaufman, L. J., C. P. Brangwynne, K. E. Kasza, E. Filippidi, V. D. Gordon, T. S. Deisboeck, and D. A. Weitz. 2005. Glioma expansion in collagen I matrices: Analyzing collagen concentration-dependent growth and motility patterns. Biophysical journal 89:635-650.

35. Payne, L. S., and P. H. Huang. 2013. The pathobiology of collagens in glioma. Molecular cancer research : MCR 11:1129-1140.

36. Scherer, H. J. 1940. The forms of growth in gliomas and their practical significance. Brain 63:1-35.

37. Cuddapah, V. A., S. Robel, S. Watkins, and H. Sontheimer. 2014. A neurocentric perspective on glioma invasion. Nat Rev Neurosci 15:455-465.

38. Han, J., J. C. Daniel, N. Lieska, and G. D. Pappas. 1994. Immunofluorescence and biochemical studies of the type VI collagen expression by human glioblastoma cells in vitro. Neurological research 16:370-375.

39. Ogawa, K., M. Oguchi, Y. Nakashima, and H. Yamabe. 1989. Distribution of collagen type IV in brain tumors - an immunohistochemical study. J Neuro-Oncol 7:357-366.

40. Kwak, E. A., S. Ahn, and J. Jaworski. 2015. Microfabrication of Custom Collagen Structures Capable of Guiding Cell Morphology and Alignment. Biomacromolecules 16:1761-1770.

41. Wang, N., E. Ostuni, G. M. Whitesides, and D. E. Ingber. 2002. Micropatterning tractional forces in living cells. Cell Motil Cytoskel 52:97-106.

42. Odawara, A., M. Gotoh, and I. Suzuki. 2013. Control of neural network patterning using collagen gel photothermal etching. Lab Chip 13:2040-2046.

43. Wan, C. R., E. M. Frohlich, J. L. Charest, and R. D. Kamm. 2011. Effect of Surface Patterning and Presence of Collagen I on the Phenotypic Changes of Embryonic Stem Cell Derived Cardiomyocytes. Cell Mol Bioeng 4:56-66.

44. Tang, M. D., A. P. Golden, and J. Tien. 2004. Fabrication of collagen gels that contain patterned, micrometer-scale cavities. Adv Mater 16:1345-+.

45. Fukuda, J., A. Khademhosseini, J. Yeh, G. Eng, J. J. Cheng, O. C. Farokhzad, and R. Langer. 2006. Micropatterned cell co-cultures using layer-by-layer deposition of extracellular matrix components. Biomaterials 27:1479-1486.

46. Yu, S. M., Y. Li, and D. Kim. 2011. Collagen mimetic peptides: progress towards functional applications. Soft Matter 7:7927-7938.

47. Martin, R., L. Waldmann, and D. L. Kaplan. 2003. Supramolecular assembly of collagen triblock peptides. Biopolymers 70:435-444.

48. Services, F. a. D. A.-U. S. D. o. H. a. H. 1997. The Sourcing and Processing of Gelatin to Reduce the Potential Risk Posed by Bovine Spongiform Encephalopathy (BSE) in FDA-Regulated Products for Human Use.

49. Liu, D., M. Nikoo, G. Boran, P. Zhou, and J. M. Regenstein. 2015. Collagen and gelatin. Annual review of food science and technology 6:527-557.

50. Wang, S., K. Agyare, and S. Damodaran. 2009. Optimisation of hydrolysis conditions and fractionation of peptide cryoprotectants from gelatin hydrolysate. Food Chem 115:620-630.

51. Terta, M., G. Blekas, and A. Paraskevopoulou. 2006. Retention of selected aroma compounds by polysaccharide solutions: A thermodynamic and kinetic approach. Food Hydrocolloid 20:863-871.

52. Proksch, E., D. Segger, J. Degwert, M. Schunck, V. Zague, and S. Oesser. 2014. Oral Supplementation of Specific Collagen Peptides Has Beneficial Effects on Human Skin Physiology: A Double-Blind, Placebo-Controlled Study. Skin Pharmacol Phys 27:47-55.

53. Xhauflaire-Uhoda, E., K. Fontaine, and G. E. Pierard. 2008. Kinetics of moisturizing and firming effects of cosmetic formulations. International journal of cosmetic science 30:131-138.

54. Bauza, E., G. Oberto, A. Berghi, C. F. Dal, and N. Domloge. 2004. Collagen-like peptide exhibits a remarkable antiwrinkle effect on the skin when topically applied: in vivo study. International journal of tissue reactions 26:105-111.

55. Lees, J. F., M. Tasab, and N. J. Bulleid. 1997. Identification of the molecular recognition sequence which determines the type-specific assembly of procollagen. The EMBO journal 16:908-916.

56. Bourhis, J. M., N. Mariano, Y. Zhao, K. Harlos, J. Y. Exposito, E. Y. Jones, C. Moali, N. Aghajari, and D. J. Hulmes. 2012. Structural basis of fibrillar collagen trimerization and related genetic disorders. Nature structural & molecular biology 19:1031-1036.

57. Zanaboni, G., A. Rossi, A. M. T. Onana, and R. Tenni. 2000. Stability and networks of hydrogen bonds of the collagen triple helical structure: influence of pH and chaotropic nature of three anions. Matrix Biology 19:511-520.

58. Pauling, L., and R. B. Corey. 1951. The structure of fibrous proteins of the collagen-gelatin group. Proceedings of the National Academy of Sciences of the United States of America 37:272-281.

59. Bella, J., M. Eaton, B. Brodsky, and H. M. Berman. 1994. Crystal and molecular structure of a collagen-like peptide at 1.9 A resolution. Science 266:75-81.

60. Bella, J., and H. M. Berman. 1996. Crystallographic evidence for C alpha-H...O=C hydrogen bonds in a collagen triple helix. Journal of molecular biology 264:734-742.

61. Emsley, J., C. G. Knight, R. W. Farndale, M. J. Barnes, and R. C. Liddington. 2000. Structural basis of collagen recognition by integrin alpha2beta1. Cell 101:47-56.

62. Cram, D. J. 1988. The Design of Molecular Hosts, Guests and Their Complexes. Chem Scripta 28:263-274.

63. Kim, C. W. A., and J. M. Berg. 1993. Thermodynamic Beta-Sheet Propensities Measured Using a Zinc-Finger Host Peptide. Nature 362:267-270.

64. Rauscher, S., S. Baud, M. Miao, F. W. Keeley, and R. Pomes. 2006. Proline and glycine control protein self-organization into elastomeric or amyloid fibrils. Structure 14:1667-1676.

65. Chiti, F., M. Stefani, N. Taddei, G. Ramponi, and C. M. Dobson. 2003. Rationalization of the effects of mutations on peptide and protein aggregation rates. Nature 424:805-808.

66. Minor, D. L., and P. S. Kim. 1994. Measurement of the Beta-Sheet-Forming Propensities of Amino-Acids. Nature 367:660-663.

67. Buehler, M. J. 2006. Nature designs tough collagen: explaining the nanostructure of collagen fibrils. Proceedings of the National Academy of Sciences of the United States of America 103:12285-12290.

68. Wenger, M. P. E., L. Bozec, M. A. Horton, and P. Mesquida. 2007. Mechanical properties of collagen fibrils. Biophysical journal 93:1255-1263.

69. Yang, L., K. O. Van der Werf, C. F. C. Fitie, M. L. Bennink, P. J. Dijkstra, and J. Feijen. 2008. Mechanical properties of native and cross-linked type I collagen fibrils. Biophysical journal 94:2204-2211.

70. Buehler, M. J. 2006. Nature designs tough collagen: Explaining the nanostructure of collagen fibrils. Proceedings of the National Academy of Sciences of the United States of America 103:12285-12290.

71. Veld, P. J., and M. J. Stevens. 2008. Simulation of the mechanical strength of a single collagen molecule. Biophysical journal 95:33-39.

72. Murad, S., D. Grove, K. A. Lindberg, G. Reynolds, A. Sivarajah, and S. R. Pinnell. 1981. Regulation of collagen synthesis by ascorbic acid. Proceedings of the National Academy of Sciences of the United States of America 78:2879-2882.

73. Canty, E. G., Y. Lu, R. S. Meadows, M. K. Shaw, D. F. Holmes, and K. E. Kadler. 2004. Coalignment of plasma membrane channels and protrusions (fibripositors) specifies the parallelism of tendon. The Journal of cell biology 165:553-563.

74. Strasser, S., A. Zink, M. Janko, W. M. Heckl, and S. Thalhammer. 2007. Structural investigations on native collagen type I fibrils using AFM. Biochemical and biophysical research communications 354:27-32.

75. Wenstrup, R. J., J. B. Florer, W. G. Cole, M. C. Willing, and D. E. Birk. 2004. Reduced type I collagen utilization: a pathogenic mechanism in COL5A1 haplo-insufficient Ehlers-Danlos syndrome. Journal of cellular biochemistry 92:113-124.

76. Ameye, L., and M. F. Young. 2002. Mice deficient in small leucine-rich proteoglycans: novel in vivo models for osteoporosis, osteoarthritis, Ehlers-Danlos syndrome, muscular dystrophy, and corneal diseases. Glycobiology 12:107R-116R.

77. Kalamajski, S., and A. Oldberg. 2010. The role of small leucine-rich proteoglycans in collagen fibrillogenesis. Matrix biology : journal of the International Society for Matrix Biology 29:248-253.

78. Kadler, K. E., Y. Hojima, and D. J. Prockop. 1987. Assembly of collagen fibrils de novo by cleavage of the type I pC-collagen with procollagen C-proteinase. Assay of critical concentration demonstrates that collagen self-assembly is a classical example of an entropy-driven process. The Journal of biological chemistry 262:15696-15701.

79. Danielsen, C. C. 1981. Mechanical properties of reconstituted collagen fibrils. A study on reconstitution methodology and influence of in vitro maturation. Connective tissue research 9:51-57.

80. Kadler, K. E., D. F. Holmes, J. A. Trotter, and J. A. Chapman. 1996. Collagen fibril formation. Biochem J 316:1-11.

81. Helseth, D. L., Jr., and A. Veis. 1981. Collagen self-assembly in vitro. Differentiating specific telopeptide-dependent interactions using selective enzyme modification and the addition of free amino telopeptide. The Journal of biological chemistry 256:7118-7128.

82. Wood, G. C., and M. K. Keech. 1960. The formation of fibrils from collagen solutions. 1. The effect of experimental conditions: kinetic and electron-microscope studies. Biochem J 75:588-598.

83. Yeromonahos, C., B. Polack, and F. Caton. 2010. Nanostructure of the fibrin clot. Biophysical journal 99:2018-2027.

84. Berne, B. J. 1974. Interpretation of the light scattering from long rods. Journal of molecular biology 89:755-758.

85. Casassa, E. F. 1955. Light Scattering from Very Long Rod-Like Particles and an Application to Polymerized Fibrinogen. J Chem Phys 23:596-597.

86. Zhu, J. L., and L. J. Kaufman. 2014. Collagen I Self-Assembly: Revealing the Developing Structures that Generate Turbidity. Biophysical journal 106:1822-1831.

87. Birk, D. E., J. M. Fitch, J. P. Babiarz, K. J. Doane, and T. F. Linsenmayer. 1990. Collagen fibrillogenesis in vitro: interaction of types I and V collagen regulates fibril diameter. Journal of cell science 95 (Pt 4):649-657.

88. de Wild, M., W. Pomp, and G. H. Koenderink. 2013. Thermal Memory in Self-Assembled Collagen Fibril Networks. Biophysical journal 105:200-210.

89. Hwang, J. S., and H. Z. Cummins. 1982. Dynamic Light-Scattering-Studies of Collagen. J Chem Phys 77:616-621.

90. Payne, K. J., T. A. King, and D. F. Holmes. 1986. Collagen Fibrillogenesis Invitro - an Investigation of the Thermal Memory Effect and of the Early Events Occurring during Fibril Assembly Using Dynamic Light-Scattering. Biopolymers 25:1185-1207.

91. Fletcher, G. C. 1976. Dynamic Light-Scattering from Collagen Solutions .1. Translational Diffusion-Coefficient and Aggregation Effects. Biopolymers 15:2201-2217.

92. Robitaille, M. C., R. Zareian, C. A. DiMarzio, K. T. Wan, and J. W. Ruberti. 2011. Small-angle light scattering to detect strain-directed collagen degradation in native tissue. Interface Focus 1:767-776.

93. Bard, J. B., and J. A. Chapman. 1973. Diameters of collagen fibrils grown in vitro. Nature: New biology 246:83-84.

94. Trelstad, R. L., K. Hayashi, and J. Gross. 1976. Collagen fibrillogenesis: intermediate aggregates and suprafibrillar order. Proceedings of the National Academy of Sciences of the United States of America 73:4027-4031.

95. Yang, Y. L., and L. J. Kaufman. 2009. Rheology and Confocal Reflectance Microscopy as Probes of Mechanical Properties and Structure during Collagen and Collagen/Hyaluronan Self-Assembly. Biophysical journal 96:1566-1585.

96. Gobeaux, F., E. Belamie, G. Mosser, P. Davidson, and S. Asnacios. 2010. Power law rheology and strain-induced yielding in acidic solutions of type I-collagen. Soft Matter 6:3769-3777.

97. Lai, G. L., Y. Li, and G. Y. Li. 2008. Effect of concentration and temperature on the rheological behavior of collagen solution. Int J Biol Macromol 42:285-291.

98. Stein, A. M., D. A. Vader, D. A. Weitz, and L. M. Sander. 2011. The Micromechanics of Three-Dimensional Collagen-I Gels. Complexity 16:22-28.

99. Motte, S., and L. J. Kaufman. 2013. Strain stiffening in collagen I networks. Biopolymers 99:35-46.

100. Storm, C., J. J. Pastore, F. C. MacKintosh, T. C. Lubensky, and P. A. Janmey. 2005. Nonlinear elasticity in biological gels. Nature 435:191-194.

101. Munster, S., L. M. Jawerth, B. A. Leslie, J. I. Weitz, B. Fabry, and D. A. Weitz. 2013. Strain history dependence of the nonlinear stress response of fibrin and collagen networks. Proceedings of the National Academy of Sciences of the United States of America 110:12197-12202.

102. Shayegan, M., and N. R. Forde. 2013. Microrheological characterization of collagen systems: from molecular solutions to fibrillar gels. PloS one 8:e70590.

103. Velegol, D., and F. Lanni. 2001. Cell traction forces on soft biomaterials. I. Microrheology of Type I collagen gels. Biophysical journal 81:1786-1792.

104. Latinovic, O., L. A. Hough, and H. D. Ou-Yang. 2010. Structural and micromechanical characterization of type I collagen gels. J Biomech 43:500-505.

105. Parekh, A., and D. Velegol. 2007. Collagen gel anisotropy measured by 2-d laser trap microrheometry. Ann Biomed Eng 35:1231-1246.

106. Forgacs, G., S. A. Newman, B. Hinner, C. W. Maier, and E. Sackmann. 2003. Assembly of collagen matrices as a phase transition revealed by structural and rheologic studies. Biophysical journal 84:1272-1280.

107. Yang, Y. L., L. M. Leone, and L. J. Kaufman. 2009. Elastic Moduli of Collagen Gels Can Be Predicted from Two-Dimensional Confocal Microscopy. Biophysical journal 97:2051-2060.

108. Piechocka, I. K., A. S. G. van Oosten, R. G. M. Breuls, and G. H. Koenderink. 2011. Rheology of Heterotypic Collagen Networks. Biomacromolecules 12:2797-2805.

109. Carr, M. E., and J. Hermans. 1978. Size and Density of Fibrin Fibers from Turbidity. Macromolecules 11:46-50.

110. Zhu, J., and L. J. Kaufman. 2014. Collagen I self-assembly: revealing the developing structures that generate turbidity. Biophysical journal 106:1822-1831.

111. Mezger, T. G. 2006. The rheology handbook: for users of rotational and oscillatory rheometers.

112. Winter, H. H., and F. Chambon. 1986. Analysis of Linear Viscoelasticity of a Cross-Linking Polymer at the Gel Point. J Rheol 30:367-382.

113. Winter, H. H. 1987. Can the Gel Point of a Cross-Linking Polymer Be Detected by the G' - G" Crossover. Polym Eng Sci 27:1698-1702.

114. Yeromonahos, C., B. Polack, and F. Caton. 2010. Nanostructure of the Fibrin Clot. Biophys. J. 99:2018-2027.

115. Brokaw, J. L., C. J. Doillon, R. A. Hahn, D. E. Birk, R. A. Berg, and F. H. Silver. 1985. TURBIDIMETRIC AND MORPHOLOGICAL-STUDIES OF TYPE-I COLLAGEN FIBER SELF ASSEMBLY INVITRO AND THE INFLUENCE OF FIBRONECTIN. Int. J. Biol. Macromol. 7:135-140.

116. MacKintosh, F. C., J. Kas, and P. A. Janmey. 1995. Elasticity of semiflexible biopolymer networks. Physical review letters 75:4425-4428.

117. Del Duca, D., T. Werbowetski, and R. F. Del Maestro. 2004. Spheroid preparation from hanging drops: characterization of a model of brain tumor invasion. J Neurooncol 67:295-303.

118. Alberts, B. 2008. Molecular biology of the cell. Garland Science, New York.

119. Friedl, P., and E. B. Brocker. 2000. The biology of cell locomotion within three-dimensional extracellular matrix. Cell Mol Life Sci 57:41-64.

120. Petroll, W. M., and L. S. Ma. 2003. Direct, dynamic assessment of cell-matrix interactions inside fibrillar collagen lattices. Cell Motil Cytoskel 55:254-264.

121. Zaman, M. H., L. M. Trapani, A. Siemeski, D. MacKellar, H. Gong, R. D. Kamm, A. Wells, D. A. Lauffenburger, and P. Matsudaira. 2006. Migration of tumor cells in 3D matrices is governed by matrix stiffness along with cell-matrix adhesion and proteolysis.

Proceedings of the National Academy of Sciences of the United States of America 103:10889-10894.

122. Cen, L., W. Liu, L. Cui, W. J. Zhang, and Y. L. Cao. 2008. Collagen tissue engineering: Development of novel biomaterials and applications. Pediatr Res 63:492-496.

123. Glowacki, J., and S. Mizuno. 2008. Collagen scaffolds for tissue engineering. Biopolymers 89:338-344.

124. Grinnell, F., and W. M. Petroll. 2010. Cell Motility and Mechanics in Three-Dimensional Collagen Matrices. Annu Rev Cell Dev Bi 26:335-361.

125. Wolf, K., M. te Lindert, M. Krause, S. Alexander, J. te Riet, A. L. Willis, R. M. Hoffman, C. G. Figdor, S. J. Weiss, and P. Friedl. 2013. Physical limits of cell migration: Control by ECM space and nuclear deformation and tuning by proteolysis and traction force. Journal of Cell Biology 201:1069-1084.

126. Kadler, K. E., A. Hill, and E. G. Canty-Laird. 2008. Collagen fibrillogenesis: fibronectin, integrins, and minor collagens as organizers and nucleators. Curr Opin Cell Biol 20:495-501.

127. Raub, C. B., J. Unruh, V. Suresh, T. Krasieva, T. Lindmo, E. Gratton, B. J. Tromberg, and S. C. George. 2008. Image correlation spectroscopy of multiphoton images correlates with collagen mechanical properties. Biophysical journal 94:2361-2373.

128. Raub, C. B., V. Suresh, T. Krasieva, J. Lyubovitsky, J. D. Mih, A. J. Putnam, B. J. Tromberg, and S. C. George. 2007. Noninvasive assessment of collagen gel microstructure and mechanics using multiphoton Microscopy. Biophysical journal 92:2212-2222.

129. Roeder, B. A., K. Kokini, and S. L. Voytik-Harbin. 2009. Fibril Microstructure Affects Strain Transmission Within Collagen Extracellular Matrices. J Biomech Eng-T Asme 131.

130. Achilli, M., and D. Mantovani. 2010. Tailoring Mechanical Properties of Collagen-Based Scaffolds for Vascular Tissue Engineering: The Effects of pH, Temperature and Ionic Strength on Gelation. Polymers-Basel 2:664-680.

131. Chiti, F., and C. M. Dobson. 2006. Protein misfolding, functional amyloid, and human disease. Annual review of biochemistry 75:333-366.

132. Gross, J., and D. Kirk. 1958. The heat precipitation of collagen from neutral salt solutions: some rate-regulating factors. The Journal of biological chemistry 233:355-360.

133. Williams, B. R., R. A. Gelman, D. C. Poppke, and K. A. Piez. 1978. Collagen fibril formation. Optimal in vitro conditions and preliminary kinetic results. The Journal of biological chemistry 253:6578-6585.

134. Wood, G. C. 1960. The formation of fibrils from collagen solutions. 2. A mechanism of collagen-fibril formation. Biochem J 75:598-605.

135. Comper, W. D., and A. Veis. 1977. The mechanism of nucleation for in vitro collagen fibril formation. Biopolymers 16:2113-2131.

136. Comper, W. D., and A. Veis. 1977. Characterization of nuclei in in vitro collagen fibril formation. Biopolymers 16:2133-2142.

137. Mickel, W., S. Munster, L. M. Jawerth, D. A. Vader, D. A. Weitz, A. P. Sheppard, K. Mecke, B. Fabry, and G. E. Schroder-Turk. 2008. Robust Pore Size Analysis of Filamentous Networks from Three-Dimensional Confocal Microscopy. Biophysical journal 95:6072-6080.

138. Zoumi, A., A. Yeh, and B. J. Tromberg. 2002. Imaging cells and extracellular matrix in vivo by using second-harmonic generation and two-photon excited fluorescence. Proceedings of the National Academy of Sciences of the United States of America 99:11014-11019.

139. Williams, R. M., W. R. Zipfel, and W. W. Webb. 2005. Interpreting second-harmonic generation images of collagen I fibrils. Biophysical journal 88:1377-1386.

140. Brightman, A. O., B. P. Rajwa, J. E. Sturgis, M. E. McCallister, J. P. Robinson, and S. L. Voytik-Harbin. 2000. Time-lapse confocal reflection microscopy of collagen fibrillogenesis and extracellular matrix assembly in vitro. Biopolymers 54:222-234.

141. Margaron, Y., L. Bostan, J. Y. Exposito, M. Malbouyres, A. M. Trunfio-Sfarghiu, Y. Berthier, and C. Lethias. 2010. Tenascin-X increases the stiffness of collagen gels without affecting fibrillogenesis. Biophys Chem 147:87-91.

142. Kreger, S. T., B. J. Bell, J. Bailey, E. Stites, J. Kuske, B. Waisner, and S. L. Voytik-Harbin. 2010. Polymerization and Matrix Physical Properties as Important Design Considerations for Soluble Collagen Formulations. Biopolymers 93:690-707.

143. Jawerth, L. M., S. Munster, D. A. Vader, B. Fabry, and D. A. Weitz. 2010. A Blind Spot in Confocal Reflection Microscopy: The Dependence of Fiber Brightness on Fiber Orientation in Imaging Biopolymer Networks. Biophysical journal 98:L1-L3.

144. Lang, N. R., S. Munster, C. Metzner, P. Krauss, S. Schurmann, J. Lange, K. E. Aifantis, O. Friedrich, and B. Fabry. 2013. Estimating the 3D Pore Size Distribution of Biopolymer Networks from Directionally Biased Data. Biophysical journal 105:1967-1975.

145. Silver, F. H., and D. E. Birk. 1983. Kinetic-Analysis of Collagen Fibrillogenesis .1. Use of Turbidity - Time Data. Collagen Rel Res 3:393-405.

146. Gennes, P. G. d. 1979. Scaling concepts in polymer physics. Cornell University Press, Ithaca, N.Y.

147. Banerjee, P., D. Lenz, J. P. Robinson, J. L. Rickus, and A. K. Bhunia. 2008. A novel and simple cell-based detection system with a collagen-encapsulated B-lymphocyte cell line as a biosensor for rapid detection of pathogens and toxins. Lab Invest 88:196-206.

148. Gelman, R. A., and K. A. Piez. 1980. Collagen fibril formation in vitro. A quasielastic light-scattering study of early stages. The Journal of biological chemistry 255:8098-8102.

149. Silver, F. H. 1981. Type I collagen fibrillogenesis in vitro. Additional evidence for the assembly mechanism. The Journal of biological chemistry 256:4973-4977.

150. Cox, A. J., A. J. DeWeerd, and J. Linden. 2002. An experiment to measure Mie and Rayleigh total scattering cross sections. Am J Phys 70:620-625.

151. Ferri, F., M. Greco, G. Arcovito, F. A. Bassi, M. De Spirito, E. Paganini, and M. Rocco. 2001. Growth kinetics and structure of fibrin gels. Phys Rev E 63.

152. Holmes, D. F., and K. E. Kadler. 2005. The precision of lateral size control in the assembly of corneal collagen fibrils. J. Mol. Biol. 345:773-784.

153. Graham, J. S., A. N. Vomund, C. L. Phillips, and M. Grandbois. 2004. Structural changes in human type I collagen fibrils investigated by force spectroscopy. Exp Cell Res 299:335-342.

154. Janmey, P. A., U. Euteneuer, P. Traub, and M. Schliwa. 1991. Viscoelastic Properties of Vimentin Compared with Other Filamentous Biopolymer Networks. Journal of Cell Biology 113:155-160.

155. Arevalo, R. C., J. S. Urbach, and D. L. Blair. 2010. Size-Dependent Rheology of Type-I Collagen Networks. Biophysical journal 99:L65-L67.

156. Winter, H. H. 2003. Gel Point. Encyclopedia of Polymer Science and Technology.

157. Stauffer, D., A. Coniglio, and M. Adam. 1982. Gelation and Critical Phenomena. Adv Polym Sci 44:103-158.

158. Ross-Murphy, S. B. 2007. Biopolymer gelation-exponents and critical exponents. Polym Bull 58:119-126.

159. Rao, M. A., and R. W. Hartel. 1998. Phase/state transitions in foods : chemical, structural, and rheological changes. M. Dekker, New York.

160. Scanlan, J. C., and H. H. Winter. 1991. Composition Dependence of the Viscoelasticity of End-Linked Poly(Dimethylsiloxane) at the Gel Point. Macromolecules 24:47-54.

161. Li, H. Y., and Y. H. Zhang. 2014. Modeling of the viscoelastic behavior of collagen gel from dynamic oscillatory shear measurements. Biorheology 51:369-380.

162. Zuidema, J. M., C. J. Rivet, R. J. Gilbert, and F. A. Morrison. 2014. A protocol for rheological characterization of hydrogels for tissue engineering strategies. J Biomed Mater Res B 102:1063-1073.

163. Ulrich, T. A., A. Jain, K. Tanner, J. L. MacKay, and S. Kumar. 2010. Probing cellular mechanobiology in three-dimensional culture with collagen-agarose matrices. Biomaterials 31:1875-1884.

164. Zhang, M., Y. H. Chen, G. Y. Li, and Z. L. Du. 2010. Rheological properties of fish skin collagen solution : Effects of temperature and concentration. Korea-Aust Rheol J 22:119-127.

165. Kajiwara, K., and Y. Osada. 2000. Gels handbook. Academic Press, San Diego, Calif. ; London.

166. Morse, D. C. 1998. Viscoelasticity of concentrated isotropic solutions of semiflexible polymers. 1. Model and stress tensor. Macromolecules 31:7030-7043.

167. Morse, D. C. 1998. Viscoelasticity of concentrated isotropic solutions of semiflexible polymers. 2. Linear response. Macromolecules 31:7044-7067.

168. Louis, D. N., H. Ohgaki, O. D. Wiestler, W. K. Cavenee, P. C. Burger, A. Jouvet, B. W. Scheithauer, and P. Kleihues. 2007. The 2007 WHO classification of tumours of the central nervous system. Acta neuropathologica 114:97-109.

169. Behin, A., K. Hoang-Xuan, A. F. Carpentier, and J. Y. Delattre. 2003. Primary brain tumours in adults. Lancet 361:323-331.

170. Mammoto, T., A. Jiang, E. Jiang, D. Panigrahy, M. W. Kieran, and A. Mammoto. 2013. Role of collagen matrix in tumor angiogenesis and glioblastoma multiforme progression. The American journal of pathology 183:1293-1305.

171. Bellail, A. C., S. B. Hunter, D. J. Brat, C. Tan, and E. G. Van Meir. 2004. Microregional extracellular matrix heterogeneity in brain modulates glioma cell invasion. The international journal of biochemistry & cell biology 36:1046-1069.

172. Rao, J. S. 2003. Molecular mechanisms of glioma invasiveness: the role of proteases. Nature reviews. Cancer 3:489-501.

173. Beadle, C., M. C. Assanah, P. Monzo, R. Vallee, S. S. Rosenfeld, and P. Canoll. 2008. The role of myosin II in glioma invasion of the brain. Molecular biology of the cell 19:3357-3368.

174. Bruehlmeier, M., U. Roelcke, P. Blauenstein, J. Missimer, P. A. Schubiger, J. T. Locher, R. Pellikka, and S. M. Ametamey. 2003. Measurement of the extracellular space in brain tumors using 76Br-bromide and PET. Journal of nuclear medicine : official publication, Society of Nuclear Medicine 44:1210-1218.

175. Thorne, R. G., and C. Nicholson. 2006. In vivo diffusion analysis with quantum dots and dextrans predicts the width of brain extracellular space. Proceedings of the National Academy of Sciences of the United States of America 103:5567-5572.

176. Huijbers, I. J., M. Iravani, S. Popov, D. Robertson, S. Al-Sarraj, C. Jones, and C. M. Isacke. 2010. A role for fibrillar collagen deposition and the collagen internalization receptor endo180 in glioma invasion. PloS one 5:e9808.

177. Chintala, S. K., R. Sawaya, Z. L. Gokaslan, G. Fuller, and J. S. Rao. 1996. Immunohistochemical localization of extracellular matrix proteins in human glioma, both in vivo and in vitro. Cancer letters 101:107-114.

178. Zamecnik, J. 2005. The extracellular space and matrix of gliomas. Acta neuropathologica 110:435-442.

179. Zamecnik, J., L. Vargova, A. Homola, R. Kodet, and E. Sykova. 2004. Extracellular matrix glycoproteins and diffusion barriers in human astrocytic tumours. Neuropathology and applied neurobiology 30:338-350.

180. Riemenschneider, M. J., W. Mueller, R. A. Betensky, G. Mohapatra, and D. N. Louis. 2005. In situ analysis of integrin and growth factor receptor signaling pathways in human glioblastomas suggests overlapping relationships with focal adhesion kinase activation. The American journal of pathology 167:1379-1387.

181. Tonn, J. C., S. Wunderlich, S. Kerkau, C. E. Klein, and K. Roosen. 1998. Invasive behaviour of human gliomas is mediated by interindividually different integrin patterns. Anticancer Res 18:2599-2605.

182. Haugland, H. K., B. B. Tysnes, and O. B. Tysnes. 1997. Adhesion and migration of human glioma cells are differently dependent on extracellular matrix molecules. Anticancer Res 17:1035-1042.

183. Engelholm, L. H., S. Ingvarsen, H. J. Jurgensen, T. Hillig, D. H. Madsen, B. S. Nielsen, and N. Behrendt. 2009. The collagen receptor uPARAP/Endo180. Front Biosci 14:2103-2114.

184. Takahashi, S., H. Yamada-Okabe, K. Hamada, S. Ohta, T. Kawase, K. Yoshida, and M. Toda. 2011. Downregulation of uPARAP mediates cytoskeletal rearrangements and decreases invasion and migration properties in glioma cells. J Neuro-Oncol 103:267-276.

185. Ivkovic, S., C. Beadle, S. Noticewala, S. C. Massey, K. R. Swanson, L. N. Toro, A. R. Bresnick, P. Canoll, and S. S. Rosenfeld. 2012. Direct inhibition of myosin II effectively blocks glioma invasion in the presence of multiple motogens. Molecular biology of the cell 23:533-542.

186. Vicente-Manzanares, M., X. Ma, R. S. Adelstein, and A. R. Horwitz. 2009. Non-muscle myosin II takes centre stage in cell adhesion and migration. Nature reviews. Molecular cell biology 10:778-790.

187. Aguilar-Cuenca, R., A. Juanes-Garcia, and M. Vicente-Manzanares. 2014. Myosin II in mechanotransduction: master and commander of cell migration, morphogenesis, and cancer. Cell Mol Life Sci 71:479-492.

188. Betapudi, V. 2014. Life without double-headed non-muscle myosin II motor proteins. Frontiers in chemistry 2:45.

189. Zhong, J., A. Paul, S. J. Kellie, and G. M. O'Neill. 2010. Mesenchymal migration as a therapeutic target in glioblastoma. Journal of oncology 2010:430142.

190. Friedl, P. 2004. Prespecification and plasticity: shifting mechanisms of cell migration. Curr Opin Cell Biol 16:14-23.

191. Demuth, T., and M. E. Berens. 2004. Molecular mechanisms of glioma cell migration and invasion. J Neurooncol 70:217-228.

192. Lauffenburger, D. A., and A. F. Horwitz. 1996. Cell migration: a physically integrated molecular process. Cell 84:359-369.

193. Laukaitis, C. M., D. J. Webb, K. Donais, and A. F. Horwitz. 2001. Differential dynamics of alpha 5 integrin, paxillin, and alpha-actinin during formation and disassembly of adhesions in migrating cells. The Journal of cell biology 153:1427-1440.

194. Kiss, A., P. Horvath, A. Rothballer, U. Kutay, and G. Csucs. 2014. Nuclear motility in glioma cells reveals a cell-line dependent role of various cytoskeletal components. PloS one 9:e93431.

195. Szabo, B., R. Unnep, K. Marko, Z. Kornyei, E. Mehes, and A. Czirok. 2011. Inhibition of Myosin II Triggers Morphological Transition and Increased Nuclear Motility. Cytoskeleton 68:325-339.

196. Ulrich, T. A., E. M. de Juan Pardo, and S. Kumar. 2009. The mechanical rigidity of the extracellular matrix regulates the structure, motility, and proliferation of glioma cells. Cancer research 69:4167-4174.

197. Umesh, V., A. D. Rape, T. A. Ulrich, and S. Kumar. 2014. Microenvironmental stiffness enhances glioma cell proliferation by stimulating epidermal growth factor receptor signaling. PloS one 9:e101771.

198. Pathak, A., and S. Kumar. 2012. Independent regulation of tumor cell migration by matrix stiffness and confinement. Proceedings of the National Academy of Sciences of the United States of America 109:10334-10339.

199. Cheng, Y., J. Zhao, W. Qiao, and K. Chen. 2014. Recent advances in diagnosis and treatment of gliomas using chlorotoxin-based bioconjugates. American journal of nuclear medicine and molecular imaging 4:385-405.

200. Hagemann, C., J. Anacker, R. I. Ernestus, and G. H. Vince. 2012. A complete compilation of matrix metalloproteinase expression in human malignant gliomas. World journal of clinical oncology 3:67-79.

201. Wang, M., T. Wang, S. Liu, D. Yoshida, and A. Teramoto. 2003. The expression of matrix metalloproteinase-2 and -9 in human gliomas of different pathological grades. Brain tumor pathology 20:65-72.

202. Zhao, Y., A. Xiao, C. G. diPierro, J. E. Carpenter, R. Abdel-Fattah, G. T. Redpath, M. B. Lopes, and I. M. Hussaini. 2010. An extensive invasive intracranial human glioblastoma xenograft model: role of high level matrix metalloproteinase 9. The American journal of pathology 176:3032-3049.

203. Abe, T., T. Mori, K. Kohno, M. Seiki, T. Hayakawa, H. G. Welgus, S. Hori, and M. Kuwano. 1994. Expression of 72 kDa type IV collagenase and invasion activity of human glioma cells. Clinical & experimental metastasis 12:296-304.

204. Badiga, A. V., C. Chetty, D. Kesanakurti, D. Are, M. Gujrati, J. D. Klopfenstein, D. H. Dinh, and J. S. Rao. 2011. MMP-2 siRNA inhibits radiation-enhanced invasiveness in glioma cells. PloS one 6:e20614.

205. Wang, J., Y. Li, J. Wang, C. Li, K. Yu, and Q. Wang. 2012. Increased expression of matrix metalloproteinase-13 in glioma is associated with poor overall survival of patients. Medical oncology 29:2432-2437.

206. Wang, L., J. Yuan, Y. Tu, X. Mao, S. He, G. Fu, J. Zong, and Y. Zhang. 2013. Co-expression of MMP-14 and MMP-19 predicts poor survival in human glioma. Clinical & translational oncology : official publication of the Federation of Spanish Oncology Societies and of the National Cancer Institute of Mexico 15:139-145.

207. Fingleton, B. 2008. MMPs as therapeutic targets--still a viable option? Seminars in cell & developmental biology 19:61-68.

208. Coussens, L. M., B. Fingleton, and L. M. Matrisian. 2002. Matrix metalloproteinase inhibitors and cancer: trials and tribulations. Science 295:2387-2392.

209. Wolf, K., I. Mazo, H. Leung, K. Engelke, U. H. von Andrian, E. I. Deryugina, A. Y. Strongin, E. B. Brocker, and P. Friedl. 2003. Compensation mechanism in tumor cell migration: mesenchymal-amoeboid transition after blocking of pericellular proteolysis. The Journal of cell biology 160:267-277.

210. Sabeh, F., R. Shimizu-Hirota, and S. J. Weiss. 2009. Protease-dependent versus -independent cancer cell invasion programs: three-dimensional amoeboid movement revisited. The Journal of cell biology 185:11-19.

211. Huttenlocher, A., and A. R. Horwitz. 2011. Integrins in Cell Migration. Csh Perspect Biol 3.

212. Ivaska, J. 2012. Unanchoring integrins in focal adhesions. Nature cell biology 14:981-983.

213. Gladson, C. L. 1996. Expression of integrin alpha v beta 3 in small blood vessels of glioblastoma tumors. Journal of neuropathology and experimental neurology 55:1143-1149.

214. Zaidel-Bar, R., C. Ballestrem, Z. Kam, and B. Geiger. 2003. Early molecular events in the assembly of matrix adhesions at the leading edge of migrating cells. Journal of cell science 116:4605-4613.

215. Riemenschneider, M. J., W. Mueller, R. A. Betensky, G. Mohapatra, and D. N. Louis. 2005. In situ analysis of integrin and growth factor receptor signaling pathways in human glioblastomas suggests overlapping relationships with focal adhesion kinase activation. American Journal of Pathology 167:1379-1387.

216. Paulus, W., I. Baur, A. S. Beutler, and S. A. Reeves. 1996. Diffuse brain invasion of glioma cells requires beta 1 integrins. Lab Invest 75:819-826.

217. Friedl, P., K. S. Zanker, and E. B. Brocker. 1998. Cell migration strategies in 3-D extracellular matrix: Differences in morphology, cell matrix interactions, and integrin function. Microsc Res Techniq 43:369-378.

218. Training, A. C. o. P. 2015. ACS guidelines and evaluation procedures for undergraduate Bachelor's degree programs. American Chemical Society, Washington, DC.

219. Brown, P. 2001. Understanding solubility through excel spreadsheets. J Chem Educ 78:268-270.

220. Cress, N. L., M. A. Robinson, L. Corner, R. L. Legge, and L. A. Ricardez-Sandoval. 2012. Problem-solving and concept integration using a computational tool in first-year undergraduate chemical engineering. Education for Chemical Engineers 7:e133-e138.

221. Loyson, P. 2010. Teaching Kinetics Using Excel. J Chem Educ 87:998-998.

222. Wong, K. W. W., and J. P. Barford. 2010. Teaching Excel VBA as a problem solving tool for chemical engineering core courses. Education for Chemical Engineers 5:e72-e77.

223. Martini, S. R., and C. J. Hartzell. 2015. Integrating Computational Chemistry into a Course in Classical Thermodynamics. J Chem Educ 92:1201-1203.

224. Bennett, N. S., and B. F. Taubman. 2013. Reading Journal Articles for Comprehension Using Key Sentences: An Exercise for the Novice Research Student. J Chem Educ 90:741-744.

225. Drake, B. D., G. M. Acosta, and R. L. Smith. 1997. An effective technique for reading research articles - The Japanese KENSHU method. J Chem Educ 74:186-188.

226. Tilstra, L. 2001. Using journal articles to teach writing skills for laboratory reports in general chemistry. J Chem Educ 78:762-764.

227. Gawalt, E. S., and B. Adams. 2011. A Chemical Information Literacy Program for First-Year Students. J Chem Educ 88:402-407.

228. Jensen, D., R. Narske, and C. Ghinazzi. 2010. Beyond Chemical Literature: Developing Skills for Chemical Research Literacy. J Chem Educ 87:700-702.

229. Roecker, L. 2007. Introducing students to the scientific literature. J Chem Educ 84:1380-1384.

230. Commission, A. P. 2012. Advancing graduate education in the chemical sciences. American Chemical Society, Washington, DC.

231. 2012. In Challenges in Chemistry Graduate Education: A Workshop Summary, Washington (DC).

232. Feldon, D. F., J. Peugh, B. E. Timmerman, M. A. Maher, M. Hurst, D. Strickland, J. A. Gilmore, and C. Stiegelmeyer. 2011. Graduate Students' Teaching Experiences Improve Their Methodological Research Skills. Science 333:1037-1039.

233. Ethington, C. A., and A. Pisani. 1993. The RA and TA Experience - Impediments and Benefits to Graduate Study. Res High Educ 34:343-354.